ALMA MATER STUDIORUM
UNIVERSITÀ DI BOLOGNA

DEPARTMENT OF
CIVIL, CHEMICAL, ENVIRONMENTAL AND MATERIALS ENGINEERING

SECOND CYCLE MASTER'S DEGREE IN
EARTH RESOURCES ENGINEERING

Effect of spatial variability on uranium diffusion in the three facies of the Opalinus Clay at Mont Terri

Supervisor
Prof. Villiam Bortolotti

Co-Supervisors
Dr. Marco De Lucia
Prof. Stefano Bonduà

Candidate
Marco Fabbri

Graduation Session III
Academic Year 2023/2024

Abstract

This study, conducted in the framework of an Erasmus exchange at GFZ Helmholtz Centre for Geosciences (Potsdam, Germany), investigates the impact of spatial variability on uranium diffusion in the Opalinus Clay formation at Switzerland's Mont Terri underground laboratory; a facility built to research the geological storage of high-level radioactive waste. Using 2D reactive transport simulations with the open-source research code POET developed at GFZ, the research examined three distinct facies: sandy, carbonate-rich, and shaly, each with different porosity ranges and chemical retention capacities. Geostatistical simulations of porosity with varying correlation lengths (5-20m) and anisotropy ratios were used to derive spatially variable effective diffusion coefficients. Two distinct boundary conditions were tested: uranium diffusion from a linear source and from a punctual source, both simulated over one million years. Results indicate that the carbonate-rich facies allows significantly further uranium migration due to reduced chemical buffering. Larger correlation lengths produced more extensive uranium spreading, with a maximum migration length of 33m for linear sources and coverage of 975m^2 for punctual sources under isotropic conditions. When incorporating more realistic hydro-geochemical gradients into the initial state for the simulations, uranium diffusion increased significantly, reaching 48.25m distance and 2066.3m^2 coverage in the carbonate-rich facies when diffusing into increasing background concentrations. These findings highlight the fact that, while geochemistry of the formation has the largest impact on uranium migration, spatial variability can not be neglected as source of uncertainty on long-term radionuclide transport in potential repository sites.

Table of contents

1 Introduction

1.1 Introduction

The relevant challenges in terms of global reduction of CO_2 emissions, and the consequent research of carbon-free energy sources, have reawaken the discussion about the role of nuclear energy worldwide. Despite the threat of a nuclear war which has characterized the toughest years of the Cold War, the idea of exploiting the power created from the nuclear fission to produce energy started spreading, with the first commercial power stations built in the 1950s.

Nowadays, the nuclear energy accounts for 9% of the world's electricity production, coming from 440 power reactors operating in 31 countries [S1].

The latest data show that nuclear is the second source of low-carbon energy, only after hydro power energy, with an electricity generation of more than 2.6 million of GWh in 2022 [S2].

In the future scenario, the production of electricity form nuclear power is expected to grow, replacing part of the share related to fossil fuels. As a result, the amount of spent fuel coming from the energy production sector is going to increase. Moreover, nuclear energy is not the only source of high-level nuclear waste, which also derives from medical imaging and research studies. Despite the first reactor was built more than 70 years ago, the disposal of radioactive waste materials is still an urgent topic. Due to technical challenges, the evaluation of the most efficient disposal method for nuclear waste materials is under discussion. The consequence is that almost the previously produced spent fuel is not disposed yet. Regarding the term nuclear waste, a variety of different radioactive elements are taken into considerations. Nevertheless, the most relevant element from a technical and political point of view is uranium. In this complicated context, politics has set a threshold for the evaluation of a safe disposal site. The integrity of the disposal site has to be guaranteed for a time period of 1 million years. Accordingly, no radioactivity traces can pass the defined borders of the disposal site within the defined time period. The consequence is that only particular technologies and natural conditions allow such long disposal period, along which the minimum environmental hazard has to be guaranteed. The disposal into deep marine environment was taken into consideration at first, but it was evaluated that the most suitable solution is underground repositories [1].

From a technological point of view, the spent fuel has to be placed inside a thick metal container, which can be made of carbon steel, copper-lined nodular iron, or a combination of cement and stainless steel. The main goal for the system is to prevent water, or groundwater in the context of underground disposal, to reach the radioactive material, avoiding it to spread inside the environment. To improve the impermeability of the internal structure and to avoid corrosion, the tunnel, where the container is located, is filled with bentonite: a clay, mainly made of montmorillonite, which can absorb large quantities of water and of radionuclides acting as a buffer towards water intrusions [S3]. However, the implementation of the technical barrier (spent fuel, metal container, and bentonite) comes after the localization of a proper geological formation: the multi-barrier concept. Worldwide, the current focus of the research is on the localization of rock formations characterized by specific feature. The ideal features for the host rock should be a high stability over millions of years, almost absence of underground water flow, a geochemically reducing environment, together with a hypothetical thermodynamic equilibrium between pore water and minerals. Globally, very few formations show the majority of those features, but three different host rock types have been deeply investigated: crystalline rocks, salt formations, and clays. Looking at the European geographical area, Switzerland, France, and Belgium consider clay as promising disposal formations, while Sweden and Finland are building the shelters inside crystalline formations. Regarding Germany, the choice is still under evaluation. Despite a lower thermal conductivity and mechanical stability than the other two types, clays show favorable properties:

- very low hydraulic permeability (10^{-10} to $<10^{-14}$ m/s [2])
- almost all the transport takes place through diffusion mechanisms
- retention capacity against radionuclides
- rather high stability
- lateral continuity [3].

In 2021, globally only three countries (France, Sweden and Finland) were under licensing for the construction of geological disposal facilities showing how delicate from a technical, political and social point of view this topic is [1].

It is clear that, beside the technological and social challenges, a larger number of repositories have to be planned in the next decades.

Indeed, starting from the guidelines related to the selection of a suitable host rock, other countries, such as Germany, are focused on the investigation of different rock formations. The Swiss government has pointed the Opalinus Clay formation as host rock for the disposal of the Swiss highly radioactive waste materials [4]. The choice of the exact location is under discussion. The current study, carried out under the supervision of Doctor Marco De Lucia at the GFZ Helmholtz Centre for Geosciences [S4](Potsdam, Germany), investigates the uranium diffusion in the Opalinus Clay at Mont Terri.

1.2 Lithology of the Opalinus Clay at the Mont Terri laboratory

The Opalinus Clay formed in the lower Aalenian age (Jurassic), and it is present in the northern part of Switzerland, Swiss-German foreland basin, southern Germany, and France. In 1995, the Swiss government pointed it as suitable and potential host rock for the disposal of radioactive waste materials, and since then, it has been deeply investigated at the Mont Terri underground laboratory.

The laboratory is located inside a 3900 m motorway tunnel that crosses an overthrust anticline of the Jura mountains in the northwestern part of Switzerland.

The Opalinus Clay deposited in a shallow marine environment, and the investigations on the geological history showed that it reached depths of more than 1000 m creating an overconsolidated claystone. The Opalinus Clay is part of the Dogger hydrogeological unit, together with the upper layer of limestones (180-170 Ma (million years ago)). Regarding the specific site at Mont Terri, Liassic claystones and limestones are located below the Opalinus Clay, with the claystone formation creating a very low-permeability layer together with the Opalinus Clay. The two embedding layers represents two active aquifers which cause the presence of a geochemical gradient inside the Opalinus Clay. A more detailed explanation of the involved geochemical system is provided in the chapters "Previuos Diffusion Results", and "Geochemical Gradient at Mont Terri". The investigated formation is characterized by both claystone and marl, with the presence of sandy and calcareous layers and lenses, resulting in a dark gray argillaceous to light gray silty-sand claystone with a maximum thickness of 160 meters *[Figure1/1]* [5].

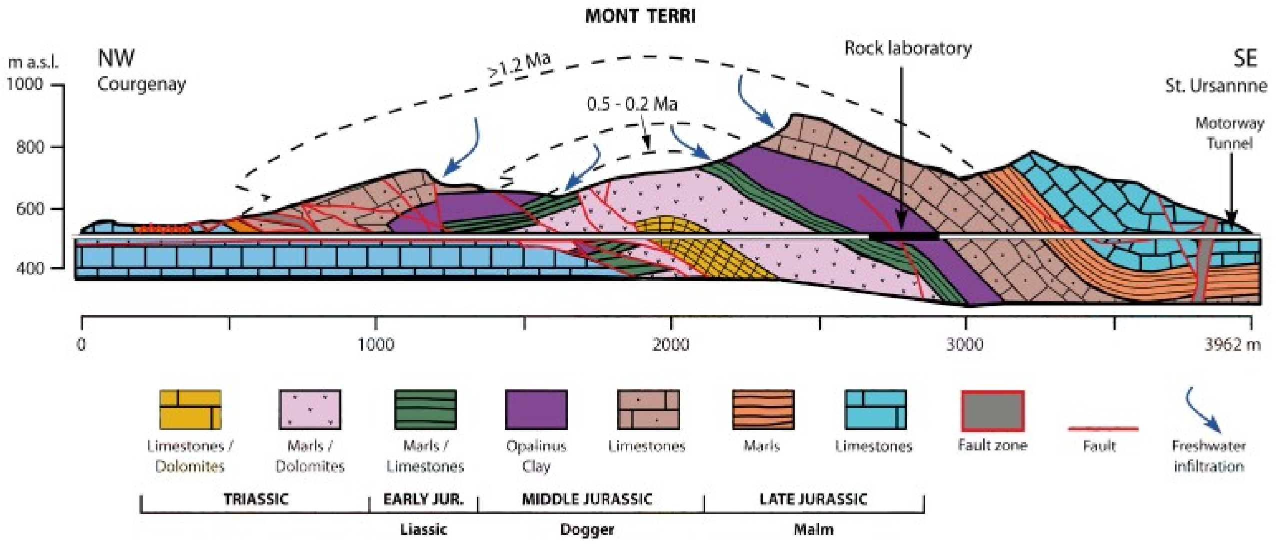

Figure 1/1. Geological cross-section through the Mont Terri anticline, with the location of the Mont Terri laboratory. Image reproduced with permission from the author [6].

The heterogeneity in terms of major minerals content leads to the classification of 3 different lithofacies (shaly, sandy and carbonate-rich sandy), and to a subdivision into 5 units.

Moving form the bottom of the formation to the top, it is possible to distinguish the major shaly facies consisting of mica-bearing calcareous claystones with lenses or with mm-thick layers of quartz in the silt fraction, a sharp transition to a thin carbonate-rich sandy facies, characterized by quartz-bearing calcareous layers of up to 10 cm thickness, a sandy facies with calcareous silty claystones, which is then overlain by a dark grey mica-bearing and slightly silty claystone attributed to the shaly facies. Finally, the uppermost unit of the Opalinus Clay consists again of a sandy facies, a light grey silty claystone with laminated silt lenses, and lenses of bioclastic material [7].

The contribution of the shaly facies to the whole formation is around 60%, while the sandy facies accounts for the 35%. The thin carbonate-rich facies comprises 5% of the rock. Through a qualitative investigation, the heterogeneity between the different facies could be considered almost negligible. However, the differences in mineralogical contest result in a variation of the petrophysical properties (porosity) and thus in the diffusion phenomena, as it is reported in the chapter "Facies-dependent Porosity" (Chapter 4). As a consequence, it is better to define and highlight the mineralogy of each facies. Regarding the shaly facies, the amount of clay minerals was estimated to be around 68%; illite, kaolinite and the illite-smectite unit (montmorillonite) as major clay minerals components for the whole formation. Then, the shaly facies is mostly made of calcite and quartz, both accounting around 16%. The carbonate-rich facies is characterized by a lower content of clay minerals (24%), but by more calcite (44%), and even the quartz fraction increases up to 31%. The quartz content for the sandy facies does not differ from the carbonate-rich case, but the clay content is estimated around 59%, and the calcite fraction decreases up to 7%, with a mean value of 13%.

The differences in terms of mineral contents between two same facies, but located at different depths of the formation, are negligible. Moreover, the latest studies have revealed the possibility to subdivide the three facies into five subfacies, exploring in a very detailed way the mineral and chemical properties that characterize the formation [8].

1.3 Diffusion as the only transport mechanism

The low values of permeability for the majority of clay formations result in a diffusive transport as only transport mechanism. In a fluid, diffusion phenomena are related to the random movement of molecules which is not dependent on the magnitude and direction of the flow, but it can be classified as a thermal motion (dependence on the temperature) [9].

Once a heterogeneous condition for the concentration of the species (S) occurs – there is a concentration gradient in the fluid – more molecules from the higher concentration regions move towards the lower ones than vice versa. The consequence is the apparent transport of molecules from the region at higher concentration to the one at lower concentration as result of Brownian motion.

This transport mechanism is quantified at a macroscopic scale by the Fick's First Law, which states that the flux (mass flow rate) (kg/s/m^2) of the molecules is function of the gradient of the concentration c (kg/m^3):

$$\phi = -d_0 \nabla(c)$$

"d_0" is the molecular diffusion coefficient [L^2T^1], which is an isotropic value, and it is given by the Stokes-Einstein equation [10].

$$d_0 = \frac{k_B T}{(6\pi \mu_b r_a)}$$

For a diluted species *a*, in a phase *b*, the coefficient is proportional to the Boltzmann constant k_B (1.38E-23 J/K), and the absolute temperature T (˚C + 273.15). While the value decreases as the phase viscosity μ_b increases, and as the radius r_a of the particle increases. This results in smaller molecular diffusion coefficient for molecules diluted in a liquid, rather than a gaseous phase.

Regarding diffusive transport in liquid phases, once there are no other transport mechanisms involved, the transport equation turns to be the Fick's Second Law:

$$\frac{\partial c}{\partial t} = \nabla \cdot [d_0 \nabla(c)]$$

The diffusive transport equation in a porous media can be written as:

$$\omega \frac{\partial c}{\partial t} = \nabla \cdot [\omega D_f \nabla(c)]$$

where ω is the porosity, D_f is the diffusion coefficient in "free" water, and for POET, the transport operator applied in the current study, in a 2D scenario the equation for the species S is:

$$\frac{\partial C}{\partial t} = \frac{\partial}{\partial x}\left[D_{fx}\frac{\partial C}{\partial x}\right] + \frac{\partial}{\partial y}\left[D_{fy}\frac{\partial C}{\partial x}\right] \text{ where } C = \frac{m(S)}{V_{tot}} \text{ and } c = \frac{m(S)}{V_{sol}} = \frac{C}{\omega}$$

Performing reactive-transport simulations in POET relies on a simplification. The porosity is considered homogeneous and constant inside the simulated model, and this allows the treatment spatially heterogeneous diffusion coefficients which are scaled by the porosity.

The motion of molecules in porous media is affected by tortuosity, which is a dimensionless quantification of the effect of heterogeneous pore structures on the path of the molecules (the tortuosity is defined as the length of the actual travel path taken by the solute divided by the straight-line distance [11]). The modified path results in a longer diffusive length to be covered which implies the definition of the effective diffusion coefficient as the molecular diffusion coefficient in “free water” divided by the tortuosity θ to the power of two:

$$D_e = \frac{D_f}{\theta^2}$$

Under the assumption of grains as perfect insulators, and accounting the relationship between the formation factor *F* (ratio between the specific electrical resistance of a sediment with a solution and the specific resistance of the free solution) and the porosity ω given by the Archie’s law, the effective diffusion coefficient can be defined as the diffusion coefficient in “free” water times the porosity [11]:

$$D_e = D_f \cdot \omega$$

1.4 Diffusion and sorption in clay formations

Beside the theory of diffusive mechanisms, the diffusion in the clay formation is the consequence of the interaction between the clay minerals and the pore water molecule. The wider principles behind the coupling of transport phenomena and chemical reactions are reported in more accurate way in the “Basics of reactive-transport” chapter (Chapter 1.5). However, herein an overview of the effects on diffusive transport due to the electrostatics interaction of solid and liquid phases is presented. As previously mentioned, one of the most relevant features of clays as host rocks is the retention capacity against radionuclides, and it is important to investigate this behavior. The retention capacity is enhanced by the petrophysical properties of clay formation, which is characterized by very low values of permeability, but by large porosity and accessible surface, as a consequence of the granulometry of clays. The transport of radionuclides is modified by the electrostatics interactions, and it is even more buffered by the sorption processes occurring on the surface of clay minerals. The latter mechanism is described later on. The surface of clay minerals is characterized by a negative charge, which is the consequence of alkaline conditions in clay formations.

The presence of the negative surface charge leads to the formation of a compensating region inside the pore water close to the minerals. The region is called diffuse double layer (DDL), and it attracts cationic species while repulsing anionic ones. When the pores are small enough to make two layers to get in contact one with the other, then the anion exclusion phenomenon takes place. What derives is s buffered diffusive transport for anionic species with respect to cationic and neutral species. The relevance of the diffuse double layer increases as the ionic strength of the pore water decreases.

Whereby, the length covered by radionuclides depends on the chemical conditions of pore water and the mineralogy of the host rock. Experimentally measured effective diffusion coefficients for different species quantifies how the diffusive pathway of that specific species is affected by the exact chemical and mineralogical conditions occurring in the sample.

There is another important feature of clay minerals that buffers the diffusion of radionuclides: sorption. Sorption is a set of processes that immobilize dissolved radionuclides by adsorbing them on the charged surface of minerals. The two dominant mechanisms are cation exchange and surface complexation.

The former one is a consequence of the negative surface charge of minerals which turn into cation exchangers, releasing bounded cations and adsorbing cationic radionuclide species and vice versa. The latter process is surface complexation and it represents the chemical bonding of pore water molecules with functional hydroxyl groups located on the basal and edge site of the clay minerals. Based on the location of the hydroxyl group, the resulted complexes are called outer-sphere complexes or inner-sphere ones [4].

1.5 Basics of reactive transport

The concept of reactive transport is to couple the hydrodynamics and the chemical reactions involved in porous media. The chemical reactions, such as dilution or precipitation of minerals, affect the transport mechanism via changes in the transport parameters (porosity, permeability and effective diffusion coefficient), but at the same time the hydrodynamics, transporting chemical species in the pores of the medium, modifies the thermodynamical equilibrium of the occurring chemical reactions. The coupling of those phenomena represents a challenging step for a lot of different subjects investigating the interaction of a porous media with fluids. The creation of a model which is able to reproduce as close to the reality as possible the evolution of a real media, accounting both the microscopic and the macroscopic phenomena, over a fixed period of time is the key objective. The uses for those models range from the underground storage of CO_2 to the bioremediation of contaminated sites. In the current chapter, the major laws and concepts that are the basis of the geochemistry:

- concentration, activity and ionic strength
- chemical equilibrium
- reaction kinetics.

Once the geochemistry is defined, it has to be coupled with the transport mechanisms thanks to specific equations.

After the phases and the relative species (S_j) involved are defined, the activity of one species points out which is the effective or apparent concentration of that species that takes part in a reaction. The defining equation of activity is reported herein:

$$[S_j]=\gamma_j c(S_j)$$

where $[S_j]$ is the activity of the species j, $c(S_j)$ is its concentration, and γ_j is species-dependent parameter which is described later on in this chapter.

It is better to highlight that, talking about solutions inside porous media, the concentration of one species can be defined as its mass divided by the total volume of the porous media or by the volume of the solution (taking into account the porosity of the matrix):

$$C=\frac{m(S)}{V_{tot}}$$

$$c=\frac{m(S)}{V_{sol}}=\frac{C}{\omega}$$

For the evaluation of the chemical or physical-chemical interactions in a solution, two different parameters have to be considered: the concentration of species j in solution, and its charge z, since the Ionic Strength of a solution is defined as

$$I=\frac{1}{2}\sum_{j=1}^{N\,species} z_j^2 c(S_j)$$

For solutions with an elevated value of ionic strength (I), the activity of the single species will be affected by the ionic strength of the solution, and it is not possible to consider the activity of one species $[S_j]$ equal to the concentration for that species ($c(S_j)$). The Debye-Hückel model is the simplest approach to approximate the activity of species for moderately concentrated solutions [12]:

$$[S_j]=\gamma_j c(S_j)$$

$$\ln(\gamma_j) = -A z_j^2 \frac{\sqrt{I}}{1+B\bar{a}\sqrt{I}}$$

where A and B are positive constants, and the ions are considered as spheres of radius equal to ā.

By chemical equilibrium it is meant that all the activities of each species involved in the chemical reaction are constant in time. However, this condition is rarely reached in real case scenarios due to the presence of unfavorable kinetics, but there are simplified models in which the considered reactions are always at equilibrium. Moreover, modifying the system from outside, the equilibrium can be shifted toward the products or the reagents, but the system itself minimizes those effects [S5].

The equilibrium constant for a general reaction, such as

$$aA + bB = cC + dD$$

is defined as the products of activities of the reaction products divided by those of the reactants, each elevated by the corresponding stoichiometric coefficient α_j (Law of mass action) when measured at equilibrium:

$$K_{eq} = \frac{[C]^c [D]^d}{[A]^a [B]^b} = \prod_j [S_j]^{\alpha_j}$$

Depending on the type of reaction (endothermic or exothermic), for a condition of constant pressure, the equilibrium constant can increase or decrease as the temperature increases or decreases, or vice versa.

Actually, the chemical equilibrium is a dynamic condition, where the direct and inverse reactions take place but their effects can not be detected because they have the same velocity:

$$v_{dir} = k_{dir} [A]^a [B]^b$$

$$v_{inv} = k_{inv} [C]^c [D]^d$$

and as a consequence:

$$K_{eq} = \frac{k_{dir}}{k_{inv}}$$

The feasibility of a chemical reaction is enhanced when, from a thermodynamic point of view, the stability of the products is higher than the one of the reactants. Nevertheless, this is not a sufficient condition. A chemical reaction may proceed so slow that it can be considered almost still. The branch of the chemistry which focuses on the rate at which chemical reactions proceed is kinetics. Once there are *n* species involved, it is possible to define the reaction rate I_r as the variation in time of the activity of each species divided by their stoichiometric index($\alpha_{j,r}$).

$$\forall j \quad I_r = \frac{-1}{\alpha_{j,r}} \frac{d[S_j]}{dt}$$

Taking into account the principle of the law of mass action, the reaction kinetics, at a fixed temperature, is a function of the activity of the species *j* $[S_j]$, each one elevated to an experimental coefficient defined as the partial order of reaction for that species:

$$I_r = k_r \prod_j [S_j]^{\beta_j}$$

The k_r is the reaction rate constant, and it comprises all the other mechanisms that affect the reaction rate besides the activity of the species. The most famous representation of that constant is the Arrhenius equation, which defines its temperature dependence:

$$k_r = \mathrm{A}\,\mathrm{e}^{\left(\frac{-E_a}{RT}\right)}$$

This is an exponential relationship between the absolute temperature and k_r, where A is the per-exponential factor (or Arrhenius factor), E_a is the activation energy, and R the universal gas constant.

As previously mentioned, the concept of reactive transport wants to quantify the interactions between transport mechanisms and geochemistry. The four major phenomena involved are: the hydrodynamic flow of transporting phase, transport of solute species, geochemical reactions between solution and rock forming minerals, and porosity changes.

In details, the water flow affects the transport of the chemical species, which causes a change in the geochemical reactions due to either adding or subtracting reactants. The two main phenomena related to geochemistry are dissolution and precipitation. In this work, these two reactions are not explained in details, however, the Law of Mass Action applies also to mineral reactions with the caveat that the value of the activity for a mineral involved in these two reactions is conventionally set to 1 [10].

A change in the chemical equilibrium in both dissolution and precipitation reactions causes a variation in rock porosity, with a consequent change in permeability (and hence water flow) and tortuosity and hence diffusion coefficient and sorption capacity.

There are two main methods for the coupling of transport mechanisms and geochemistry:

- global implicit,
- operator splitting.

The former one is the most expensive in terms of computation time and memory use. This is a consequence of the approach which solves, at the same time, both transport and geochemistry merging together all the equations in one single problem. Such complexity allows to work only on relatively simple models. The latter method solves instead the two algebraic-differential problems in series within each time step, turning into a less precise approach, with issue in the convergency particularly if the chemistry involved is complex.

The operator splitting method can be solved in a sequential iterative (SIA) or in a sequential non iterative approach (SNIA). The second is the one implemented in POET.

Regarding the chemical reactions taken into consideration for the following investigated scenarios, two different processes are accounted for inside the reactive-transport simulations. As mentioned in the “Diffusion and Sorption in Clay formations” chapter (Chapter 1.4), the two mechanisms are the electrostatic interaction (cation exchange) and the sorption of radionuclides. Both are quantified inside the chemistry file, and they are indicated as “EXCHANGE” and “SURFACE”. The format of the file is .pqi, and it is read by the chemistry operator once the simulation is launched. The Cation Exchange Capacity (CEC) measures the negative charge of the solid phase of a soil balanced by exchangeable cations, and it can be expressed in meq/kg, where meq are milliequivalents. The CEC of a soil can be empirically correlated to the clay (<2 μm) and organic carbon (C) content, at neutral ph, via the following formula:

$$CEC(meq/kg) = 7 \cdot (\%\,clay) + 35 \cdot (\%\,C)$$

Taking into consideration two ions A^+ and B^+, the ion exchange reaction is:

$$A^{+} + B\text{-}X = A\text{-}X + B^{+}$$

where X is the soil exchanger, and the distribution of the species is given by the law of mass action:

$$K_{A/B} = \frac{[A\text{-}X][B^{+}]}{[B\text{-}X][A^{+}]}$$

with square brackets denoting activities.

A detailed definition and investigation of the mechanisms involved in what is defined as Surface Complexation does not deal with the purpose of the current paper, and it is explained by Appelo et al. [11]. Nevertheless, herein the equation of the Gibbs free energy for the surface complexation is presented. The concept behind sorption accounts for two effects: a chemical bond between the ion and the surface atoms, and an electrostatic effect that depends on the surface charge. This definitions results in two different terms inside the equation of the surface complexation (Gibbs free energy):

$$\Delta G = \Delta G_{chem} + \Delta G_{coul}$$

where ΔG_{coul} is the Coulombic term, and it quantifies the electrical work required to move ions away from a charge surface. ΔG_{chem} represents the chemical energy in the bonds.

1.6 POET and PHREEQC as simulating software

For the purpose of the current study, all the scenarios of interest are simulated in POET [13], a coupled reactive transport simulator which uses PHREEQC [14] as chemical engine (sub-model related to the chemistry).

POET is a reactive-transport software massively parallel, which is able to run on multi-cores computers and HPC clusters. Developed by De Lucia et al. [13] at the GFZ [S4] and University of Potsdam, POET works as a framework for testing speeding-up algorithms, involving PHREEQC results stored in cache, interpolation of earlier performed geochemical simulations, and machine learning. Technically, POET already consists in the sequential not iterative coupling of one transport (diffusion) module, which is "TUG (Transport on Uniform Grids)" and PHREEQC. Regarding TUG, diffusion is simulated based on finite integral differences for homogeneous grids. The numerical scheme is "Alternating Direction Implicit", which combines the precision of explicit schemes with the larger stability condition of implicit ones and therefore allows using large time steps. The diffusion coefficient is spatially variable and anisotropic; in facts, it is implemented as a 2D vector. At the contrary, the porosity is considered homogeneous and constant for the whole grid. Moreover, the model is always considered isotherm, without any feedback between the chemistry involved and the porosity or permeability.

POET has been developed using C++ as programming language, but it also features an R interpreter, which allows to dynamically load user code which is particularly helpful for machine learning. All POET input scripts are R files. In addition, the R package "PoetUtils" contains all the functions that enable the user to visualize and work on the results in the R environment.

The coupling with PHREEQC is based on the "iphreeqc" package [14], which is developed in C++ in order to couple PHREEQC with languages such as R or python. Actually, the latest version of POET has implemented a more efficient extension of "iphreeqc" which drastically reduces the use of the native interface of PHREEQC, which works via scripting. Instead, the recent extension involves the memory data structures directly.

PHREEQC is globally considered the reference program for geochemical simulations. In order to simply summarize its features, it is an open-source software, deeply established in the scientific community, based on the mass action law.

1.6.1 Performing a reactive transport simulation via POET software

The reactive transport simulating software POET is based on the coupling of two different submodels: TUG and PHREEQC. At first, the single coupling iteration simulates the transport mechanisms, thanks to the sub-model TUG, and then the chemistry is involved via the use of PHREEQC sub-model. This procedure is repeated at each time step. Indeed, the user provides two types of files to POET. The former one is related to the geometry and transport properties, such as the diffusion coefficient, or the type of injection (punctual, row-wise), or the dimension of the grid, and also the file related to the chemistry in form of a PHREEQC input script is linked (the format of the file is “.pqi”). The former file is an R file which is then transformed into a binary format “.qs” to be read by POET. The latter file is the ‘run-time’ file, which contains the settings related to duration of the simulation, in terms of number of iterations, time stepping, and which iterations are to be stored on disk. Once the simulation is concluded, those iterations are saved in an output directory indicated by the user when launching the simulation. There is no graphical interface of POET; indeed, all the simulations are launched from the terminal. POET only works on Linux operating systems.
Herein, a schematic representation of the starting command is reported:

```
“ mpirun  -np N  [...]/poet  [runtime-file].R  [input-file].qs  [output-directory]_res “.
```

N is the number of cores or CPUs involved to perform the simulation. The number of cores differs working on different servers.
The command to perform the initialisation is:

```
“[...]/poet_init  [input-file].R  [input-file].qs”.
```

1.7 Previous simulations for the Uranium diffusion performed at the GFZ

As previously mentioned, the aim of this work is to investigate the impact of the spatial variability of the petrophysical properties of the Opalinus Clay on the diffusion of radioactive components. Since the application of spatial variability is a new approach for this type of analysis, in the context of the Opalinus Clay, the obtained results have to be compared to previous analysis under the hypothesis of homogeneity of the petrophysiscal properties. Starting from the same chemical and mineralogical conditions for the pore water and the rock matrix, the comparison between heterogeneous and homogeneous cases results in the evaluation of the differences due to the spatial variability. The four papers of Hennig et al [4] are the starting point for the analysis. In those articles the diffusion of uranium inside the Opalinus Clay is deeply investigated through 1D simulations performed with PHREEQC.

The first paper [15] highlights the mineralogical heterogeneity of the Opalinus Clay formation with a series of simulations resulting in different uranium profiles working on the three different facies. The results prove that the diffusion is dependent on the single facies. The different mineralogical pattern of the three facies modifies the pore water composition as a consequence of the rearranged chemical equilibrium of the reactions between the rock minerals and the diluted components (calcite-carbonate-ion equilibrium). Pore water composition, and in particular the calcium and carbonate concentrations, is considered to most important parameter for the quantification of the uranium profiles, since it regulates the presence of Uranium(VI) in the form of the ternary anionic component $CaUO_2(CO_3)_3^{2-}$and the sorption mechanism enhanced by the anion exclusion phenomenon. Hennig et al. obtains similar migration distances for the carbonate-rich facies and the sandy facies, with a maximum distance from the injection point equal to 26 meters. While for the case of the shaly facies, where the sorption mechanism is more relevant, the maximum migration cavers 16 meters.

The second paper [16] concerns the variation in diffusion migration length once multi-component (MC) diffusion simulations are performed, instead of the single components models (SC). The use of MC implies the definition of a different diffusion coefficient for each of the species involved, together with the further characterization of the diffusion double layer (DDL) adhering clay mineral surfaces. For every facies, the MC models showed a shorted migration length of U(VI) than SC, mainly due to the consideration of the DDL. However, the use of MC models is much more time consuming rather than SC ones. In these terms, a workflow to transfer MC models into SC simulations, thanks to the calibration of effective diffusion and distribution coefficients, was developed. The simulations showed a maximum migration length of 35 meters.

The third paper [17] is less relevant in the context of the results obtained in the current study. Hennig et al. evaluates the influence of varying the stability constant on the length covered by the diffusion of uranium. All the parameters of the pore water chemistry and the mineralogy of the rock are untouched but the stability constant which influences the presence of the predominant anionic ternary group for U(VI) $CaUO_2(CO_3)_3^{2-}$, with respect to the neutral ternary complex. Modifying the value of the stability constant of 1.33 log units a variation in the migration length of 5 m up to 7 m occurs (investigating both the sandy and shaly facies). The interaction with the diffusive double layer, concept introduced in the second paper [16], causes the change in migration length. However, due to the small difference, the influence of the variation of the stability constant is considered negligible.

The last paper [6] introduces the geochemical gradients into the models for a more accurate evaluation of the uranium migration. Homogeneous initial conditions are not suitable for investigating the uranium diffusion on the host rock scale. Regarding the pore water chemistry, available concentration profiles have to be taken into consideration. The Opalinus Clay formation is embedded by two aquifers which have led to the formation of geochemical gradients inside the host rock. In order to evaluate the present-day profiles two different approaches were performed: data-driven approach, and a conceptual scenario. The influence of the evaluated profiles was evaluated on a one million years scenario, which was then compared to the homogeneous case [16]. No relevant differences were experimented using an SC or MC approach, but the results show a maximum increase in the migration length of 24 meters compared to the homogeneous case. The partial pressure of CO_2 has the highest influence on uranium diffusion.

2 Thesis Objectives

In the context of safety assessments of nuclear waste disposal, the Opalinus Clay has been investigated as suitable host rock for more than 25 years. A large amount of research has been carried out with the purpose of obtaining a detailed characterization of the formation, in order to reproduce representative models and predict the migration of uranium radionuclides via diffusion mechanisms. For a time period of 1 Ma, which is legally considered the amount of time required for the natural degradation of radionuclides, the length covered by the diffusion of uranium must not overcome a specified threshold. Starting from the studies of Hennig et al. [4], a variety of interesting results are presented. However, despite the heterogeneity of the formation has been considered so far, the implementation of the spatial variability, related to the host rock properties, has been completely neglected. The current study wants to play a key role in the evaluation of the effects of the spatial variability, resulting in a relevant, despite rather simplified, starting point for deeper analyses in the future. In order to assess the influence of the spatial variability via 2D reactive-transport simulations with POET , four main objectives are presented:

- Assess the capabilities of POET with respect to spatial and temporal discretization for given model setups, which involves a careful and extended scoping analysis
- The second objective is to implement an appropriated spatial variability (in terms of diffusion coefficients) in the reactive transport simulations. A literature research on available data concerning the Opalinus Clay at Mont Terri is envisaged to derive geostatistical Parametrization and plausible ranges of the geostatistical simulations.
- The third objective is to assess the differences in terms of uranium migration length between the three facies of the Opalinus Clay once the spatial variability is accounted for. In particular, the variation is evaluated for two different boundary conditions.
- The fourth objective is the evaluation of the combined effects of spatial variability and the implementation of a more representative model incorporating the actual stratification of the Opalinus Clay at Mont Terri, including the expected geochemical gradient.

The current study does not fucus, and it is not based, on a detailed analysis of the geochemistry processes involved in a real case scenario.

3 Scoping Analysis

The use of POET, and the implemented coupling between TUG and PHREEQC, allows, and will allow in the future, a variety of promising innovations regarding reactive-transport simulations. Nevertheless, since it is the fist time that POET is applied to a real-life case, overcoming the previous use for algorithm development, a deep characterization of its capabilities is required, before proceeding with the implementation of the case study model. Regardless, a careful scoping analysis is needed every time a new model is investigated. In particular, the coupling with chemistry may complicate the convergence of the results and it may lead to the discover of some bugs. The first part of the research focuses on the evaluation and the investigation of the responses that the softwares provide as a consequence of the change of a series of parameters (sensitivity analysis). Only after an accurate scoping analysis the user is able to prioritize the parameters involved in the simulations and build an accurate model to replicate the phenomena of interest. As a result, a series of scoping 2D simulations are performed in the context of uranium migration inside the Opalinus Clay. New updates to the transport software are constantly implemented, and the first step is the introduction of a compressed binary file format (".qs"), which is the one used for all the simulations presented in this work. Scatter plots related to the aqueous concentration of the main components for the new file format and the former one (".rds") have not shown any difference or discrepancy. The aqueous concentrations are obtained by simulating the uranium migration in a 2x1 meters model, discretized in 100x50 cells, with homogeneous pore water diffusion coefficients along the x-axis and the y-axis.

As it is presented in the following chapter, a major role in the convergence of the results while coupling two simulators for reactive-transport analysis is played by the time step. The time step, together with the number of iterations, are two fundamental parameters chosen by the user. A preliminary investigation on the effects of varying the time step is carried out. The results coming from two simulations with time steps equal to 7200 s and 3600 s, and a number of iterations of 1000 and 2000, show that there is a convergence for the aqueous components with concentrations above 10^{-6} molal, while for smaller value the convergence is not perfectly guaranteed. The presented behavior can be associated to a systematic error which occurs during the coupling and it can be observed only for small values of aqueous concentrations. The coupling accounts the surface complexation involved between the pore water chemistry and the rock minerals. Even applying spatial variability to the pore water diffusion coefficient, small discrepancies are observed for scatter plot related to rather low aqueous concentrations. The final method used to apply spatial variability into reactive-transport simulations is explained in details in Paragraph 5.2. However, a deeper analysis on the effects of the choice of the times step is fostered after an unexpected result while comparing two simulations with time steps of 1800 s and 900 s. The cumulative analysis of the S(-2) species *[Figure1/3]* shows a relevant detachment between the two trends which confirms that the choice of the time step has an influence on the results. With cumulative analysis it is meant plotting the trend of the sum of one species concentration as a function of the simulations saved (time). The approach is based on simulating the same scenario – reproducing the uranium migration into Opalinus Clay with isotropic pore water coefficient for a time period of 6 hours– with 7 different time steps, and even modifying the value of the diffusion coefficient. Since the model is based on the Fick's Second Law, to replicate a simulation with a pore water diffusion coefficient ten times bigger than the one of interest, the number of iterations for the new simulation must be ten times the one used for the previous one. The cumulative analysis for U(6) is plotted *[Figure2/3]*. The difference in the trend lines proves the presence of a bug. The relationship between the discrepancies and the precision of the solution scheme is investigated by performing a series of simulations, using different values of the time step, without accounting for both the chemical processes ("SURFACE", "EXCHANGE"). Those simulations are indicated as "NoChem" simulations. The precision of the solution scheme for diffusion can be considered insignificant as a bug source *[Figure3/3]*. The frequency of the coupling with PHREEQC, which can be associated to the choice of time discretization, is identified as the cause of lack of convergence between the results. Once the chemistry is considered inside the simulations, the sequential coupling, which is implemented in POET, is characterized by a systematic error, which is inversely proportional to the number of iterations considered. Accordingly, once the chemistry is evaluated more often, the intrinsic error decreases. The discrepancies related to this kind of error are technically irreducible. Accordingly, the scoping analysis plays a key role in evaluating the best setup for the final purpose minimizing the discrepancies.

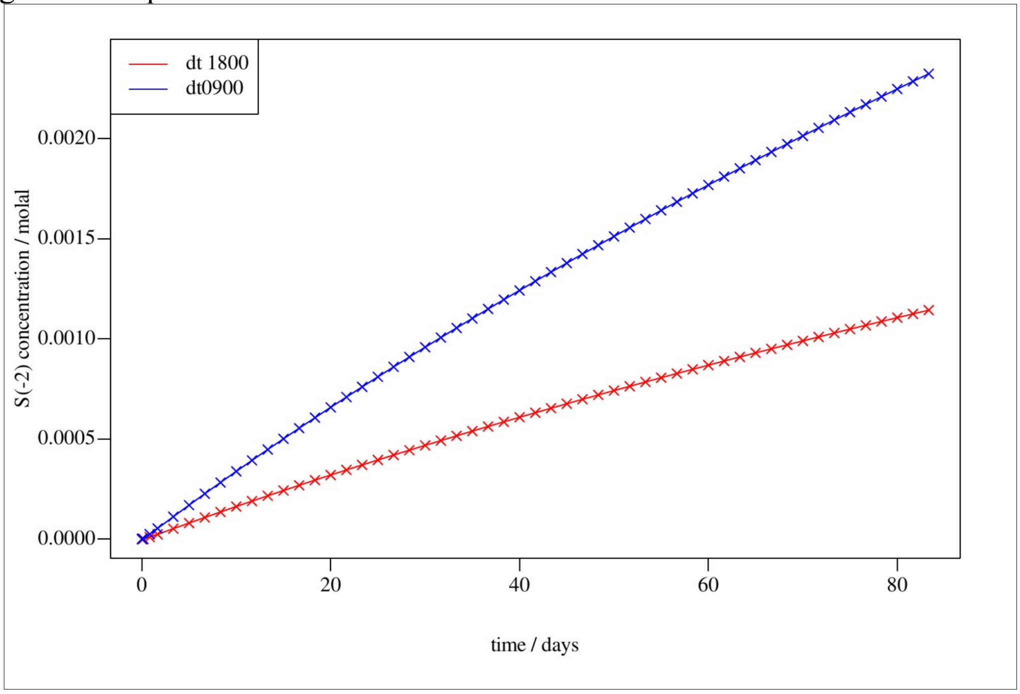

Figure 1/3. Discrepancies in the cumulative analyses of the aqueous concentration of S(-2) when using a time step of 1800 s (red line) and a time step of 900 s (blue line).

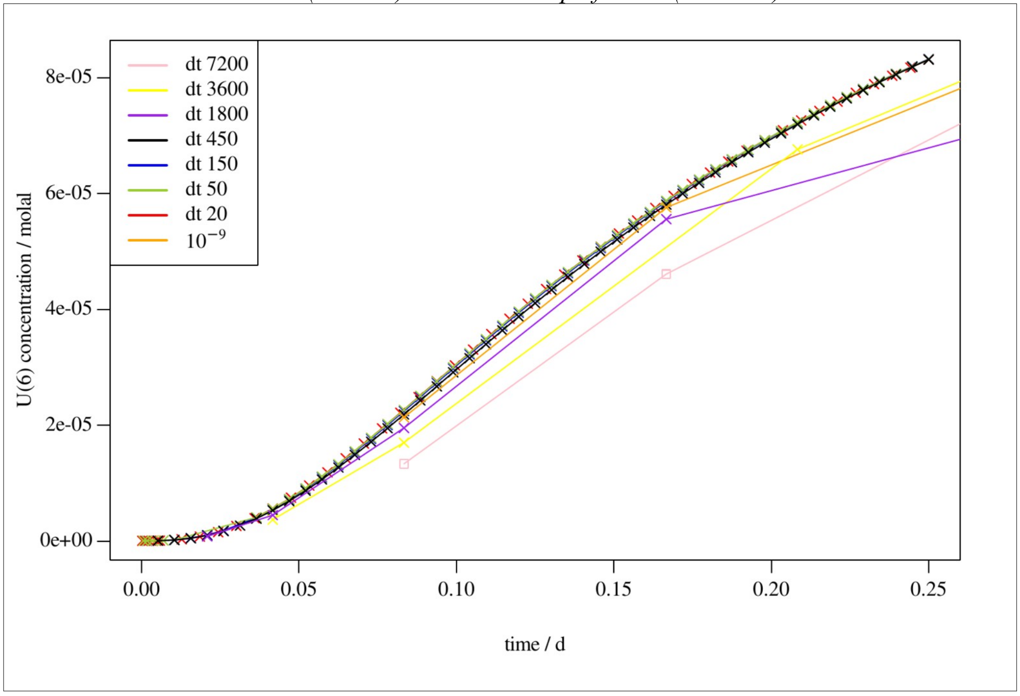

Figure2/3. Discrepancies in the cumulative analyses of the aqueous concentration of U(6) when using a series of different time steps (each time step is measured in seconds).

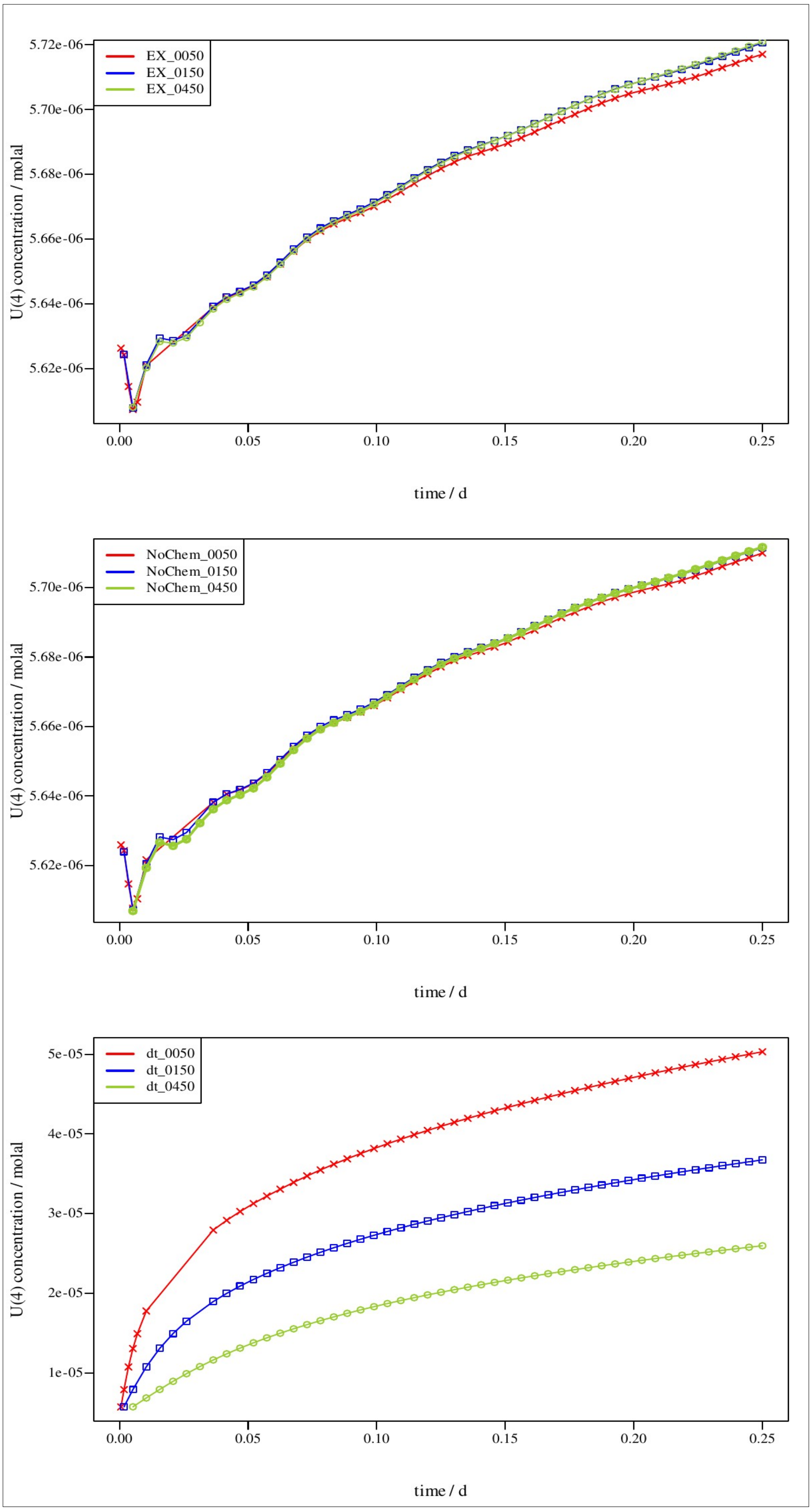

Figure3/3. Three cumulative analyses of U(4) for the same three time steps (50 s, 150 s, 450 s) while simulating in three different boundary conditions. The plot at the top of the image shows the results once only the EXCHANGE chemical processes are involved. The plot in the middle presents the results coming from simulations where no chemical processes are involved. The last one shows the discrepancies in the cumulative analyses when chemistry is considered inside the simulation.

What is revealed after a more detailed investigation on the chemistry files is that there is an intrinsic error by PHREEQC when dealing with very small values and which can be minimized imposing a more restrictive convergence tolerance for the solution of chemistry.
Once the source of the discrepancies is identified, the most efficient parameters of the model are investigated. The goal is to find the largest possible time step to reach the one million years simulation times with the least amount of needed iterations, without losing accuracy in the results. The optimal discretization of the model is evaluated iteratively, with a final grid of 100x100 cells for a 50x50 meters model. The final model is obtained looking at the time step analysis, which is explained in the following chapter. Once both the two chemical mechanisms are taken into consideration, the length covered by uranium migration in *Figure5/3* leads to the choice of the final model. It can be mentioned that a 50x50 meters model in few cases is not perfectly suitable, but in order to present comparable results it is not changed along the simulating process.

3.1 Evaluation of the optimal time step

Performing reactive transport simulations which involve phenomena taking place in one million years can be very time consuming. Accordingly, the choice of the time step is crucial. Two different "in-series" approaches were investigated to reduce the number of required iterations, following an increase in the time step. First of all, instead of working in terms of seconds the measurement unit of the time step is switched to years. The consequent variation of the measurement unit of the pore water diffusion coefficient is required, which is the most important input parameter for the reactive transport simulation. Indeed, from a measurement unit of squared meters divided by seconds, the values of the diffusion coefficient are adjusted as:

$$\alpha_x = D_f \cdot 365.25 \cdot 24 \cdot 3600$$
$$\alpha_y = D_f \cdot 365.25 \cdot 24 \cdot 3600$$

The latter approach can be considered the most critical and impacting in terms of the convergence of the results. Regarding simulations involving the resolution of partial differential equation, the Courant-Friedrichs-Lewi law gives the maximum time step which allows the convergence of the results. Herein, the Courant-Friedrichs-Lewi is indicated as the stability condition:

$$\Delta t \leq \frac{min(\Delta x^2, \Delta y^2)}{4 \cdot max(\alpha_x, \alpha_y)}$$

The values of Δx and Δy represents the discretization (size in meters divided by the number of cell) along the two axis of a 2D grid. For a 100x100 meters grid discretized in a 100x100 cells grid, the stability condition provides a maximum time step of 250 years. Which mean that 4000 iterations are necessary to simulate one million years. Despite the statement of the stability condition, a deeper analysis of the accuracy loss, as consequence of higher value of the time step, is performed. The study is performed for two different cases, both homogeneous not accounting the spatial variability: transport simulation (no chemistry involved *[Figure1/6]*), and reactive transport simulation (accounting the chemistry, which means accounting cation exchange phenomena and adsorption ad the mineral surface (Paragraph 1.4). Regarding the pure diffusion scenario, increasing the time step does not influence the results which converge in each case. The plot of the vertical concentration profile for all the uranium against the distance covered by the uranium is built accounting the simulations with five different time steps: 500 years, 1,000 years, 2,000 years, 5,000 years, and 10,000 years. *Figure4/3* shows the resulting plot.

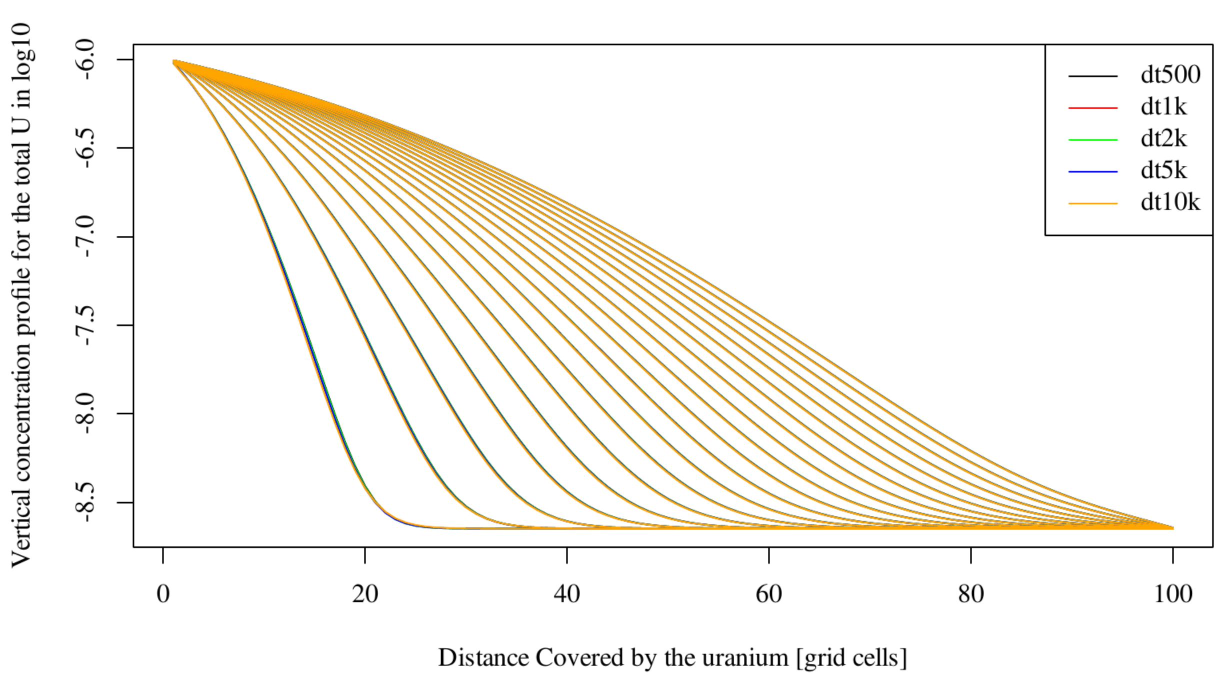

Figure4/3. Sum of the vertical concentration profiles for U(4), U(5), and U(6) for each saved iteration. The same quantity is plotted for 5 different time steps, which are evaluated in years. The fact that no chemistry is accounted for in the simulations leads to a perfect overlapping of the profiles (convergence).

The promising result, with all the profiles overlapped, derives from not accounting for the chemistry, indeed the most impacting in terms of CPU time needed. This means that the diffusion scheme implemented in TUG is stable and precise well over the theoretical CFL condition. Unfortunately, the case of interest for the current paper is the reactive transport simulation. The same approach is followed even for the latter scenario. However, in this case the time step related to the stability condition is taken into consideration to exactly quantify the lack of convergence. Together with the one equal to 250 years, the simulations are performed with four other time steps: 5,000 years, 2,000 years, and two time steps made of a combination of different values. The first one uses a Δt of 250 years for the first 50,000 years, and a time step of 5,000 years until one million years. The second one combines five different values, between 250 years and 5,000 years. The use of this kind of time step, which covers the whole simulating period being subdivided in a series of ascending time steps, aims to show a compromise, in terms of discrepancies, between simulations with large single values for the time step and the one related to the stability condition (highly time consuming). As expected, looking at the same plot as the one for the previous case, there is no complete convergence of the results. Indeed, simulations involving the chemistry display discrepancies due to time discretization, in particular during the first iterations. Nevertheless, the focus of the scoping analysis is to obtain the best convergence for the iteration related to a time period of 1 Ma. Despite this, looking at the trend for different iterations is interesting. Once all the concentration profiles related to each saved iteration are plotted, the presence of large discrepancies does not allow a clear visual representation. Accordingly, the concentration profiles related to just three iterations are reported inside *Figure5/3*. Namely, the three iterations correspond to 50,000 years, 500,000 years, and 1 Ma. However, the aim is not just a qualitative analysis, but a quantitative one. Accordingly, the absolute differences in terms of covered distance (in meters), with respect to the results obtained with the Δt set by CFL equal to 1, are evaluated for each time step, and regarding two different concentrations along the vertical profile. The two selected concentrations are $10^{-6.8}$ molal and 10^{-8} molal *[Figure6/3]*. A plot showing the trade-off between the accuracy (difference from the results related to the ones obtained applying the stability condition) and the computing time which is expected to be proportional to the number of iterations. Via *Figure7/3* it is possible to evaluate the optimal time step for the future simulations. On the left side of the plot both the trends from the two concentrations, which are related to the first iteration, show a decrease in the distance moving from higher values of time step to smaller one. Each one of the "multi-time steps" is characterized by a first step of 250 years, resulting in same outputs as for the stability condition.

Regarding the first iteration, the trend of the absolute difference is in accordance with what was expected. Beside this, the iteration that is considered more relevant for what concerns the convergence of results is the last one. For a concentration of $10^{-6.8}$ molal the values of the distance are still inversely proportional to the number of iterations. This is not reproduced for a concentration of 10^{-8} molal. In this case, the combination of a time step of 250 years and 5,000 years results in an even bigger distance than the single time step equal to 5,000 years. The most relevant result is a rather small difference, which is around 0.25 meters, for a time step equal to 2,000 years (yellow diamond). Looking at the previous plot it is possible to evaluate that, the distance covered by a concentration of uranium of 10^{-8} molal after one million years falls in the interval between 18 and 22 meters. The use of a time step of 2,000 years implies a simulation characterized by 500 iterations, resulting in one eighth of the ones related to the stability condition. Under the hypothesis of a linear correlation between the number of iterations and the time cost for one simulation, the choice of 2,000 years time step would allow to save 87.5% of the time. Accordingly to this analysis, the presence of a systematic error, in the range of 0.3 and 0.25 meters, is considered feasible.

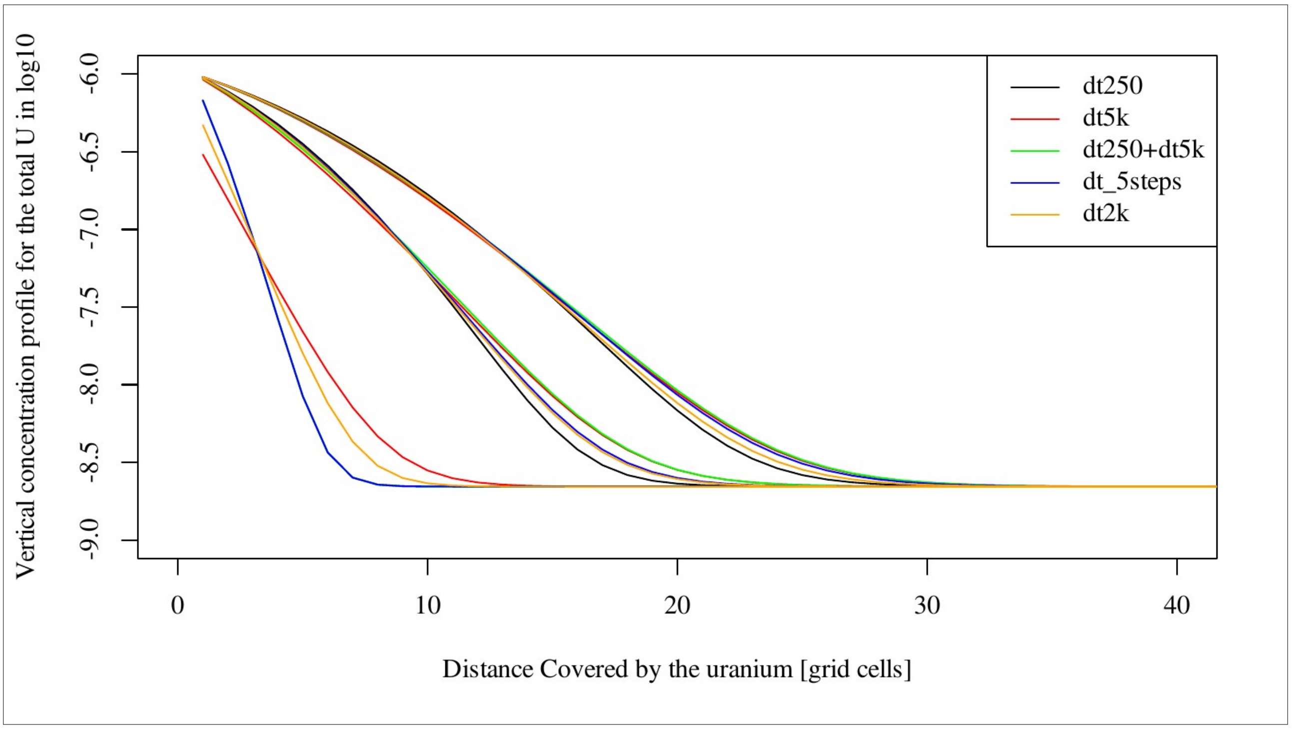

Figure5/3. The vertical concentration profiles of the total uranium for the first, the last and the iteration in the middle are plotted once simulating with 5 different time step, and accounting for the chemical process in each case. Moving towards the last iteration (longer simulating time) the discrepancies between the trends decrease.

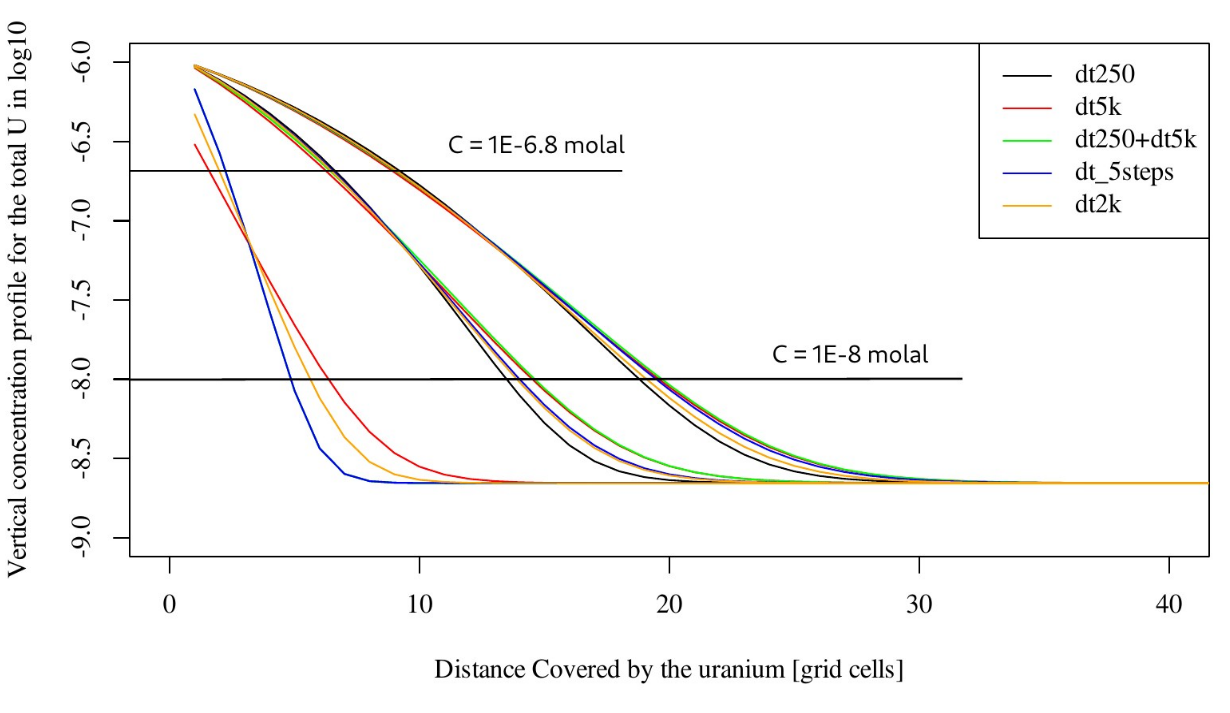

Figure6/3. Regarding the quantification of the discrepancies between the vertical concentration profiles, the two concentrations of interest are indicated.

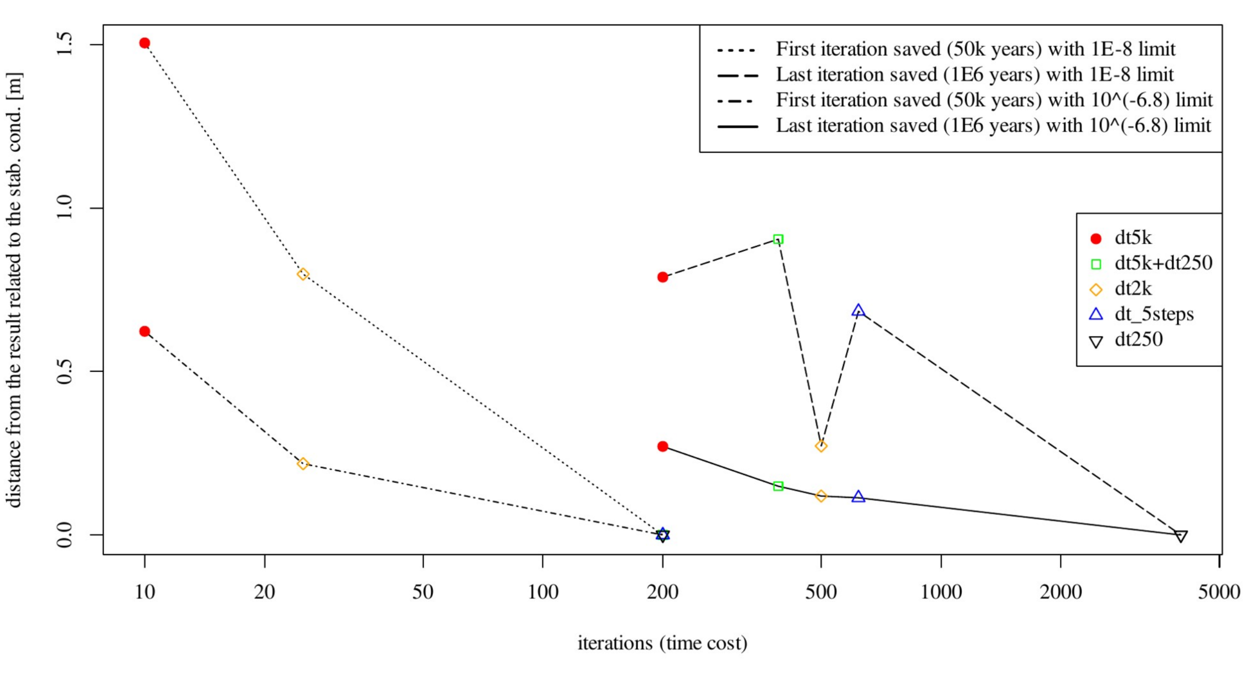

Figure7/3. For two different values of the aqueous concentration of the total U, the differences between the distance covered accounting for a time step of 250 y, which is evaluated via the stability condition, and the ones related to the other time step are plotted. The approach is applied for the first and the last iteration (left and right side of the plot). Focusing on the last iteration, for an aqueous concentration of 10^{-8} molal, a time step of 2000 y shows the best result (yellow diamond).

As previously mentioned, the simulated diffusion of uranium in one million years covers more or less 20 meters. More accurate evaluations are shown in the following chapters. Accordingly, the use of 100x100 meters is considered exaggerated. A new simulating approach based on a 50x50 meters grid, still discretized in a 100x100 cells grid, is considered more suitable. However, modifying the dimensions of the grid results in the variation of the maximum time step applicable. Indeed, the stability condition is proportional to the square of the grid element size. The consequence of reducing the real dimension of the grid is a reduction in the maximum allowable time step. Following the Courant-Friedrichs-Lewi law the new value is 50 years. The previous trade-off analysis may be compromised from the new consideration. Therefore, to prove that the results achieved for the former stability condition can be considered valid, the plot regarding the vertical concentration profiles for the new maximum time step and the previous one is built. Showing small discrepancies even for very short time periods – between 25,000 years and 200,000 – would allow to predict a rather suitable convergence of the results for larger time periods and, as a consequence, to consider the previous analysis reliable. *Figure8/3* presents the vertical concentration profiles with almost negligible discrepancies for the last iteration, which corresponds to a simulating period of 200,000 years. As a consequence, the previous scoping analysis, performed starting from a time step a CFL time step of 250 years, is considered valid even for all the following simulations working on a 50x50 meters grid.

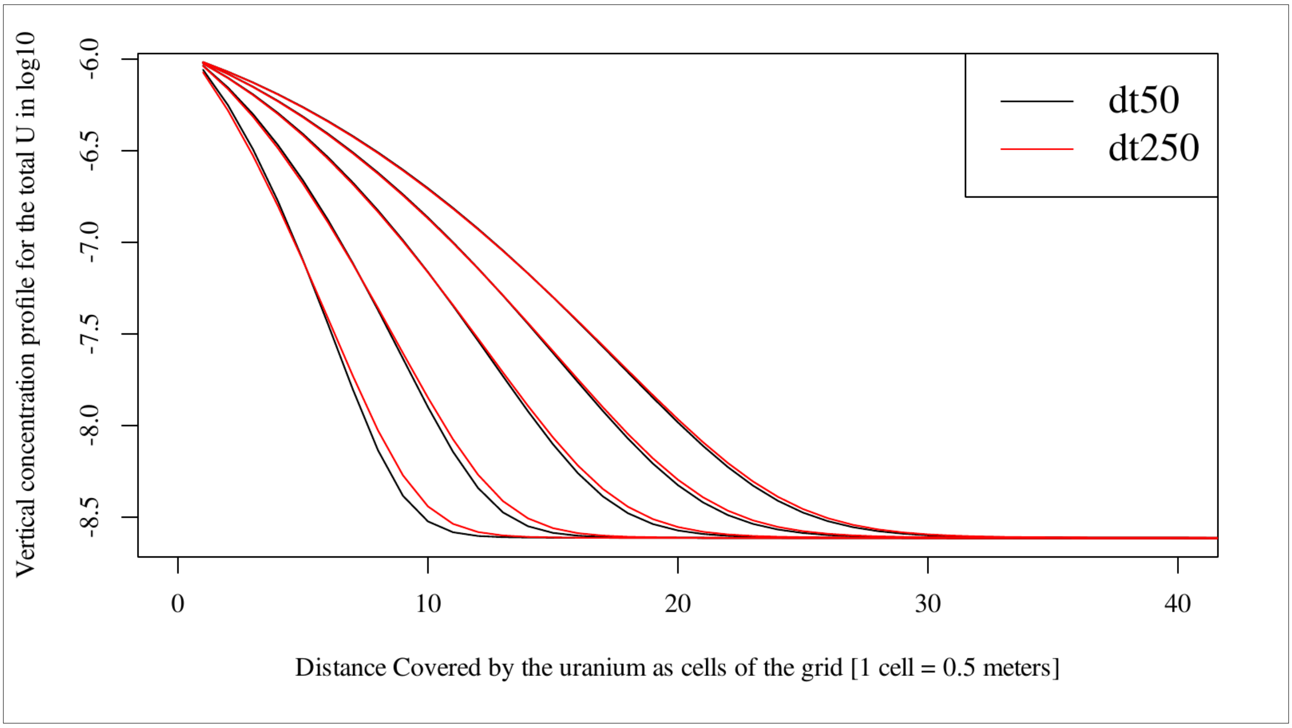

Figure8/3. Vertical concentration profiles related to a time step of 50 years (black line) and 250 years (red line). The first time step is retrieved from the stability condition accounting for a 50x50 meters model. The second one is related to a 100x100 meters model.

4 Facies-dependent Porosity

The evaluation of porosity for clays and argillaceous rocks requires accurate measurements due to the geological structure of the matrix, which leads to the classification of four different types of water contained inside the clay:

- interlayer water that is located between the sheet structures
- strongly adsorbed water at the clay mineral surfaces
- loosely-held water in the diffusive layer
- free water.

It can be derived that the quantity of water located inside the clay is highly dependent on the mineralogical, and consequently geochemical, conditions of the clay itself.

The Opalinus Clay comprises three different main litho-facies, which are not homogeneously spread inside the clay system. The most abundant is the shaly facies, which accounts for 60% of the volume. The sandy facies covers 35% of the matrix, while a less relevant facies (5%) is the carbonate-rich sandy facies [2].

Each facies is characterized by different proportions of rock-forming minerals, leading to a classification in five subfacies which, however, are not further investigated in this work [8].

The studies at the Mont Terri laboratory revealed that the formation is divided into five layers constituted by the repetition of the three litho-facies. Moving from the bottom of the formation to the top, it is possible to distinguish a shaly facies consisting of mica-bearing calcareous claystones with lenses or with mm-thick layers of quartz in the silt fraction, a sharp transition to a thin carbonate-rich sandy facies, characterized by quartz-bearing calcareous biodetritic layers of up to 10 cm thickness, a sandy facies with calcareous silty claystones, which is then overlain by a dark grey mica-bearing and slightly silty claystone attributed to the shaly facies. Finally, the uppermost unit of the Opalinus Clay consists again of a sandy facies, a light gray silty claystone with laminated silt lenses, and lenses of bioclastic material [7].

Several experiments have been carried out regarding the evaluation of porosity inside the different facies. One of the newest papers, following the results that were previously obtained, shows how the porosity increases as the clay minerals content increases. In particular, the trend follows a concave curve. Going through a simplified explanation of the phenomenon, the porosity of the shaly facies is determined by two main factors: an interlayer porosity between clay aggregates, and one related to the geometric incompatibilities between plat (clay) and granular (carbonate) minerals. The first one is directly proportional to the clay mineral content, while the second one depends on the presence of carbonate minerals in the clay matrix, which have a major role at the time of deposition, leading to the higher porosities with respect to sand minerals [18].

All these considerations result in different ranges of porosity for the facies. For the purposes of the current work the porosity, for clay rich layers, is assumed to be 10-25%. On the other hand, sand layers have a porosity of 6-14%. Regarding the carbonate-rich layer, the literature presents different results. Houben et al. [19] reports that the porosity for carbonate-rich layers is the same for sand layers, while others [4] show values which are closer to the values of the shaly facies. For the purpose of the thesis, the porosity of the carbonate-rich facies is considered equal to the one of the sandy facies.

5 Spatial variability in the context of the Opalinus Clay

5.1 Basics of geostatistics

The petrophysical and the mineralogical properties of a formation change moving from one point to another. Geostatistics is the branch of statistics dealing with spatial variability of regionalized variables in terms of distance-dependent self-correlation of these variables.. Regarding the same property, the fact that a value sampled at a certain location is intuitively expected to be more similar to the ones sampled close to its location rather than far away samples, is the fundamental assumption. The modeling of the spatial variability results in the definition of a distance threshold, beyond which the variability of the property is independent from available samples.

Once the value of the property and the location of the samples are retrieved, the most common method to quantify the spatial variability is the variogram function. It is one of the autocorrelation functions, together, for instance, with the geostatistical covariance. However, the second one presents some challenges and it is considered less practical. Generally speaking, the variogram is a monotonically increasing function of the distance. In partcular, it can be considered a model, which a Random Function is assumed to follow, or it can be a function intrinsic to the variable. In the second case, the purpose is to evaluate the experimental variogram based on the available samples. Accordingly to the second definition, this statistic expresses the change in variance of the property as a function of the distance between the samples (also called lag), and is defined as the sum of the squared differences of two samples $Z(x_i)$ at distance h divided by twice the number of couples of samples separated by that distance N(h) over the whole domain:

$$\gamma(\vec{h}) = \frac{1}{2N(\vec{h})} \sum_{i=\vec{0}}^{N(\vec{h})} [Z(x_i) - Z(x_i + \vec{h})]^2$$

Once the semivariance-distance plot is created, the objective is to find which of the standardized models (equations) fit the values best. The most important models are horizontal, linear, spherical, exponential, and Gaussian *[Figure1/5]*.

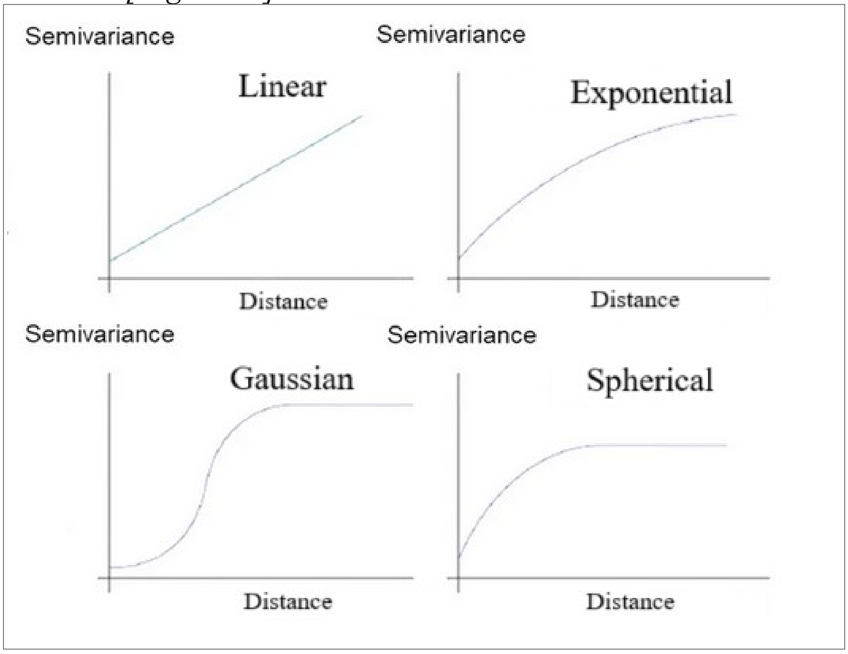

Figure1/5. Graphical representation of the 4 most important models for the variogram function. Modified image from Cai et al. [20].

To evaluate the best model, the operator works on a series of parameters, available for each model, that can be modified in order to slightly reshape or shift the model to fit the majority of the realizations (sampled values). It is very common for geostatistical studies not to find a model that perfectly represents all the values, so the priority is to fit the first values (values closer to the origin). In these terms, a reliable evaluation of the spatial variability for small distances is guaranteed. The main parameters defining all variogram models are the nugget effect, the range, and the sill *[Figure2/5]*.

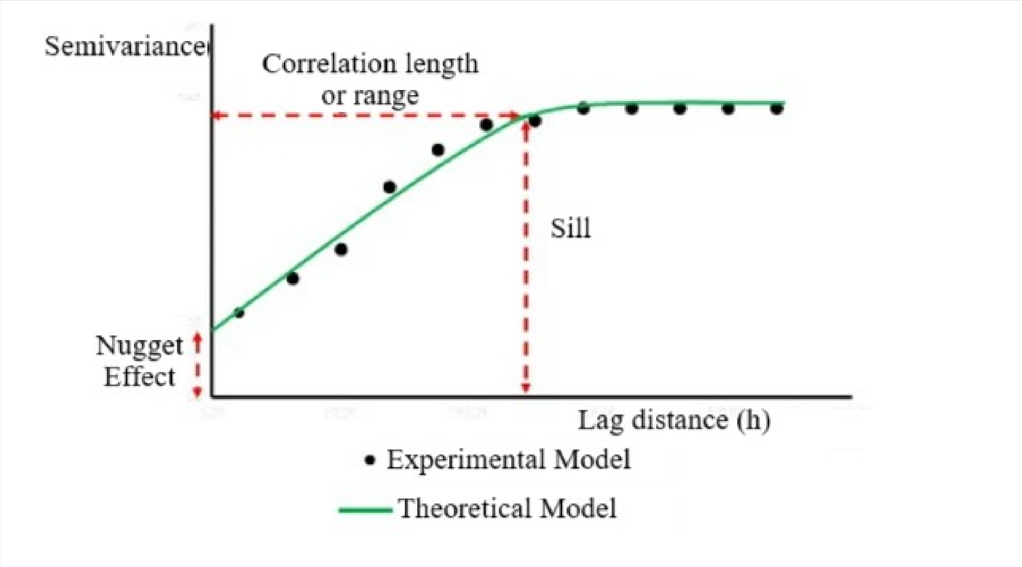

Figure2/5. Graphical representation of the main variogram parameters: the sill, the range, and the nugget effect. Modified image from Rocha et al. [21].

The nugget effect, which is the intercept on the y-axis, quantifies the background noise that affects the measures. The noise can be associated to the spatial variations that occur at smaller distances than the lag. The sill is the magnitude of maximum variance, while the range quantifies the distance beyond which there is no more spatial correlation between the values but there is random variability [22].

The distance h in the variogram definition is actually a vector. Accordingly, the correlation distance is dependent on the direction. Lot of of soil properties present anisotropic behaviors, which means different models for different directions, or only for some directions a proper model can be retrieved. Introducing the concept of anisotropic variograms, two other parameters must be taken into consideration: the ratio, and the angle. The former one represents the ratio between the range along the direction of maximum variability, defined by the angle between the x axis and its direction, and the range of the variogram in the orthogonal direction, which is that of minimum variability. For a condition of isotropy, the value of the ratio of the variogram is equal to 1 because the value of the range is equal along each direction.

The usual value pointed as the sill is the variance of the population of the realizations. However, the presence of a trend in the sample causes the lack of the sill in the semivariance plot, as for the linear model.

Once the experimental variogram is defined, it can be used for the spatial prediction of unsampled locations, namely estimation, or it can be used for simulation.

Regarding the first approach, kriging is the group of techniques enabling the estimation of unknown values using the experimental variogram model as an input parameter. Kriging is a BLUE (Best Linear Unbiased Estimator): it is a linear interpolation method which estimates the variable at unknown locations by means of weighted average of the surrounding known data. The standard method is the ordinary kriging which evaluates an unknown sample assigning the weights to the surrounding realizations based on the spatial correlation specified by the variogram. The two assumptions under the use of ordinary kriging are the stationarity of the mean of the values and of the variogram function. The former signifies that the mean is constant among the whole dataset, and it does not depend on the location of the samples. The latter states that the variogram function exists, and it is only dependent on the separation distance, not on the starting location.

There are other types of kriging, such as universal, or block kriging, which differ from the standard one for the estimating method or for the different starting conditions and hypotheses. For example, the universal kriging can be applied when the variable has unknown mean or has no stationary mean, which has to be systematic and that can be quantified through an iterative approach. For the block kriging the same stationarity conditions have to be guaranteed, but the estimates are made in cells rather than points [22].

The current paper focuses on the second approach which exploits the variogram for simulating. The extrapolated variogram model is used to investigate the behavior of a real case scenario when different inputs are considered. The simulating phase is characterized by two different approaches: conditional and unconditional simulations. The first approach relies on the interpolation of the available data as a starting point for the simulations. The unconditional simulations do not interpolate the samples, but they are constrained to the mean, the variance, and the variogram of the data. The second approach is the one used for the purpose of the current paper. Generally speaking, the usual simulating procedure consists of generating unconditional simulations, and performing the kriging (using the same variogram) on the residuals; namely, the difference between the simulated values and the sampled values. Subtracting the results of the kriging (residuals) to the unconditional simulations, it results in conditional simulations.

5.2 Spectral method as geostatistical simulation approach

An effective approach to the spatial variability to one of the petrophysical properties of the host rock is built. The approach is based on the use of spectral simulation, method which is implemented inside an R package (SpecSim) developed by dr. Marco De Lucia.

The advantage related to the use of spectral method is that it allows to filter out the effect of randomness when comparing different cases. In particular, it is possible to draw different series of random numbers, and any variogram model can be "projected" using those series. Accordingly, the choice of different parameters for the variogram (range, angle, ratio) is the only influencing factor for the results, due to the repetitive use of the same random numbers. The "SpecSim" R package implements the described spectral method by using as inputs the different series of random values, and the paramters of the variogram. The outputs of the simulation are normal distributed values which, evaluated onto a grid, represent a possible realization of spatial variability based on the input variogram parameters. For technical reasons related to the implementation, the geostatistical simulation can be performed only on grids which have a number of cells for each side which is equal to 2 to the power of n, with n a natural number.

$$\forall n=1,2,3,\ldots \quad 2^n \times 2^n \, cells$$

However, all the simulations performed on POET work with a grid of 100x100 cells. The output grid obtained from by the spectral method is cropped to retrieve the new grid of interest. In particular, for all the cases of interest, a grid of 100x100 cells is obtained cutting a grid of 128x128 cells starting from the top left corner.

As previously mentioned, the goal of the method is to apply the concept of spatial variability to the diffusion coefficient, input parameter for the reactive transport simulation. We chose to simulate spatially variable porosity and derive an effective diffusion coefficient from the simulated porosity. In order to follow this approach, the standard distributed values are rescaled to match the porosity range of each facies. A simple linear transformation:

$$y=a\cdot x+b$$

with a and *b* extrapolated parameters, is performed to obtained a shifted and rescaled normal distribution *[Table1/5]* [S6].

Facies	Range of porosity (%)	a	b
Shaly	10-25	0.02	0.175
Sandy	6-14	0.011	0.1
Carbonate-rich	6-14	0.011	0.1

Table1/5. Porosity and the two parameters for the linear transformation for each facies.

The assumption of working with porosity values which are characterized by a normal distribution values is partially confirmed by the studies of Yven et al. [23] in the context of the mineralogical evaluation of the Callovo Oxfordian formation (France), which can be considered similar to the Opalinus Clay in terms of petrophysical properties *[Figure3/5]*.

In the context of Opalinus Clay (Mont Terri), U(VI) is much more abundant than the other species of uranium U(V) and U(IV). The consequence is the choice of the effective diffusion coefficient related to the U(VI) as parameter of reference; it is a known value as the exact D_e used by Hennig et al. [4] is taken into consideration (D_e = 1.9E-12 m^2/s). The transport sub-model (TUG) in POET requires as input the pore water diffusion coefficient. To simulate the spatial variability of the diffusion coefficient, the pore water diffusion coefficient is obtained as the ratio between the D_e of U(VI) and the rescaled spatially distributed values of the porosity.

$$D_f = \frac{D_e}{\omega}$$

It is important to mention that porosity ω is always considered constant in POET, which means that technically the only property which can be considered heterogeneous (meaning, affected by spatial variability) is the tortuosity.

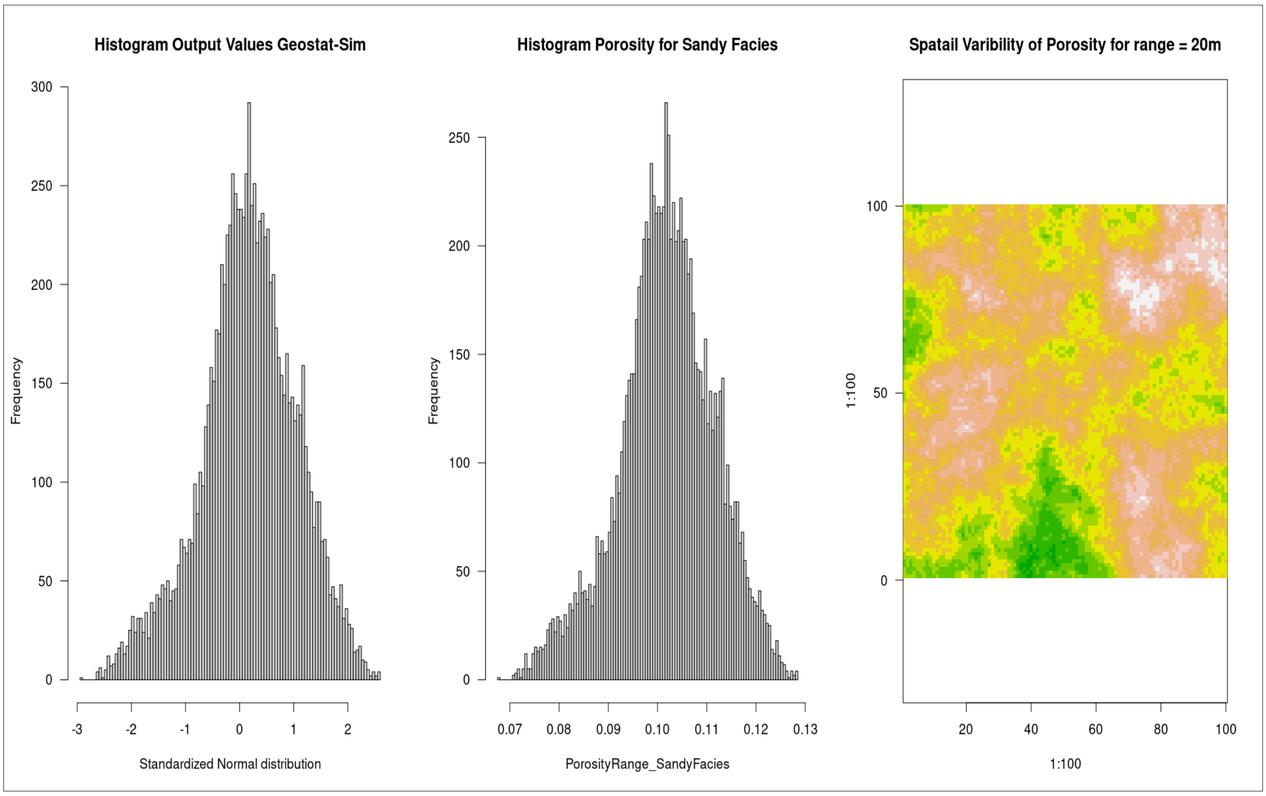

Figure3/5. Visual representation of the workflow for the implementation of the spatial variability inside the porosity. The histogram on the left presents the normal distributed output values from the geostatistical simulation. The second histogram shows the new value once they are scaled inside the porosity range. The last image shows a graphical representation of the heterogeneity of porosity for a variogram range of 20 meters.

5.3 Investigated cases

As previously explained, the simulating approach for a complete evaluation of the Opalinus Clay as suitable host rock applying the concept of spatial variability of the petrophysical properties is subdivided into different steps.

First of all, for each one of the three facies, the diffusion of the all uranium is simulated on a 50x50 meters grid. The investigating workflow, related to the geostatistical simulations, is structured as follows. Ten different series of random values are drawn, and the same values are used for each of the following cases. There are two main cases: the first one accounts for an isotropic variogram, and the second one for an anisotropic variogram. Regarding the condition of isotropy, three different values of the range – 5, 10, and 20 meters – are considered. The results are 10 ".rds" files, accordingly to the series of random values, for each of the ranges of interest (30 files in total). Inside each ".rds" file there is a vector reporting the simulated diffusion coefficient *[Figure4/5]*. Concerning the anisotropy condition, the range of the variogram is dependent on the direction, and the ratio quantifies the relationship between the two ranges. The input range, which is the one related to the indicated direction, is kept constant, and it is equal to 20 meters. Two different directions are considered. The first one takes into account an angle of the variogram equal to 0˚ (horizontal direction), while the second one an angle of 90˚ (vertical direction). Regarding both the angles, the values of interest for the ratio are 4, and 10. Namely, the range for the indicated direction is four and ten times longer than the one related to the perpendicular direction. From a graphical point of view, modifying the value of the angle, as a consequence of a ratio not equal to 1, means to create a pattern of horizontal (angle = 0°) *[Figure5/5]* or vertical (angle = 90°) *[Figure6/5]* stripes related to spatial variation of the petrophysical property. Regarding the first value for the angle, the resulting stratification is orthogonal to the main diffusion direction, while for the second it is parallel. At the end, the results are 40 ".rds" files related to the anisotropy condition.

The influence of the spatial variability is assessed for two different boundary conditions. The first one (SCENARIO1) is defined imposing an uranium-rich solution (10^{-6} molal) on the whole upper boundary of the domain. The rest of the grid has a background solution containing around 10^{-9} molal of U. The second scenario (SCENARIO2) mimics a "punctual" source of uranium, and in the models the 50th and 51st cells of the upper boundary are set with 10^{-6} molal U, resulting in a radial diffusion front. Moreover, it was specified, both in the lithological description (Chapter 1.2) and in the chapter related to previous results (Chapter 1.7), that the presence of two aquifers embedding the Opalinus Clay has caused the formation of geochemical gradients. A more suitable investigation of the influence of spatial variability for each formation requires to take into account those geochemical gradients in the simulations, as even for the homogeneous case it resulted in a longer propagation of uranium. The last step would be to create a simulation grid representative of the actual geometry and facies distribution of Opalinus Clay at Mont Terri. In the graphical representation of each case, the uranium profile related to the homogeneous case (constant value of the diffusion coefficient in the model) is reported, enabling a more precise comparison with the results obtained by Hennig et al. [4].

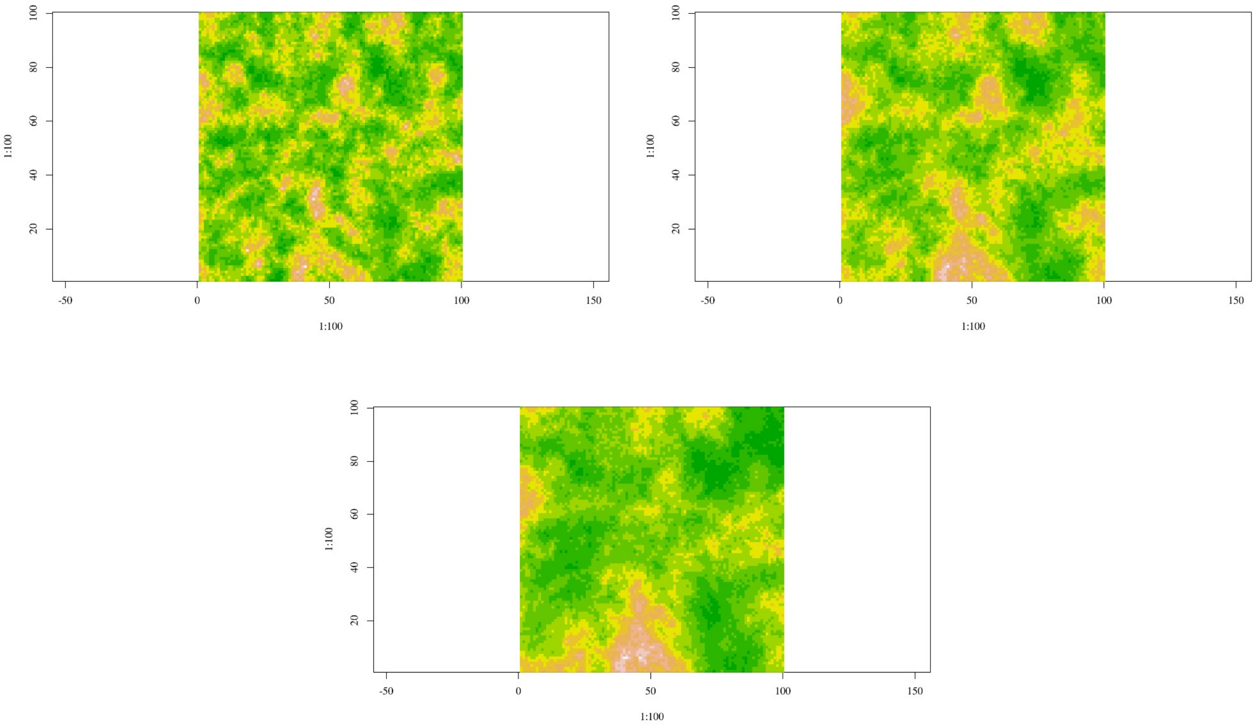

Figure4/5. Visual representation of the change in the diffusion coefficient pattern, varying the range of the variogram. The image in the top-left corner represents the heterogeneity of the diffusion coefficient for a range of 5 meters. The one in the top-right corner for a range of 10 meter. The last one for a range of 20 meters.

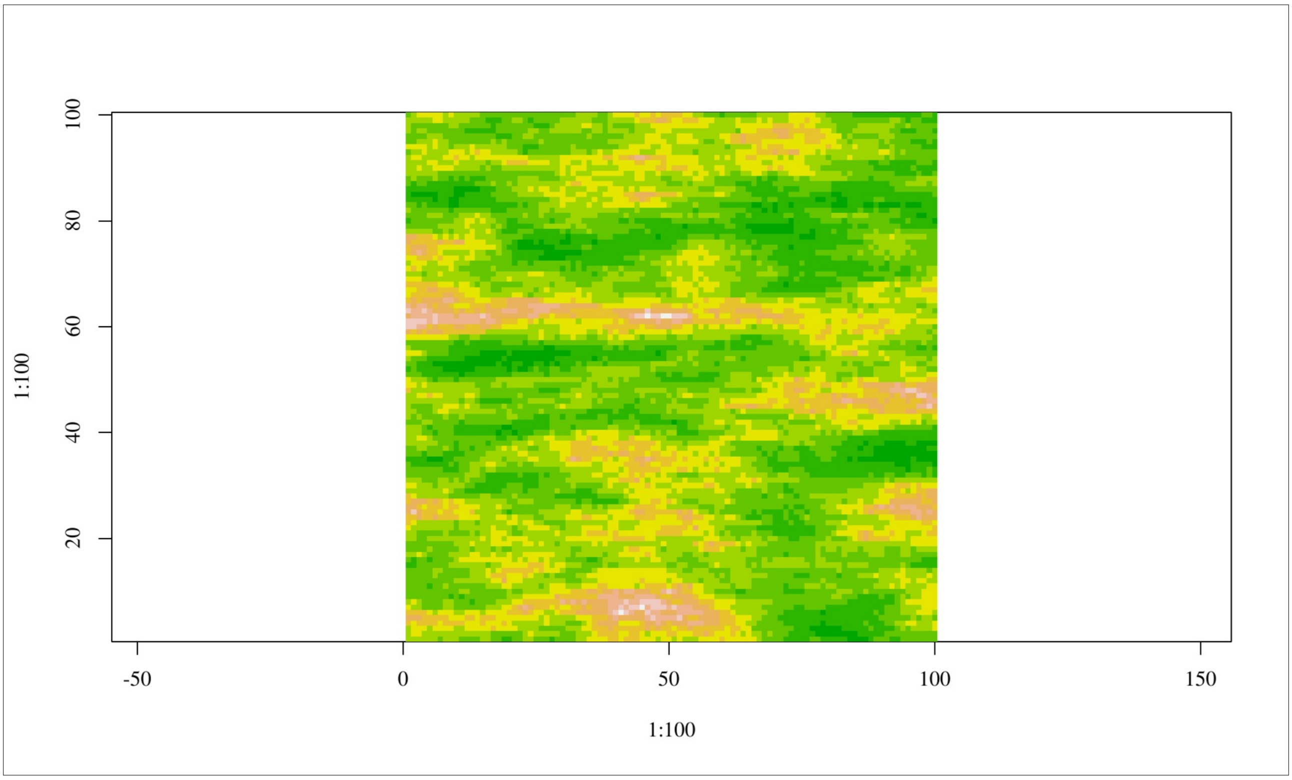

Figure5/5. Visual representation of the heterogeneity of the diffusion coefficient for the anisotropic case, where the variogram range related to the horizontal direction is 4 times the one on the vertical direction.

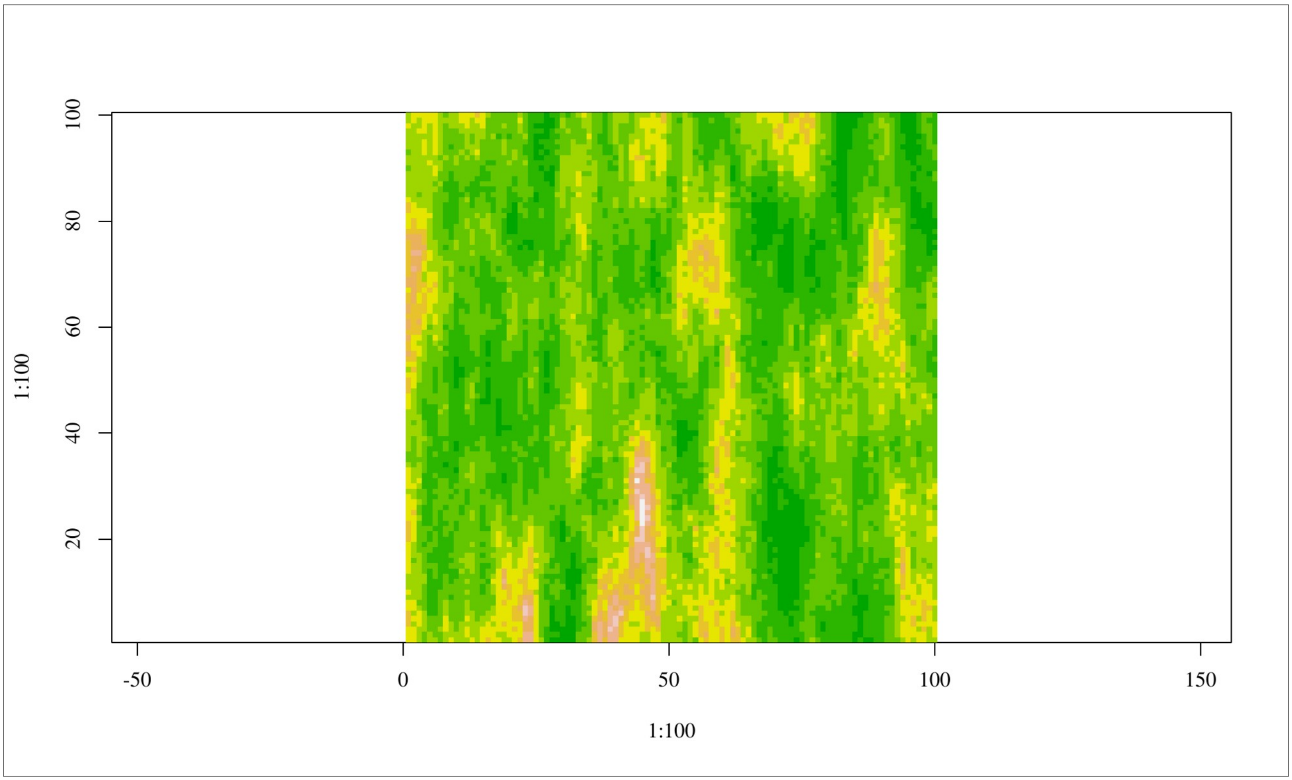

Figure6/5. Visual representation of the heterogeneity of the diffusion coefficient for the anisotropic case, where the variogram range related to the vertical direction is 4 times the one on the horizontal direction.

6 Scenario1

The first investigated scenario for each different facies sets constant boundary condition on the whole upper boundary of the 2D domain with an high aqueous concentration of uranium and otherwise the same concentrations as in the whole domain. The result is a mainly vertical migration of the uranium via diffusion. The initial conditions and the actual boundaries are adapted to reflect representative models of each facies, as is the parametrization of chemistry clay fractions for surface complexation and cation exchange capacity for cationic exchange). The homogeneous scenario where the diffusion coefficient is a constant value results in concentration profile which covers the same distance for each column of the grid, being as expected a pseudo 1D scenario. It is important to note that the diffusion coefficient for the homogeneous case has been calculated dividing the effective diffusion coefficient of uranium by the mean porosity value related to the facies of interest. This choice exploits the assumption that the distribution of the porosity within each facies is Gaussian. The effects of the spatial variability are quantified by grouping the simulations related by geostatistical range together with the corresponding homogeneous scenario, whereby only the last iteration of each simulation is retained in the following statistical analysis, after 1 million years. The following plots represent a graphical representation of the results. The isotropic and anisotropic cases are investigated for each facies.

6.1 Elaboration of the results via R software for Scenario1

The approach for the evaluation of the covered distance begins by selecting which concentration of uranium to consider as threshold discriminating the arrival time of the “injected” uranium. In the case of the sandy facies, the exact background concentration for uranium is $2.481 \cdot 10^{-9}$ molal. Since the boundary concentration is set to 10^{-6} molal, it is decided that the threshold value to quantify the distance covered is 10^{-8} molal. The choice of a threshold concentration which is an order of magnitude bigger than the background one may have an influence on the evaluation of effects of the spatial variability. Accordingly, a lower threshold values would have led to the measurement of longer distances. Nevertheless, since the same threshold concentration is investigated for each value of the variogram range, I suppose that the influence of the spatial variability on the covered length would not change.

The POET output consists of the concentration values of the all involved species at the cell centre of each cell of the 100x100 cells grid. A contouring operation is hereby performed, in order to find the y coordinate at which the threshold is exceeded for each column of the uniform grid. This method was implemented in R. First, each column of the grid is scanned to retrieve the first cell whose U concentration lies under the threshold and the one immediately above; an interpolation by inverse distance weighting is performed to find the y coordinate at which the U concentration is equal to 10^{-8} molal. The weights are chosen as the inverse of the absolute difference between the value related to the selected cell and the threshold, and the absolute difference between the value related to *ind-1* (last value higher than the threshold) and the threshold.

This evaluation returns the actual distance from the upper boundary of the profile of U concentration equal to the threshold. The hence obtained set of profiles for a specific geostatistical parametrization are then is the basis of statistical evaluation. First of all, the profile related to the mean value of the distance is calculated, followed by the interval of confidence related to a probability of 95%. The interval of confidence is evaluated summing and subtracting the mean distance for the standard deviation multiplied by the value 1.96, which represents the interval of confidence of 95% for a normal distribution. Then, the maximum distance covered is evaluated. Herein an example of the graphical representation of the statistical analysis is provided. In particular, *Figure1/6* shows the results of applying spatial variability to the pore diffusion coefficient for a non-reactive transport model (pure diffusion model without chemistry involved).

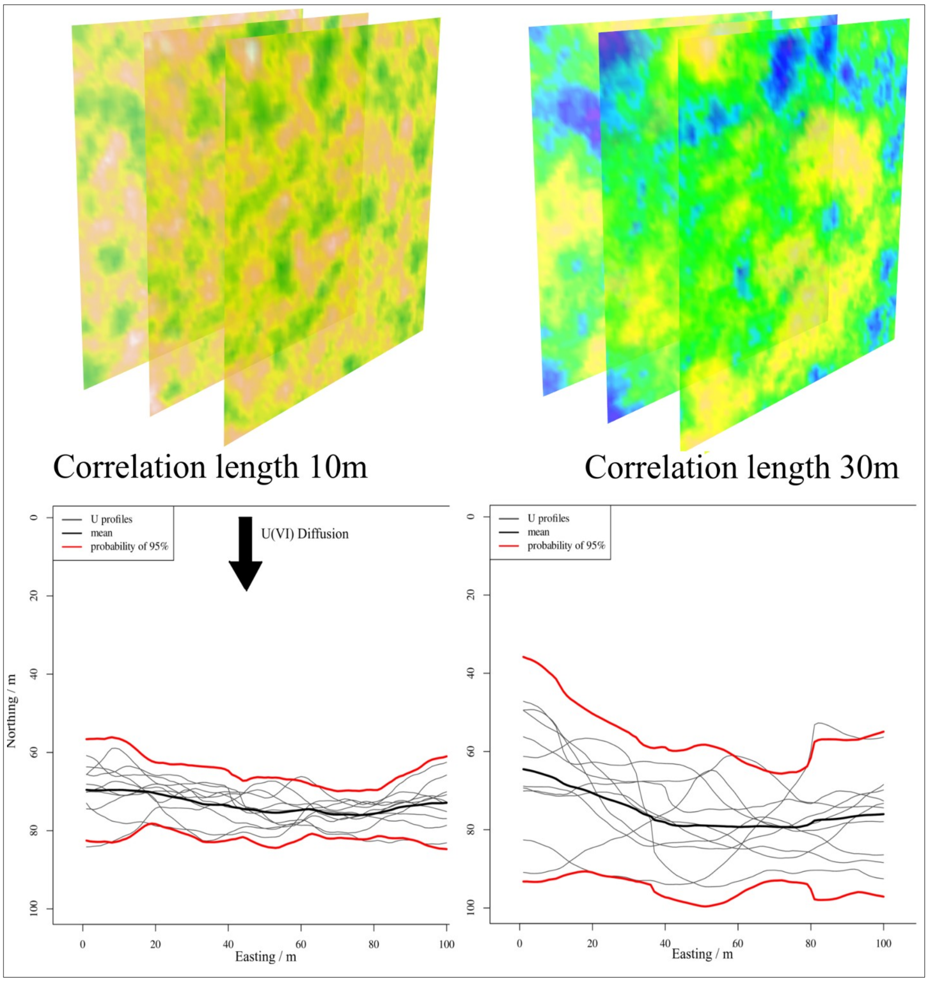

Figure1/6. Application of the method for elaborating the results related to SCENARIO1. The gray lines are the uranium concentration profiles. The two red line corresponds to a probability interval of 95%, while the black line represents the averaged covered distance. The presented concentration profiles of U come from a series of simulations accounting for two different ranges of the variogram, but without accounting for any chemical process that takes place inside the Opalinus Clay. As a result, the difference in the covered length between simulations coming from different random variable can be easily appreciated.

6.2 Sandy Facies

As mentioned before, the porosity range assumed for the sandy facies is between 6% and 14%. Following the assumption of normal distributed values, the porosity assigned to the homogeneous case is 10%. This results in a pore water diffusion coefficient of $1.9 \cdot 10^{-11}$ m^2/s for the homogeneous scenario. *Figure3/6* shows the graphical representation of the length covered by the uranium concentration profiles for the three selected ranges of the variogram. Each plot reports the average and maximum covered distances. The values related to the mean length are very similar, and this is expected since varying the range should not have an influence on the average value. Differently, performing the same simulations with an increasing value of the range should result in a wider span of covered lengths. Despite the relevant buffering effect caused by the host rock minerals, varying the geostatistical parameters the maximum covered distance changes among the three cases. A gradual spreading of the concentration profiles is observed for larger values of the variogram range (the standard deviation increases). Namely, the maximum length varies from 22.961 meters for range of 5 meters, to 23.659 meters for a range of 20 meters. This represents an increase of 3%. A correlation distance of 10 meters results in a maximum migration length of 23.283 meters.
Regarding the implementation of anisotropy inside the geostatistical simulations, the two maximum distances, covered by the uranium concentration profiles, for the 0° case and the 90° case are 23.363 meters and 23.08 meters, respectively *[Figure2/6]*. The results of both anisotropic simulations are practically indistinguishable, and they are deemed not significant for further investigations. No fingering is observed, once the angle is 90˚. Previous studies have demonstrated that there is a clear bedding stratification in the Opalinus Clay. In particular, some measurements about the anisotropy of the diffusion coefficient are also available. However, the presented results do not show any influence of the spatial variability on the uranium diffusion when anisotropy is accounted for.

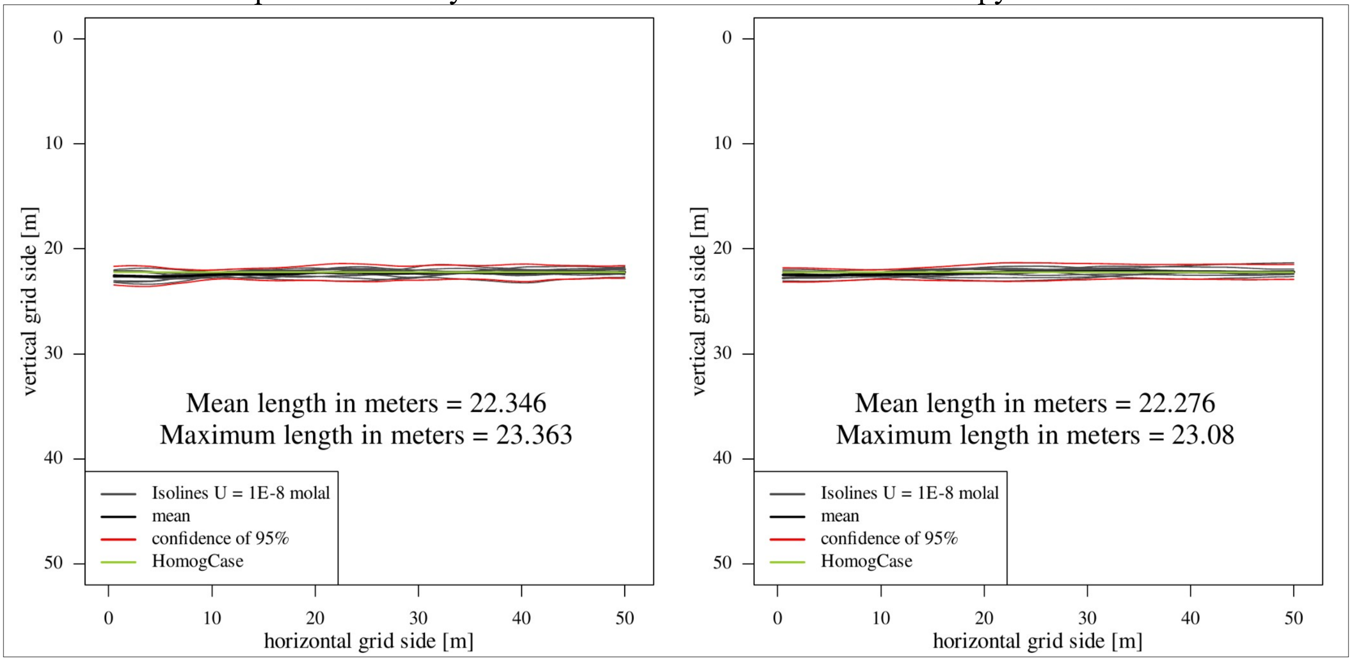

Figure2/6. Visual representation of the length covered by the concentration profiles of the total U for two different anisotropic conditions of the variogram in the sandy facies. In the plot on the left, the range of the variogram is 4 times longer along the horizontal direction than in the vertical one. In the plot on the right, the results related to the opposite case are shown.

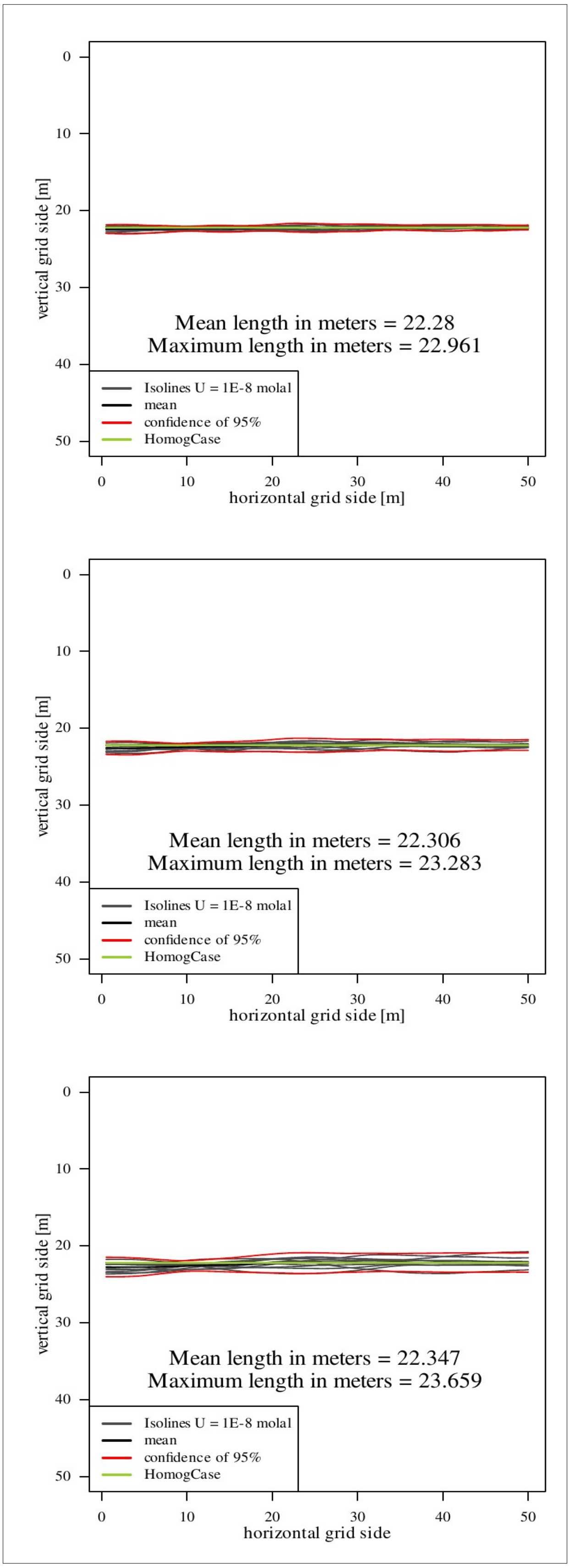

Figure3/6. Visual representation of the effect of the spatial variability on the diffusive mechanism of uranium inside the sandy facies for SCENARIO1. Inside each plot, together with the simulated profiles related to an uranium concentration of 10^{-8} molal (gray lines), the averaged covered distance (red), the probability interval of 95% (two red lines), and the profile related to the homogeneous diffusion coefficient are presented. The plot at the top is related to a variogram range of 5 meters, the second one to a range of 10 meters, and the one at the bottom to a range of 20 meters.

6.3 Carbonate-rich Facies

The range of porosity, and as a consequence the pore water diffusion coefficient, is the same of the one used for the sandy facies. The pore water chemistry does not vary with respect to the previous case, but the mineralogical content changes, and is set to representative values derived from Hennig et al. [4]. The higher content of carbonate, which qualifies the facies as calcareous sandstone, and lower clay content leads to a lesser buffering capacity by surface complexation and cation exchange. Such decreased buffering capacity should theoretically result in a longer migration of uranium. *Figure5/6* confirms the theory. The 10^{-8} molal uranium profiles, cover around 10 meters more than in the sandy facies. The effects of spatial variability are tangible even for the current case. The maximum covered length for a variogram range of 20 meters is 33.017 meters, and it is 4% longer than the one related to the minimum range of 5 meters (31.76 meters). Once again, the maximum distance obtained with a range of 10 meters is halfway, with a value of 32.275 meters. Accordingly to the previous scenario, the mean distances are very similar. Moreover, the anisotropic case shows a very comparable trend with the one presented for the sandy facies. Both the average and the maximum distances are almost equal, with slightly higher values once an angle of 0° is considered *[Figure4/6]*.

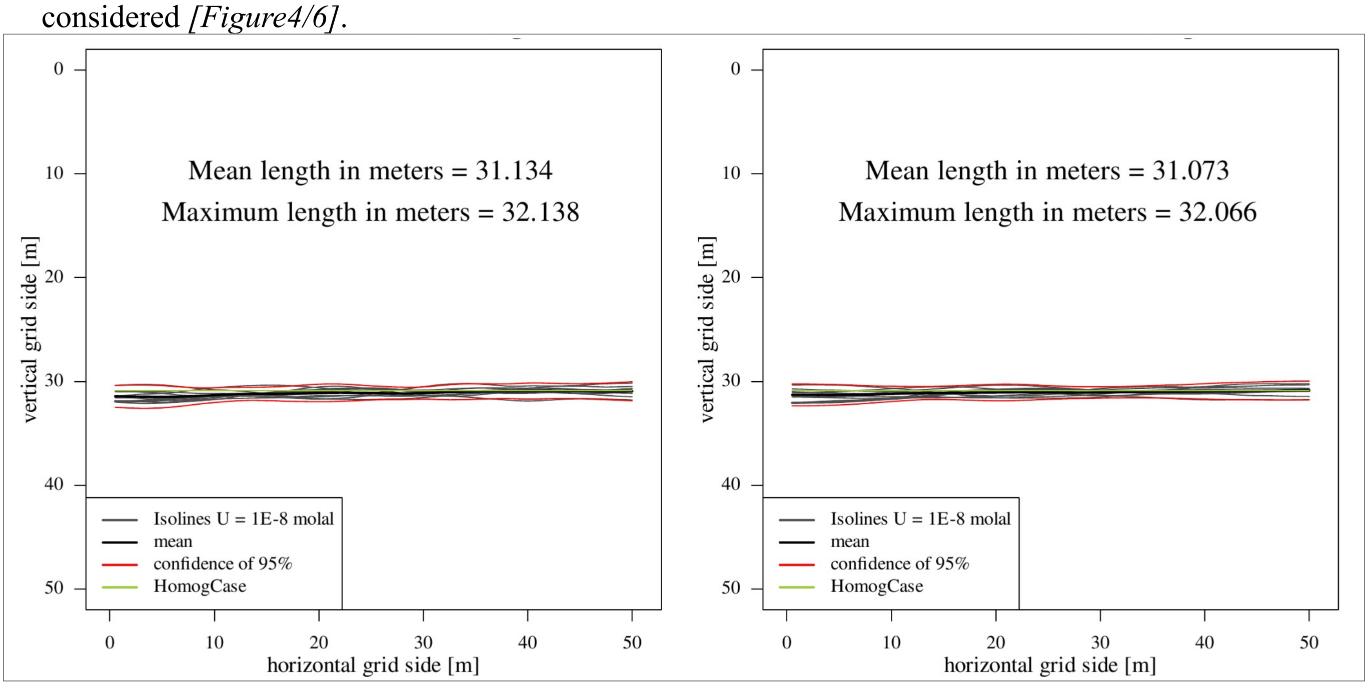

Figure4/6. Visual representation of the length covered by the concentration profiles of the total U for two different anisotropic conditions of the variogram in the carbonate-rich facies. In the plot on the left, the range of the variogram is 4 times longer along the horizontal direction than in the vertical one. In the plot on the right, the results related to the opposite case are shown.

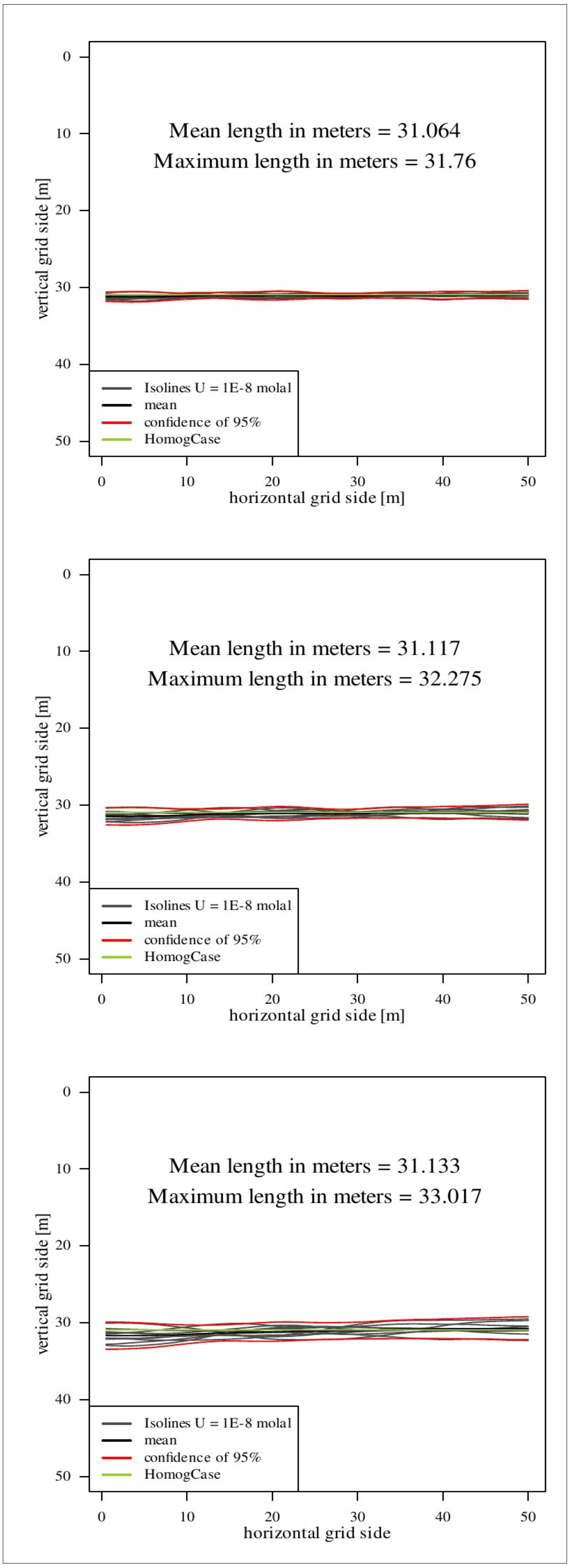

Figure5/6. Visual representation of the effect of the spatial variability on the diffusive mechanism of uranium inside the carbonate-rich facies for SCENARIO1. Inside each plot, together with the simulated profiles related to an uranium concentration of 10^{-8} *molal (gray lines), the averaged covered distance (red), the probability interval of 95% (two red lines), and the profile related to the homogeneous diffusion coefficient are presented. The plot at the top is related to a variogram range of 5 meters, the second one to a range of 10 meters, and the one at the bottom to a range of 20 meters.*

6.4 Shaly Facies

Regarding the shaly facies, the mineralogical composition, the pore water chemistry and the porosity range vary with respect of the two previous scenarios. The combination of a higher content of clay minerals and increased values of porosity results in increased buffer capacity. The results reflect this fact, with a maximum covered distance of 15.322 meters for a variogram range of 20 meters. Looking at the graphical representation of the results, the plots in *Figure7/6* show a less evident spreading of the concentration profiles moving to simulations performed with larger ranges. The effects of the spatial variability seem not as relevant as for the two previous scenarios due to the short distance covered by uranium. Graphically speaking the profiles looks less spread than in the precious cases, but a very similar trend in terms of relative difference between the maximum distances holds. The one related to a range of 20 meters is 4.2% higher than the value 14.703 meters, which is maximum distance obtained with a variogram range of 5 meters. For the simulations with range of 10 meters, the maximum distance is 14.972 meters. Once again, the average of the covered distances can be almost considered equal to the homogeneous case. The same behavior of the previous facies for the anisotropic case is observed for the shaly one *[Figure6/6]*.

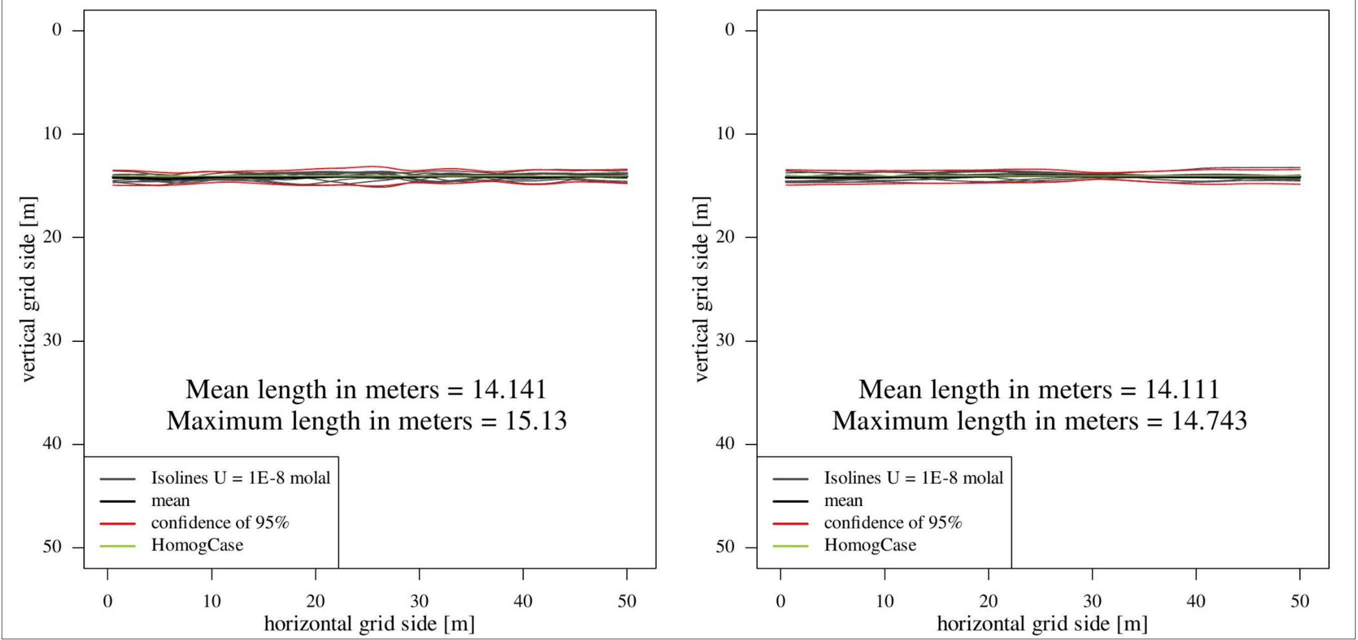

Figure6/6. Visual representation of the length covered by the concentration profiles of the total U for two different anisotropic conditions of the variogram in the shaly facies. In the plot on the left, the range of the variogram is 4 times longer along the horizontal direction than in the vertical one. In the plot on the right, the results related to the opposite case are shown.

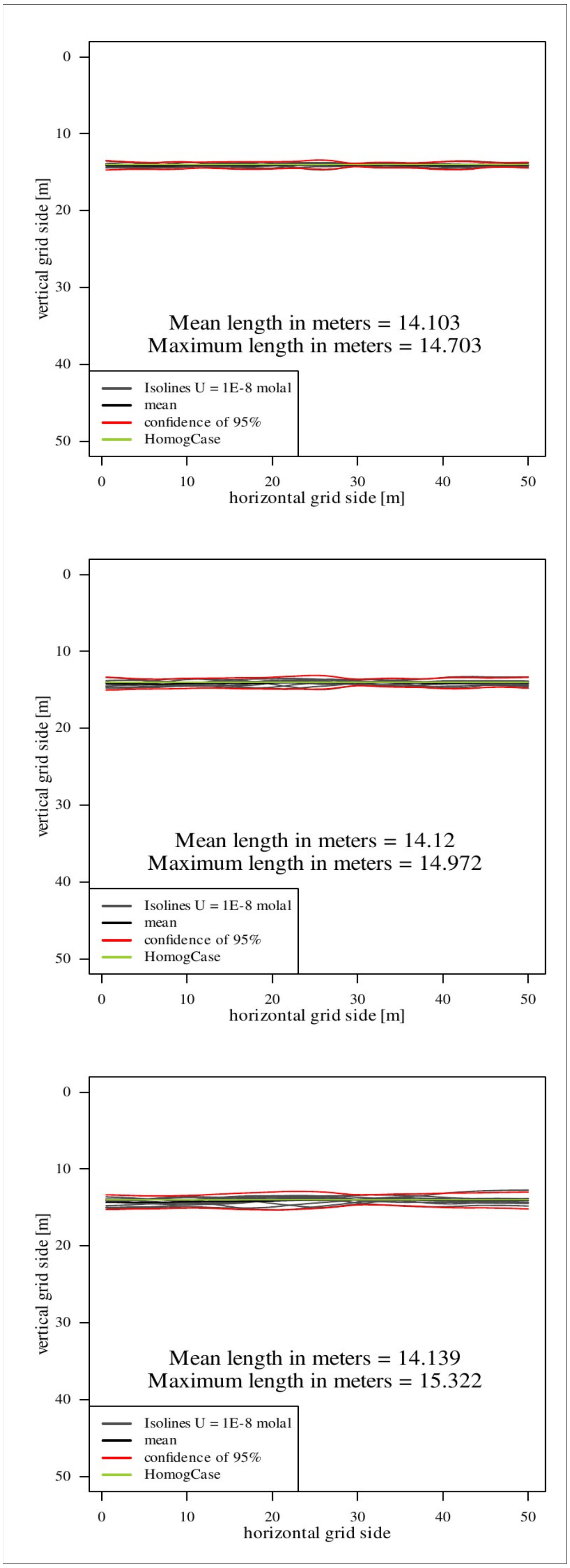

Figure7/6. Visual representation of the effect of the spatial variability on the diffusive mechanism of uranium inside the shaly facies for SCEANRIO1. Inside each plot, together with the simulated profiles related to an uranium concentration of 10^{-8} molal (gray lines), the averaged covered distance (red), the probability interval of 95% (two red lines), and the profile related to the homogeneous diffusion coefficient are presented. The plot at the top is related to a variogram range of 5 meters, the second one to a range of 10 meters, and the one at the bottom to a range of 20 meters.

7 Scenario2

When thinking about a real case scenario, the source of uranium from failing canisters is rather unlikely to be distributed along a large linear distance. While the previous hypothesis can not be excluded, the chance that a localized fail takes place is rather higher. This scenario sets the boundary conditions to have a constant source of uranium in just two cells at the top boundary of the domain, to reflect this “punctual source”. The 2D model of 50x50 meters is discretized as before into a 100x100 cells grid, and the presence of the uranium-rich solution occurs in the 50th and 51st cells of the top boundary of the grid. Everything else is equal to the Scenario 1 models. Even the approach for the selection of the pore water diffusion coefficient in the homogeneous cases does not vary. All the three different facies are investigated taking into consideration the same three ranges for the variogram. However, the anisotropic case is not considered here since no relevant effects are expected.

7.1 Elaboration of the results via R software for Scenario2

A different approach is implemented for the elaboration of the results coming from these simulations. As previously mentioned, only two cells of the top boundary of the grid are set at high constant concentration of uranium of 10^{-6} molal. The approach related to SCENARIO1 (Chapter 6) exploits the pseudo 1D nature of the simulations, which results in horizontal profiles, and making obvious how to measure the migration distance. This method is no more reliable for the new boundary conditions. The uranium migration is no more confined to a vertical propagation. Instead, the uranium profiles irradiate from the punctual source. To quantify the migration length of uranium for SCENARIO2, a new evaluating approach is implemented. The algorithm consists of a contouring operation which retrieves the coordinates of the migrating concentration profile of uranium, for a threshold concentration of interest. The operation results in a list, where for each element of the list (each element of the list corresponds to one reactive-transport simulation), there are two sub-elements showing the x and y-coordinates of the contour curve. The threshold aqueous concentration for uranium is 10^{-8} molal.

Once the coordinates of the contour curve are obtained, the Euclidean distances from the source boundaries are calculated for each knot in the contour. The operation is repeated for each profile of the ten simulations with the same parameters. The result is the evaluation of a minimum and a maximum covered distance for every scenario. Furthermore, the area covered by the injected uranium is computed using the same contour lines. This is performed with the “polyarea” function from R package “pracma”, which calculates exactly that: the area covered by a curve given its coordinates. It is not even necessary that the curve of interest is closed. However, in some specific cases, the concentration profiles arrive at the vertical boundaries, and, in order to quantify the exact covered area, the coordinates of the top-right and top-left corners of the grid were included in the curve. The method is applied for the cases involving the spatial variability and for the homogeneous case.

A third observable, which can be considered comparable to the area, is evaluated. It is the total sum of the in-flowed dissolved uranium calculated for each simulation. This value represents the sum of the concentrations of the three uranium species in the last iteration, subtracting the sum related to the initial state, which is the total background concentration. The process is carried out for each simulation involving the spatial variability and for the homogeneous case. It is expected that the trends of the covered areas and the total in-flowed uranium are similar. Moreover, it is expected that the relative standard deviation of the in-flowed uranium values, with respect to the homogeneous case, shows an increasing trend as the range of the variogram for the simulations increases. With

relative standard deviation is meant the standard deviation of the differences between the values of in-flowed uranium, related to each simulation, and the one of the homogeneous case.
All the reported measures are quantified in terms of cells of the grid. The side of each cell corresponds to 0.5 meters.

7.2 Sandy Facies

For each of the three investigated ranges of the variogram, all the profiles (black lines) are visually compared to the homogeneous simulation (green line). As it is observed for the SCENARIO1 (Chapter 6), the concentration profiles differ more from the homogeneous case as a bigger variogram range is taken into account. As a consequence, the maximum covered length by uranium concentration profiles shows its peak for simulations with a range of 20 meters *[Figure1/7]*. At the same time, the same profiles present the minimum covered distance, in accordance with the theory behind the implementation of the spatial variability. Namely, the two values are 39.92 cells (19,96 meters) and 31.89 cells (15,95 meters). Moreover, the evaluated covered areas follow the same trend. Both the minimum and the maxim values are related to a range equal to 20 meters. After being multiplied for 0.25, the biggest and the smallest covered areas in meters are around 509 m^2 and 431.5 m^2. The values related to a range of 5 meters show the smallest range for both area and distance covered. The quantity of in-flowed uranium is expected to be proportional to the area covered. *Figure2/7* aims to graphically represent the relationship between the two quantities. Looking at the plots, despite the presence of some discrepancies, the two trend can be considered similar, in particular regarding the last simulations. The whole estimation results in an increasing standard deviation (relative standard deviation between the in-flowed uranium obtained from heterogeneous simulations and the homogeneous case) once simulations with larger ranges are considered *[Table1/7]*.

Ranges [m]	5	10	20
Standard Deviation (In-flowed uranium)	$8.17 \cdot 10^{-6}$	$1.107 \cdot 10^{-5}$	$1.304 \cdot 10^{-5}$

Table1/7. Variation of the standard deviation of the concentration related to the in-flowed uranium as a function of the range of the variogram. The data are related to the sandy facies.

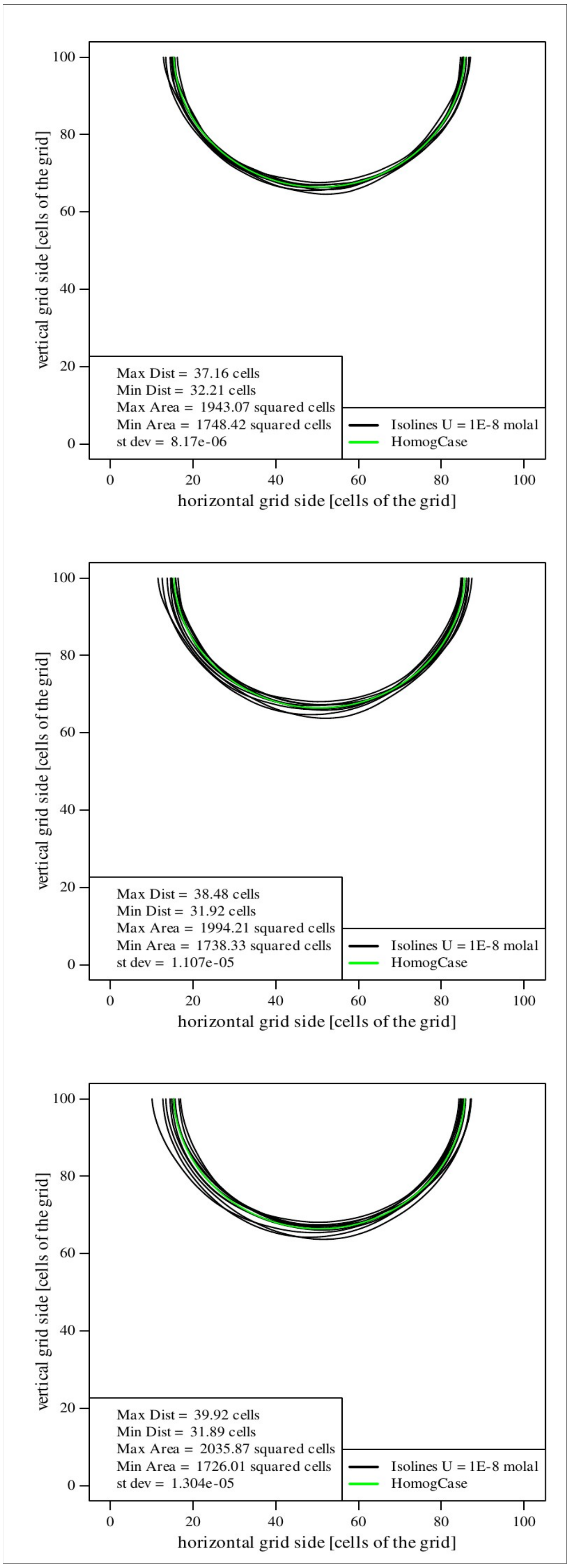

Figure1/7. Visual representation of the effect of the spatial variability on the diffusive mechanism of uranium inside the sandy facies for SCEANRIO2. Inside each plot, together with the simulated profiles related to an uranium concentration of 10^{-8} *molal (black lines), the profile related to the homogeneous diffusion coefficient is presented. The plot at the top is related to a variogram range of 5 meters, the second one to a range of 10 meters, and the one at the bottom to a range of 20 meters.*

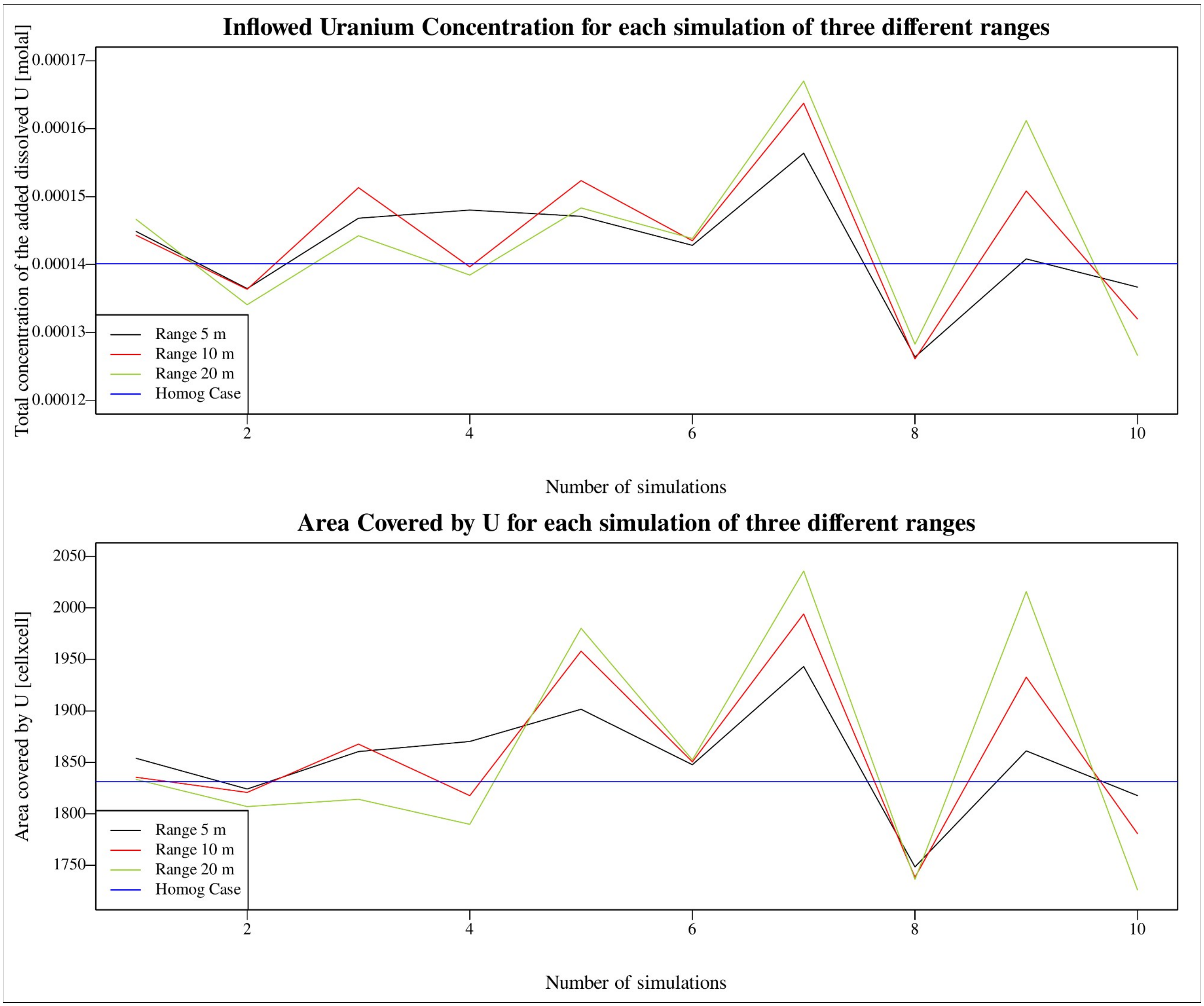

Figure2/7. The in-flowed uranium concentration and the covered area are selected to quantitatively evaluate the effects of the spatial variability. The plot at the top of the image shows the value of the total in-flowed U for each of the 10 simulations, and it presents the trends related to ranges of 5 meters (black), 10 meters (red), and 20 meters (green). The quantities related to a homogeneous diffusion coefficient are constant (blue lines). The plot at the bottom shows the trends for the area covered by an uranium concentration of 10^{-8} molal. The results are related to the sandy facies.

7.3 Carbonate-Rich Facies

The carbonate-rich facies displays again the longest migration distances *[Figure3/7]*. For each different variogram range the uranium concentration profiles reach the vertical borders of the grid. Nevertheless, the trend in terms of maximum and minimum areas and distances does not vary form the previous case. The longest and the shortest distances are both recorded among the simulations accounting a range of 20 meters. Similarly, the trends for the covered area and the for the in-flowed uranium regarding each simulation can be compared one to each other. The analysis results in a maximum covered area of 974.9 m^2, and a minimum value of 861,7 m^2, while the area covered in the homogeneous case can be rounded to 900 m^2 *[Table2/7]*. The maximum lengths and the relative standard deviations, always in terms of in-flowed uranium, are reported herein, clearly capturing an increasing spread with the range of variogram.

Range [meters]	5	10	20
Standard Deviation (In-flowed uranium)	$1.354 \cdot 10^{-5}$	$1.885 \cdot 10^{-5}$	$2.247 \cdot 10^{-5}$
Max. distance [meters]	26.67	27.12	27.94

Table2/7. Variation of the maximum distance covered by uranium diffusion and the standard deviation of in-flowed uranium concentration. The variation is function of the increasing range of the variogram. The data are related to the carbonate-rich facies.

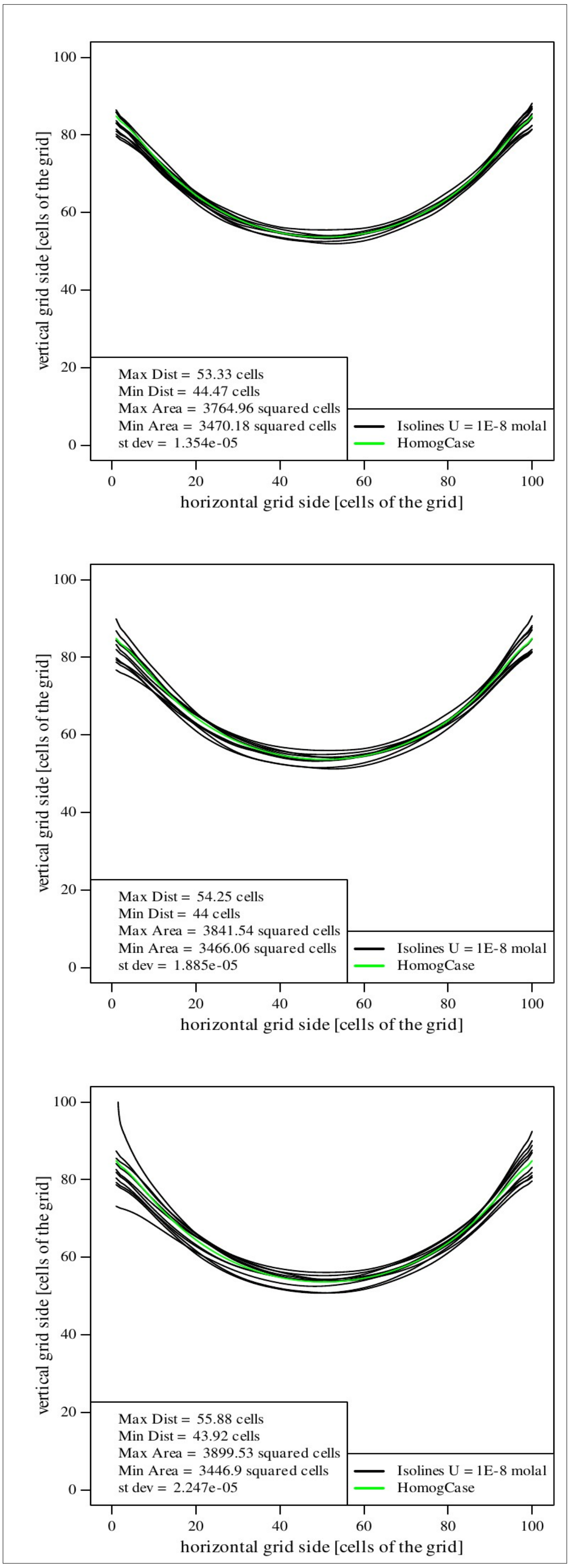

Figure3/7. Visual representation of the effect of the spatial variability on the diffusive mechanism of uranium inside the carbonate-rich facies for SCEANRIO2. Inside each plot, together with the simulated profiles related to an uranium concentration of 10^{-8} molal (black lines), the profile related to the homogeneous diffusion coefficient is presented. The plot at the top is related to a variogram range of 5 meters, the second one to a range of 10 meters, and the one at the bottom to a range of 20 meters.

7.4 Shaly Facies

The relevant role of the chemistry involved in the simulation is as clear as it is for SCENARIO1 (Chapter 6). The uranium concentration profiles cover the closest distances and the smaller areas due to the buffering effect of sorption *[Figure4/7]*. The minimum distances for the two largest ranges, 10 meters and 20 meters, are the same. However, since the minimum areas show different values and the maximum distance related to the second case (range equal to 20 meters) is larger, the order relationship of the standard deviation and covered area are respected increasing the variogram range *[Table3/7]*.

Range [meters]	5	10	20
Standard Deviation (In-flowed uranium)	$4.16 \cdot 10^{-6}$	$5.37 \cdot 10^{-6}$	$6.28 \cdot 10^{-6}$
Max. area [sq. meters]	206.28	214.49	218.73

Table3/7. Variation of the maximum area covered by uranium diffusion and the standard deviation of in-flowed uranium concentration. The variation is function of the increasing range of the variogram. The data are related to the shaly facies.

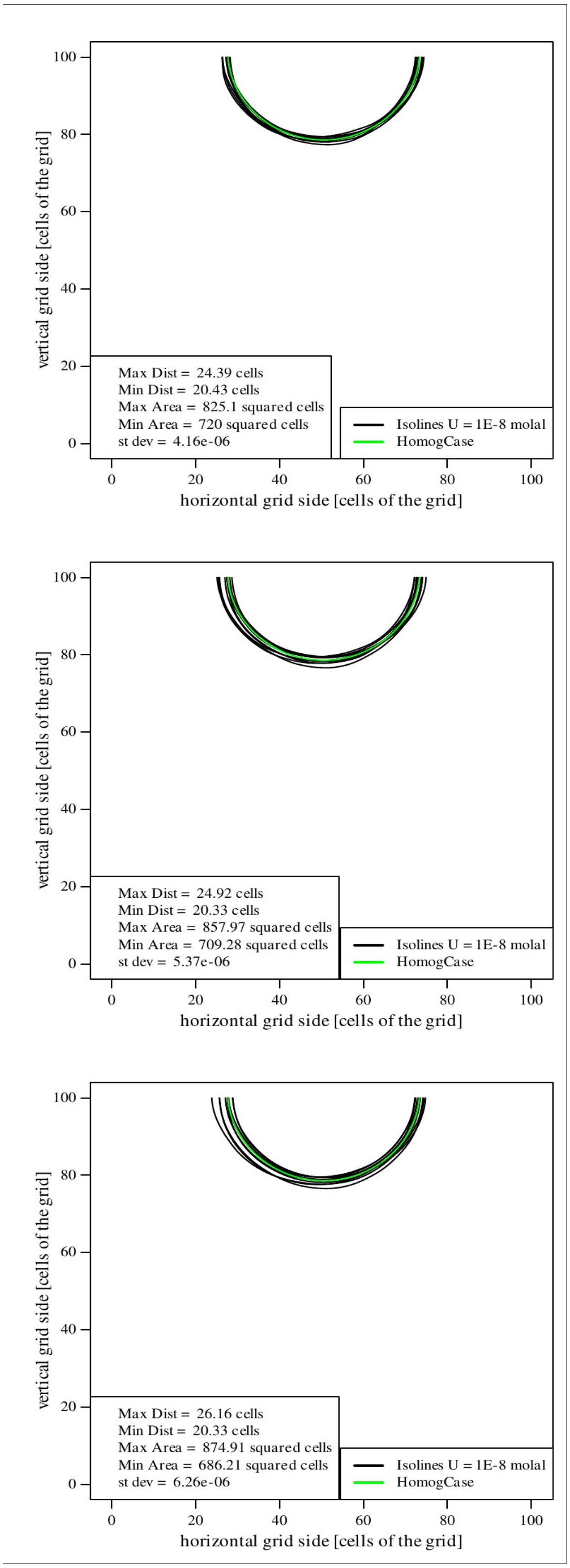

Figure4/7. Visual representation of the effect of the spatial variability on the diffusive mechanism of uranium inside the shaly facies for SCEANRIO2. Inside each plot, together with the simulated profiles related to an uranium concentration of 10^{-8} molal (black lines), the profile related to the homogeneous diffusion coefficient is presented. The plot at the top is related to a variogram range of 5 meters, the second one to a range of 10 meters, and the one at the bottom to a range of 20 meters.

8 Geochemical Gradient at Mont Terri

The assumption of initially homogeneous and constant conditions in terms of pore water geochemistry and aqueous concentrations can not stand when looking at the host rock scale. The presence of two embedding aquifers as hydro-geological boundaries leads to the formation of a geochemical gradient across the entire Opalinus Clay. The hydro-geological boundary at the hanging wall is located where the limestones of the Lower Dogger end, and the Opalinus Clay starts. The one at the footwall is the Liassic Gryphaea limestone. Defining these two boundaries, the 160 m thick Opalinus Clay is not the only formation considered, but even a 50 m thick layer of Liassic shales is included. The stratigraphic evolution of the area allowed the possibility for fresh water to infiltrate into both the aquifers and consequently to activate the hydro-geological boundaries. Mazurek et al. [18] states that the triggering event was the folding of Jura mountains 10 Ma ago. A consequent erosion of the exposed layers has taken place. The activation of the two aquifers is not simultaneous. The overlying one is considered to have been activated between 10 Ma ago, direct consequence of the folding, and 1.2 Ma ago. Instead, regarding the one at the bottom, the activation took place between 0.5 Ma and 0.2 Ma ago. Only once the fresh water infiltrations have crossed the whole formation.

At Mont Terri, the current hydro-geochemical gradient can be best understood via the chloride concentration, since the chloride species can be considered almost totally uninvolved in the chemical reactions. The concentration profile shows a steep decrease crossing the thin layer of Liassic shales, as drifting apart form the peak of gradient. The peak can be hypothetically located in the contact area between the Opalinus Clay and the Liassic shales. Differently, moving towards the hanging boundary, through the 160 m thick layer, the decreasing gradient trend is much smoother. The plot presented by Hennig et al. [6] reports the characterizing chloride gradient for the area of interest at Mont Terri *[Figure1/8]*.

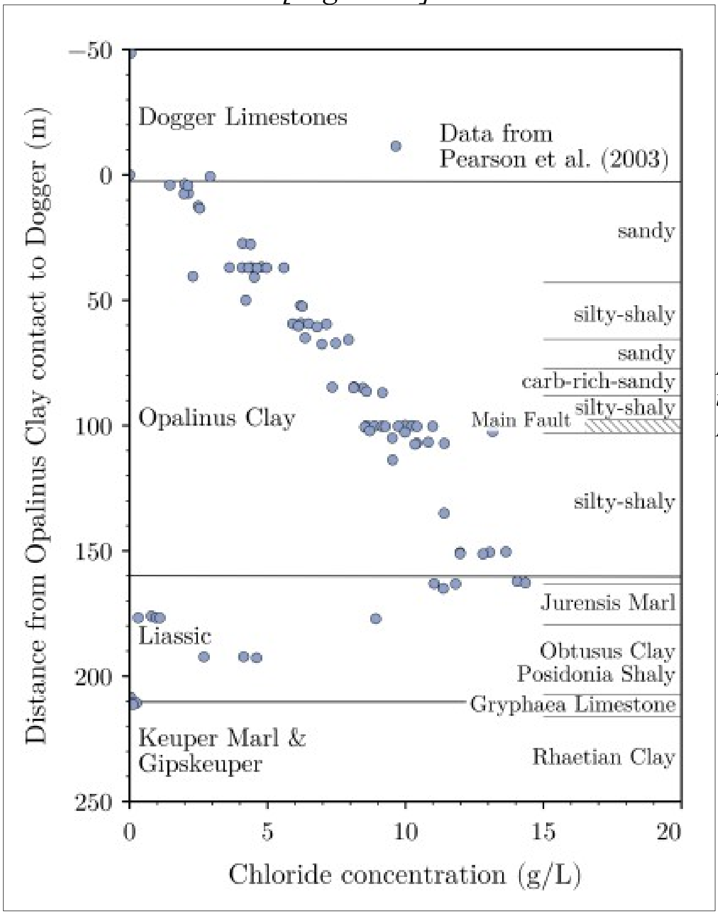

Figure1/8. Vertical concentration profile of chloride in the Opalinus Clay, and in the embedding aquifers. Image reproduced with permission from the author.

8.1 Implementation of geochemical gradient into reactive transport simulations performed on POET

To reproduce the current hydro-geochemical gradient, Hennig et al. [6] decides to perform a 6 Ma simulation on PHREEQC, where the hanging aquifer is active from the beginning, while the one at the bottom is activated only 0.5 MA before the end of the simulation. As mentioned in the introductory chapter (Chapter 1), the only transport mechanism involved in the low permeable sequence is diffusion, hence, even Hennig et al. works with a reactive-transport model which only involves diffusion. Regarding the choice of the initial conditions, in terms of concentration of chloride, together with the main pore water components, two different scenarios are investigated. The first one is based on the values retrieved from squeezing a sample of Opalinus Clay coming from the Mont Russelin anticline, which is considered a more stable area where almost constant hydro-geological conditions have been shown. The initial chloride concentration is considered to be around 18.9 g/L. The second scenario follows the assumption of Mazurek et al. [18] who proposes as starting chloride concentration 18.4 g/L. The value is obtained by the sample of stagnant groundwater retrieved from the Liassic aquifer close to Mont Russelin, where any infiltration is expected to have reached the formation. In order to perform simulations for the two scenarios, not only the initial chloride concentration is needed, but also the one of the other main pore water components (eg. Na^+, Cl^-, K^+, Ca^{2+}, Mg^{2+}, Sr^{2+}, SO_4^{2-}).

Regarding the former scenario, the values of the main components were easily retrieved during the squeezing process for the Opalinus Clay coming from the Mont Russelin. Instead, only sodium and strontium data are available from the stagnant water of the Liassic aquifer, so, regarding the other components of the second scenario, the data are picked looking at the seawater concentrations according to the time of deposition in the Jurassic. Moreover, the pore water composition for each of the bounding aquifers are obtained from samples extracted at Mont Terri. *Table1/8* reports the initial conditions for the two scenarios.

Component	Scenario 1	Scenario 2	Dogger Limestone	Liassic Limestone
Na^+ (mmol/L)	402	413	0,8	1,3
Cl^- (mmol/L)	522	508	0,08	0,2
Ca^{2+} (mmol/L)	46	26	1,9	2,1
Mg^{2+} (mmol/L)	41	33	2,7	0,7
SO_4^{2-} (mmol/L)	31	14	0,9	0,5
K^+ (mmol/L)	1,2	10,2	0,4	0,1
Sr^{2+} (mmol/L)	0,8	0,6	0,2	0,03

Table1/8. Aqueous concentration of the main pore water components for the two different scenarios, which are investigated to replicate the current hydro-geochemical system via 6 Ma simulations. The first two columns, strating from the right side of the table, presents the aqueous concentrations inside the embedding aquifers.

Following the workflow presented by Hennig et al. [6], reproducing the current hydro-geochemical gradient for the Opalins Clay at Mont Terri results in the first step for a more representative modelling of uranium diffusion across the formation. Two different approaches are investigated: the Single-Component diffusion approach (SC), and the Multi-Component diffusion approach (MC). As already pointed out in Chapter 1.7, the SC is based on the assumption that there is only one diffusion coefficient for all the pore water components, Hennig et al. takes into consideration the effective diffusion coefficient of chloride (D_e = 4.6E-12 m^2/s) as parameter of the Fick's Law. Once the model is calibrated thanks to the current chloride profile at Mont Terri, the effective diffusion coefficient is changed into the one for uranium (D_e = 1.9E-12 m^2/s), and the uranium diffusion is simulated. For the MC approach, the diffusion simulation on PHREEQC is based on the electrochemical potential, leading to the possibility to calculate the diffusive flux for each species as the sum of its diffusion inside the uncharged and charged region (pore water and diffusive double layer (DDL) for the investigated case). For every species, its own self-diffusion coefficient in water D_w (m^2/s) is indicated. The pore water diffusion coefficient is derived following the Archie's Law:

$$\frac{D_e}{\omega} = D_p = D_w \cdot \omega^n$$

Porosity is indicated with ω. The parameter *n* is an empirical value, specific for each case, and it is determined based on the SC approach simulations, whose model is previously calibrated against the chloride profile. Then, for both the approaches, the uranium diffusion simulations are performed.
The results in terms of most suitable scenarios are not that relevant for the current analysis, in particular because the MC approach is not involved in the reactive-transport simulations applied on PHREEQC and POET for this study. Nevertheless, the results achieved by Hennig et al. [4] are already presented in the Chapter 1.7, indeed using the SC approach the first scenario shows a better representation of the current chloride gradient. The chloride profile, which is used for the calibration of the model, is much more relevant for the objective of the current paper. The implementation of the hydro-geochemical gradient inside the employed model would allow to quantify the influence of spatial variability on uranium diffusion for a more geochemically and hydrogeologically realistic scenario. The results proposed by Hennig et al. [6] show a longer uranium migration once the hydro-geochemical gradient is taken into account. *Figure2/8* reports all the concentrations of the main components, together with other relevant parameters, used for the model calibration by Hennig et al.

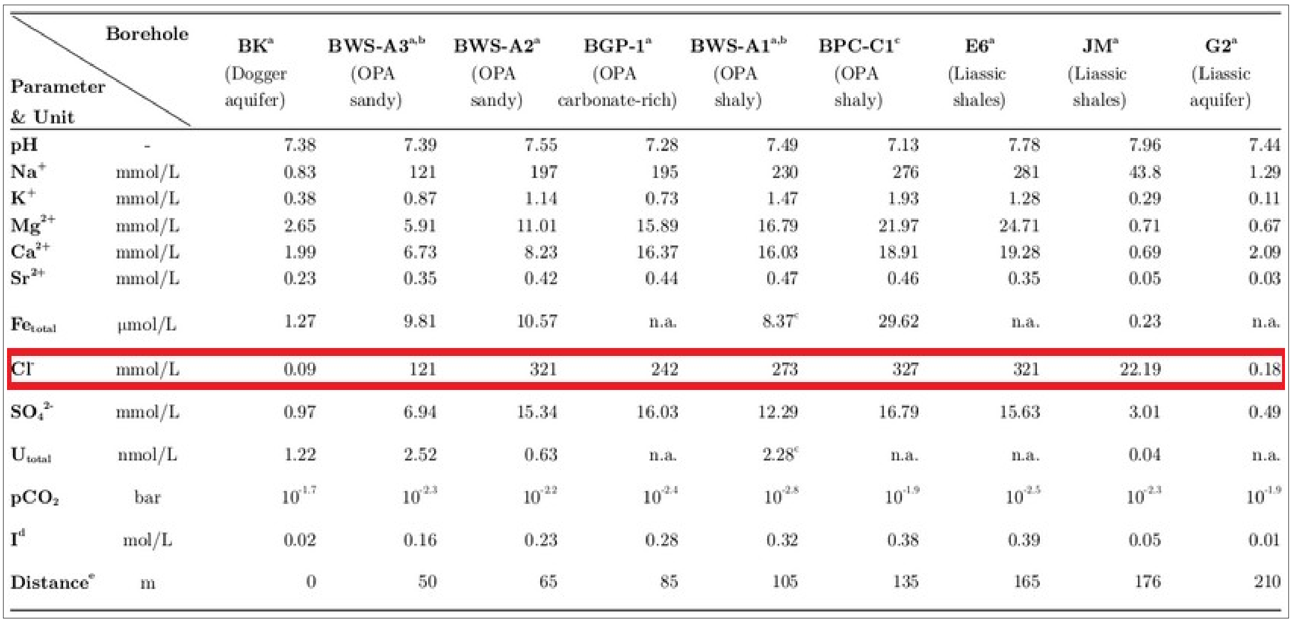

Borehole Parameter & Unit		BK^a (Dogger aquifer)	$BWS\text{-}A3^{a,b}$ (OPA sandy)	$BWS\text{-}A2^a$ (OPA sandy)	$BGP\text{-}1^a$ (OPA carbonate-rich)	$BWS\text{-}A1^{a,b}$ (OPA shaly)	$BPC\text{-}C1^c$ (OPA shaly)	$E6^a$ (Liassic shales)	JM^a (Liassic shales)	$G2^a$ (Liassic aquifer)
pH	-	7.38	7.39	7.55	7.28	7.49	7.13	7.78	7.96	7.44
Na^+	mmol/L	0.83	121	197	195	230	276	281	43.8	1.29
K^+	mmol/L	0.38	0.87	1.14	0.73	1.47	1.93	1.28	0.29	0.11
Mg^{2+}	mmol/L	2.65	5.91	11.01	15.89	16.79	21.97	24.71	0.71	0.67
Ca^{2+}	mmol/L	1.99	6.73	8.23	16.37	16.03	18.91	19.28	0.69	2.09
Sr^{2+}	mmol/L	0.23	0.35	0.42	0.44	0.47	0.46	0.35	0.05	0.03
Fe_{total}	µmol/L	1.27	9.81	10.57	n.a.	8.37^c	29.62	n.a.	0.23	n.a.
Cl^-	mmol/L	0.09	121	321	242	273	327	321	22.19	0.18
SO_4^{2-}	mmol/L	0.97	6.94	15.34	16.03	12.29	16.79	15.63	3.01	0.49
U_{total}	nmol/L	1.22	2.52	0.63	n.a.	2.28^c	n.a.	n.a.	0.04	n.a.
pCO_2	bar	$10^{-1.7}$	$10^{-2.3}$	$10^{-2.2}$	$10^{-2.4}$	$10^{-2.8}$	$10^{-1.9}$	$10^{-2.5}$	$10^{-2.3}$	$10^{-1.9}$
I^d	mol/L	0.02	0.16	0.23	0.28	0.32	0.38	0.39	0.05	0.01
$Distance^e$	m	0	50	65	85	105	135	165	176	210

Figure2/8. The partial pressure of CO2, the pH, and the concentration of the main pore water elements, retrieved from different boreholes, are reported inside the table. The highlighted values show the vertical concentration profile of Cl. The value related to the BWS-A2 borehole is not correct. Image reproduced with permission from the author.

Each row of the previous table represents the averaged values from borehole analyses at Mont Terri. In particular, for the implementation of the gradient, the vertical chloride concentration profile is retrieved, with the term “distance” indicating how far from the contact area between the hanging boundary and the Opalinus Clay the concentration value is sampled.

Distance (m)	0	50	65	85	105	135	165	176	210
Cl^- conc. (mmol/L)	0.09	121	179	242	273	327	321	22.19	0.18

Table2/8. Values of reference to replicate the vertical concentration gradient of chloride. The distances are evaluated starting from the contact area between the Dogger aquifer and the Opalinus Clay.

Looking at *Figure2/8*, the chloride concentration of borehole BWS-A2 is not the correct one (321 mmol/L). A simple mistake during the transcription of the averaged data may have occurred. The correct value (179 mmol/L) is inserted in *Table2/8*. The proof is the vertical concentration profile presented by Hennig et al. [4] in the Supplementary Material following the claimed table *[Figure3/8]*.

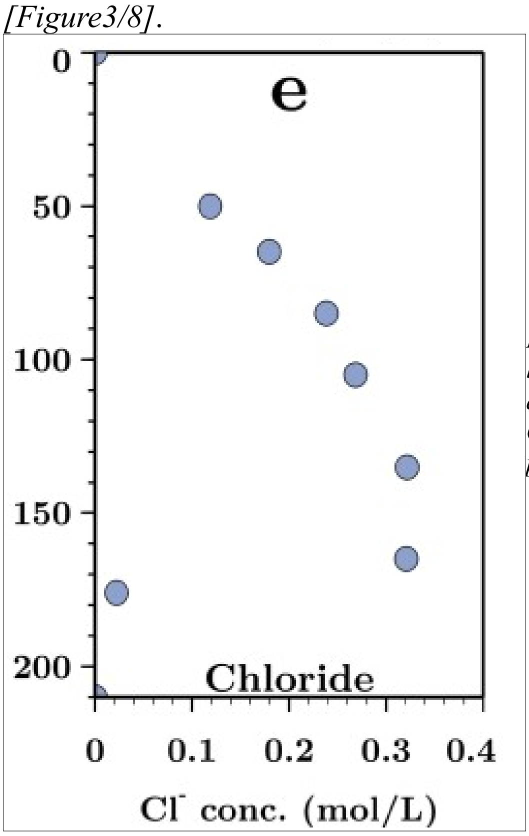

Figure3/8. Trend of the averaged chloride concentration retrieved from borehole analysis at the underground laboratory Mont Terry. The y-axis reports the distance perpendicular to the contact between the Opalinus Clay and the Dogger Limestone. Image reproduced with permission from the author.

In order to quantify the differences in terms of uranium migration two different types of simulations are performed. Accounting the geochemical gradient which only characterizes the 160 meters thick formation of the Opalinus Clay, and taking into consideration that the pore water chemistry of the sandy and carbonate-rich facies is retrieved from the borehole BWS-A3 (50 meters below the contact area between the Dogger aquifer and the Oplainus Clay), two different scenarios are investigated. It is important to underline that the pore water chemistry is equal for the two facies, but the mineralogical fractions differ. The “FRESH” condition depicts a scenario in which the migration of U goes towards less saline concentrations. In particular, it replicates the chloride gradient at the contact area between the Opalinus Clay and the Dogger aquifer. The scenario is obtained setting the “fresh water” boundary condition at the opposite boundary of the one characterized by the uranium-rich solution. The “SALINE” condition depicts the second scenario. In this case, the boundary condition set at the opposite boundary refers to the peak concentration of the chloride gradient. Looking at the CL gradient, the peak is located at the contact area between the Opalinus Clay and the Liassic shales. Concerning both the scenarios, before applying the source term for uranium, it is required to let the system equilibrate once the new condition is set at the opposite boundary. Regarding the sandy and the carbonate-rich facies, both the “FRESH” and the “SALINE” gradient effects are investigated. Instead, for what concerns the shaly facies, since the location of the most relevant layer of this facies can be assumed at the peak of the geochemical gradient, only the simulations accounting the “FRESH” scenario are performed. A different pore water chemistry is considered while simulating the uranium migration inside the shaly facies.

In order to implement the geochemical gradient, first an equilibration simulation with appropriate boundary conditions at the opposite boundaries of our domain are run for 6 million of years; the resulting concentration fields are then used as initial state when imposing source of uranium in the boundary. This process is repeated for all the three facies, and the injection of uranium simulated for both the SCENARIO1 (Chapter 6) and SCENARIO2 (Chapter 7) settings are performed, but only for a variogram range of 20 meters. The results are elaborated with the same methods as for the scenarios not accounting the geochemical gradient. Looking in details at the behavior of the uranium migration in the three different facies, the most remarkable result is, once again, the fundamental role of the chemistry (pore water chemistry and mineralogical composition of the host rock). However, the effect of the implementation of both the geochemical gradient and the spatial variability bears a detailed investigation, especially concerning the definition of geochemical constraints such as equilibrium with carbonates, which can have significant impact on the outcome of the numerical experiences. However, these aspects were outside the scope of the present work and left to investigate in future more in-depth analysis.

8.2 SCENARIO1

In order to present a meaningful graphical representation of the results, the plots show the migration length of uranium for both the homogeneous case accounting for the underlying initial geochemical gradient and the one without (Chapter 6). The latter one is reported as a gray dashed line, while a green line represent the first case. It is very clear that the role of the geochemical gradient is very relevant when the uranium migration is investigated. The initially varying concentrations along the simulation grid show a massive effect. However, the results obtained by Hennig et al. [6], while showing a similarly relevant change in terms of uranium migration when accounting for the initial gradient, go in the opposite direction with respect to the results of the current work: our simulations show longer covered lengths for the “saline” scenarios (moving towards higher concentrations), and conversely the migration towards a “fresh” condition is slowed down compared with the initially homogeneous simulation. These results are qualitative opposite with respect to the evaluation of Hennig et al. The same behavior is presented for the SCENARIO2 in the following chapter. The two approaches can not be accurately compared due to a series of differences in the implementation of the chemistry and of the gradient, which points out the need for a more detailed analysis in the future.

8.2.1 Sandy Facies

Recalling the results obtained in Paragraph 6.2, the maximum covered distance is 23.659 meters, while the two new corresponding values are 21.401 meters for the “fresh” condition, and 28.735 meters for the “saline condition”. *Table3/8* reports the maximum and the mean distances for the three cases. Since the uranium concentration profile of 10^{-8} molal migrates farther when going towards more saline conditions, the related profiles are more affected by the spatial variability resulting in a higher range of values, which is approximately quantified as the difference between the maximum value and the mean. Considering the same range of the variogram, due to the previous explanation the effects of the spatial variability on the “fresh” scenario can be considered less relevant.

Condition inside sandy facies (range = 20 meters)	No Gradient	Saline	Fresh
Mean distance [meters]	22.347	36.205	20.218
Max distance [meters]	23.659	38.735	21.401

Table3/8. Variation of the mean and maximum distances as a consequence of the implementation of the “FRESH” and “SALINE” conditions for a variogram range of 20 meters. The data are related to the sandy facies in SCENARIO1.

The result is that applying the geochemical gradient to the simulations modifies the uranium migration. For the “saline” condition, once the spatial variability is taken into consideration, the migration is enhanced at a maximum of 15.1 meters, with an averaged increase of 13.9 meters. Differently, moving towards “fresh” conditions leads to a reduction in the mean migration distance of 2.1 meters *[Figure4/8]*.

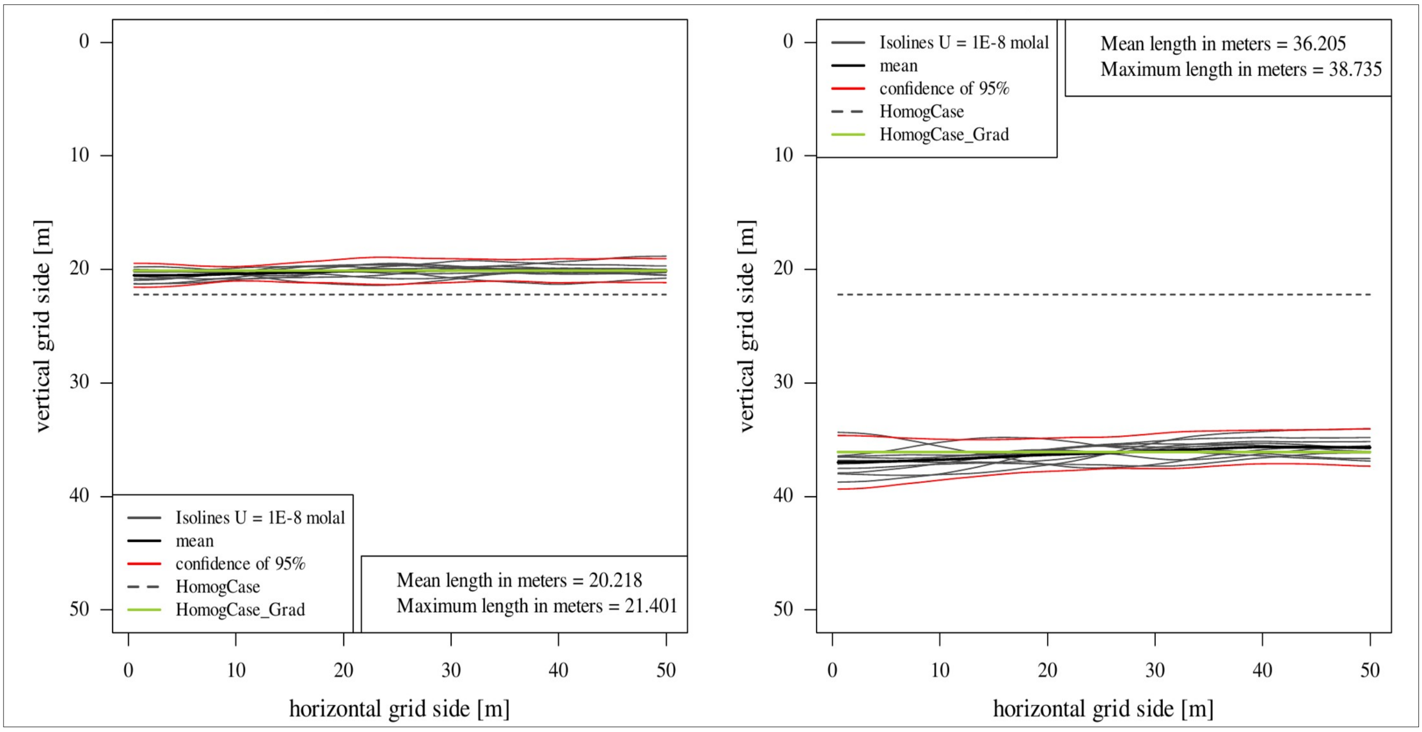

Figure4/8. Visual representation of the distance covered by the uranium concentration profiles after the implementation of the gradient for the sandy facies in SCENARIO1. The dashed line represents the distance covered by the uranium concentration profile for the homogeneous diffusion coefficient, without accounting for the geochemical gradient. The interval of probability of 95% (red lines), the averaged profile (black), and the one accounting for a homogeneous diffusion coefficient after the implementation of the gradient (green) are plotted too. The plot on the right side refers to the "FRESH" condition, while the other one reports the results for the "SALINE" condition.

8.2.2 Carbonate-Rich Facies

Regarding the uranium migration inside the carbonate-rich facies, the intrinsic chemistry of the facies leads the uranium profiles to almost cover the whole grid for the "saline" scenario. A maximum length of 48.265 meters means that the grid can be considered a limiting factor for the specific case *[Table4/8]*. The fact that the uranium almost reaches the maximum depth shifts to a secondary role the effects of the spatial variability. A more robust analysis accounting a longer y-axis has to be carried out in the future. Nevertheless, the behavior of the uranium profiles under the two different gradient conditions follows the one presented for the sandy facies. Inside the following table the mean and the maximum covered distances for the two cases and the one without accounting the gradient are reported (Chapter 6.3).

Condition inside carbonate-rich facies (range = 20 meters)	No Gradient	Saline	Fresh
Mean distance [meters]	31.133	47.56	26.672
Max distance [meters]	33.017	48.265	28.028

Table4/8. Variation of the mean and maximum distances as a consequence of the implementation of the "FRESH" and "SALINE" conditions for a variogram range of 20 meters. The data are related to the carbonate-rich facies in SCENARIO1.

Once again, for the "saline" case the uranium migration inside the facies is enhanced by the gradient *[Figure5/8]*. Looking at the maximum length, there is a positive difference of 15.2 meters. However, this value is affected by getting very close to the bottom of the grid. It is concluded that inside a longer grid the covered lengths would increase, together with the range between the mean and the maximum value due to the effects of the spatial variability. Despite the explained issue, as for the result related to the sandy facies, the range between the maximum distance and the mean distance for the "fresh" condition is smaller than the one related to the standard scenario. Namely, the longer the covered distance the more relevant the effects of the spatial variability are.

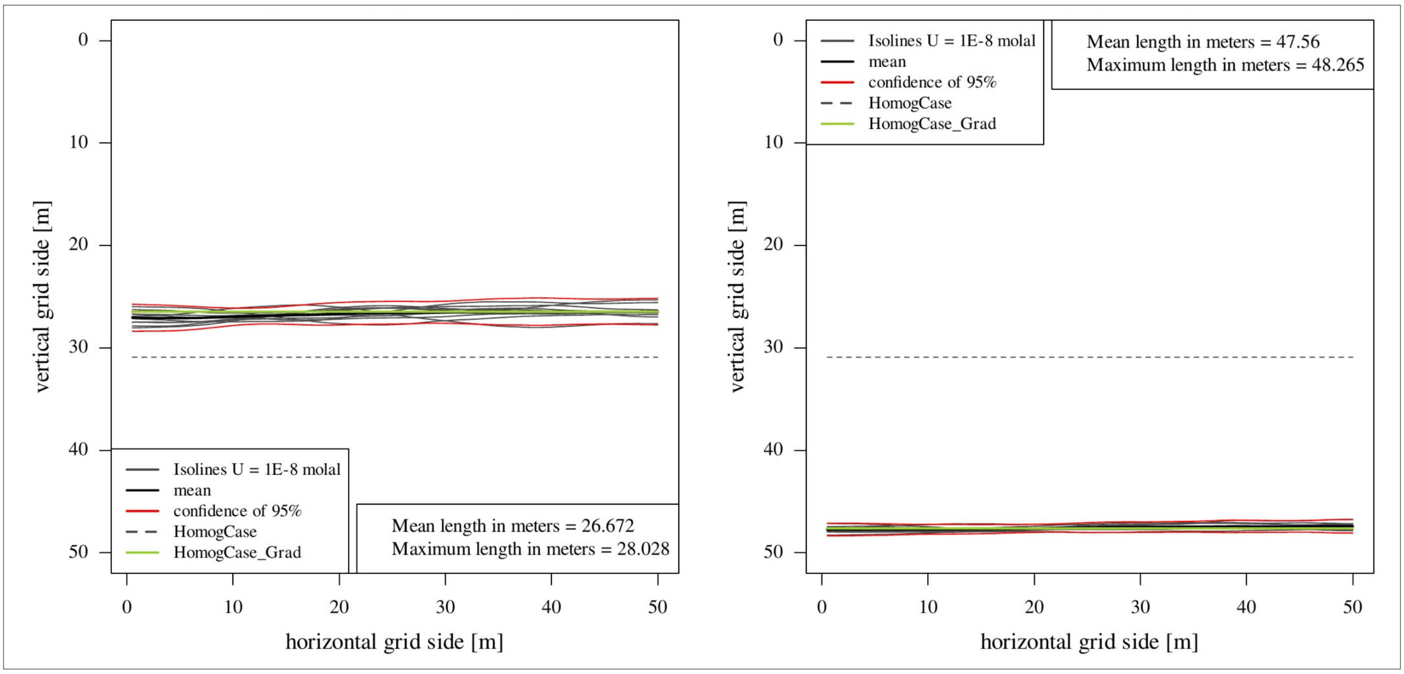

Figure5/8. Visual representation of the distance covered by the uranium concentration profiles after the implementation of the gradient for the carbonate-rich facies in SCENARIO1. The dashed line represents the distance covered by the uranium concentration profile for the homogeneous diffusion coefficient, without accounting for the geochemical gradient. The interval of probability of 95% (red lines), the averaged profile (black), and the one accounting for a homogeneous diffusion coefficient after the implementation of the gradient (green) are plotted too. The plot on the right side refers to the "FRESH" condition, while the other one reports the results for the "SALINE" condition.

8.2.3 Shaly Facies

As it is previously explained, the only investigated case for the shaly facies is the uranium migration under "fresh" condition. The results for the two other facies show a reduction in the covered length once the condition is applied. However, this is not the case for the shaly facies. *Table5/8* and *Figure6/8* present the obtained results. Looking at the plot, it is clear that the behavior does not stick to the one of the previous cases. The covered distance for the standard homogeneous scenario (without the gradient) is very close to the one related to the homogeneous case for the "fresh" condition. The data from the table confirm that a longer distance is covered by uranium migration when the gradient is implemented in the model. Namely, there is a maximum increase of 0.85 meters. Both the mean and the maximum values show a positive difference between the two cases, and, moreover, the range between the maximum and the mean value increases after the implementation of the gradient. The reason behind the explained behavior can be associated to the new condition of the pore water chemistry, which limits the buffering effect caused by the large fraction of argillaceous minerals in the shaly facies. Nevertheless, since the current work does not deeply investigate the chemistry involved, a more detailed sensitivity analysis would lead to more reliable conclusions and different results.

Condition inside shaly facies (range = 20 meters)	No Gradient	Fresh
Mean distance [meters]	14.139	14.546
Max distance [meters]	15.322	16.173

Table5/8. Variation of the mean and maximum distances as a consequence of the implementation of the "FRESH" and "SALINE" conditions. The data are related to the shaly facies in SCENARIO1.

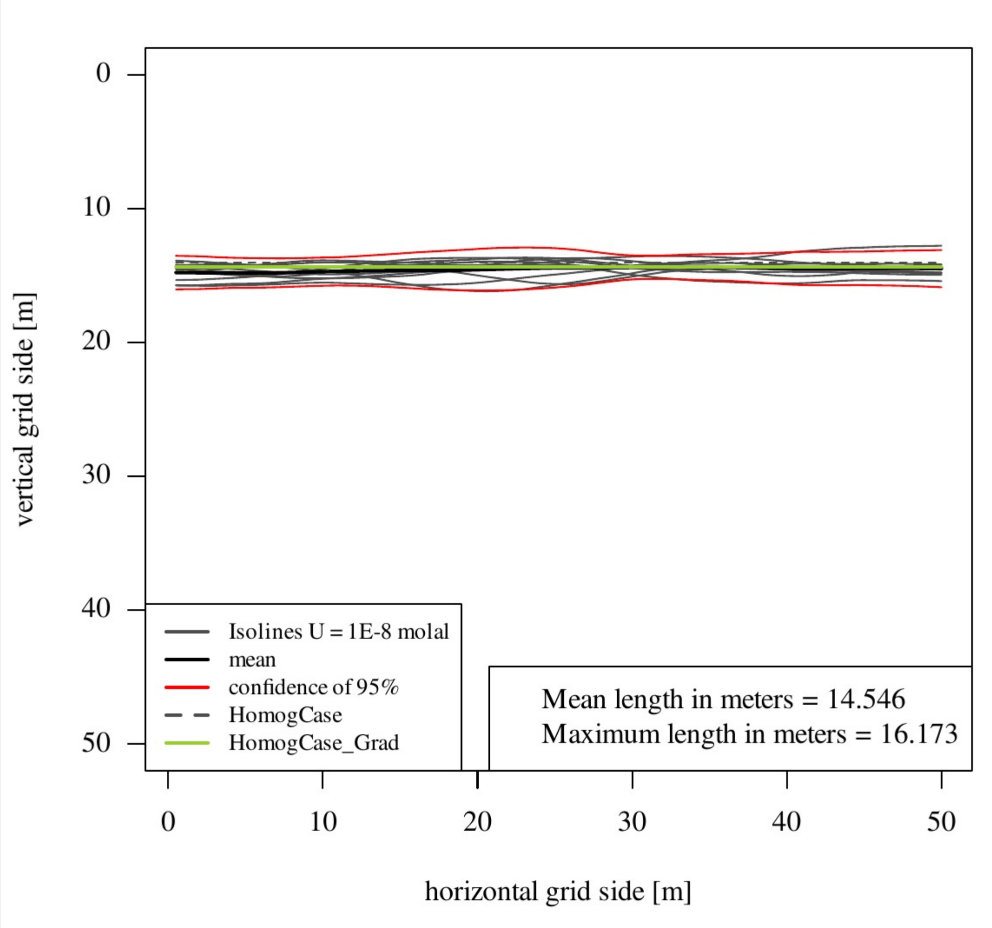

Figure6/8. Visual representation of the distance covered by the uranium concentration profiles after the implementation of the gradient for the shaly facies in SCENARIO1. The dashed line represents the distance covered by the uranium concentration profile for the homogeneous diffusion coefficient, without accounting for the geochemical gradient. The interval of probability of 95% (red lines), the averaged profile (black), and the one accounting for a homogeneous diffusion coefficient after the implementation of the gradient (green) are plotted too. The plot refers to the "FRESH" condition.

8.3 SCENARIO2

The hydrogeological gradient in the initial conditions was considered also for the punctual source of uranium of SCENARIO 2. The objective behind the current chapter is to quantified the effects of the implementation of a geochemical gradient with the different boundary conditions. Similar trends to the ones of the previous chapter are expected.

8.3.1 Sandy Facies

The opposite effects due to the implementation of the two different conditions can be observed even for SCENARIO2. Looking at *Figure7/8*, the areas and the distances involved in the uranium migration are completely different considering one condition or the other. Regarding the “saline” case, due to massive diffusion of the uranium inside the facies, the shape of the profiles does not follow the one related to the initially homogeneous scenario, without underlying gradient (green line). The accounted maximum distance is approximately 35 meters (70.08 cells), while the highest value in terms of covered area is close to 1440.6 m^2 (5762.35 squared cells) *[Table6/8]*. Differently, under “fresh” conditions the uranium concentration profiles rarely overcome the profile related to the standard homogeneous case (green line).

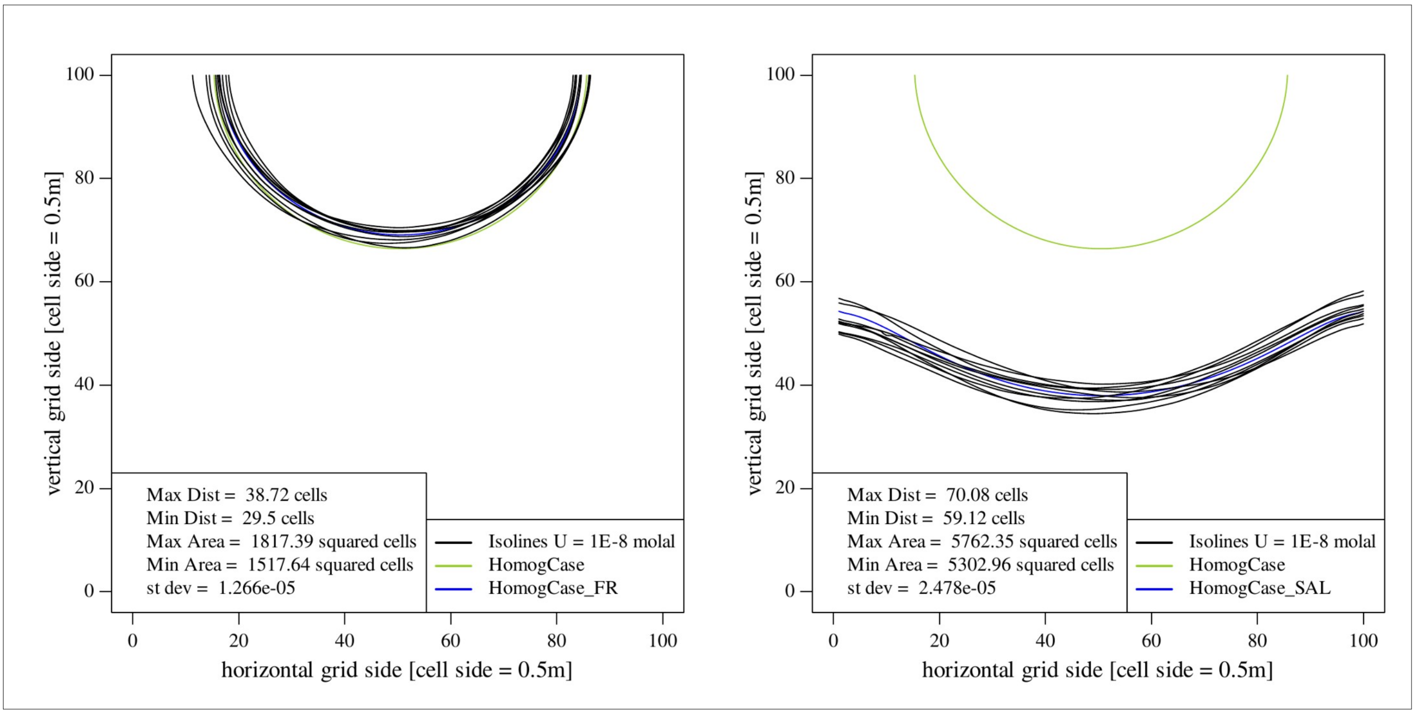

Figure7/8. Visual representation of the distance covered by the uranium concentration profiles after the implementation of the gradient for the sandy facies in SCENARIO2. The green line represents the distance covered by the uranium concentration profile for the homogeneous diffusion coefficient, without accounting for the geochemical gradient. The profile accounting for a homogeneous diffusion coefficient after the implementation of the gradient (blues) is plotted too. The plot on the right side refers to the “FRESH” condition, while the other one reports the results for the “SALINE” condition.

Condition inside sandy facies (range = 20 meters)	Max Distance		Max Area		Standard Deviation (in-flowed uranium)
	Cells	m (rounded)	Sq. Cells	m^2 (rounded)	
No Gradient	39.92	19.8	2035.87	509	$1.304\cdot10^{-5}$

Saline	70.08	35	5762.35	1440.6	$2.478\cdot10^{-5}$
Fresh	38.72	19.4	1817.39	454.3	$1.266\cdot10^{-5}$

Table6/8. Resulting values for the investigated parameters as a consequence of simulating with two new boundary conditions ("FRESH" and "SALINE") for a variogram range of 20 meters. The values related to the maximum distance and the maximum area are transformed into meters and squared meters. The results represents the uranium migration inside the sandy facies for SCENARIO2.

Performing simulations of a model where the geochemical gradient is accounted for does not guarantee that the trends of the in-flowed uranium and the covered area correspond, as it is shown in Chapter 7. In particular, the two plots related to the "saline" condition can be hardly correlated one to each other *[Figure8/8]*. The cause can be associated to migration of the uranium that reaches the vertical borders of the grid. It is supposed that, once the profiles can not propagate anymore along the horizontal direction, the two observables start showing a different trend. The uranium keeps getting inside the grid from the two boundary cells set at constant U concentration, while the increase of the area is no more proportional to the quantity of in-flowed uranium. Moreover, It can be assumed that the discordant effect, between the trends of the two quantities, is enhanced once a major part of the grid is involved in the uranium migration after the vertical borders are reached. Accordingly, the plots for the carbonate-rich facies before the implementation of the gradient do not show incomparable trends. Regarding the "fresh" condition, the two plots present similar values.

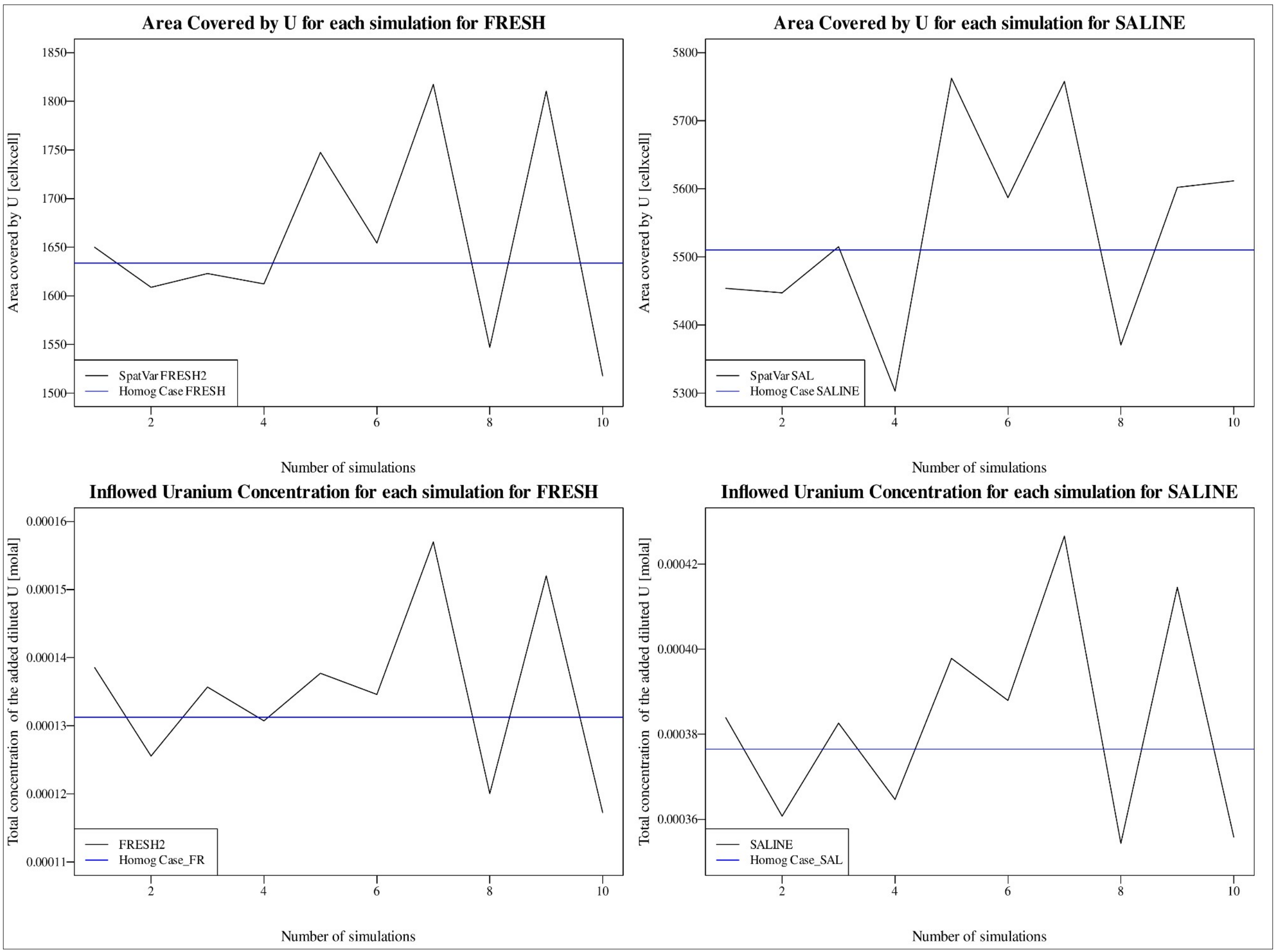

Figure8/8. Regarding the sandy facies, the trends of the total in-flowed uranium and the covered area are plotted for both the "SALINE" and "FRESH" conditions. The values related to each simulation are shown in black, while the constant value related to a homogeneous diffusion coefficient is reported in blue.

8.3.2 Carbonate-Rich Facies

The results for the carbonate-rich facies replicate the previous ones simply rescaling them due to the different chemistry and thus sorption capacity of this facies. In particular for the "fresh" condition, the uranium concentration profiles visually show a clear reduction in terms of covered areas and covered distances with respect to the homogeneous case without underlying gradient (green line) *[Figure9/8]*. The results are summarized in *Table7/8*.

Condition inside carbonate-rich facies (range = 20 meters)	Max Distance		Max Area		Standard Deviation (in-flowed uranium)
	Cells	m (rounded)	Sq. Cells	m^2 (rounded)	
No Gradient	55.88	27.9	3899.53	974.9	$2.247 \cdot 10^{-5}$
Saline	95.89	47.9	8265.25	2066.3	$4.211 \cdot 10^{-5}$
Fresh	52.76	26.4	3260.63	815.2	$2.066 \cdot 10^{-5}$

Table7/8. Resulting values for the investigated parameters as a consequence of simulating with two new boundary conditions ("FRESH" and "SALINE") for a variogram range of 20 meters. The values related to the maximum distance and the maximum area are transformed into meters and squared meters. The results represents the uranium migration inside the carbonate-rich facies for SCENARIO2.

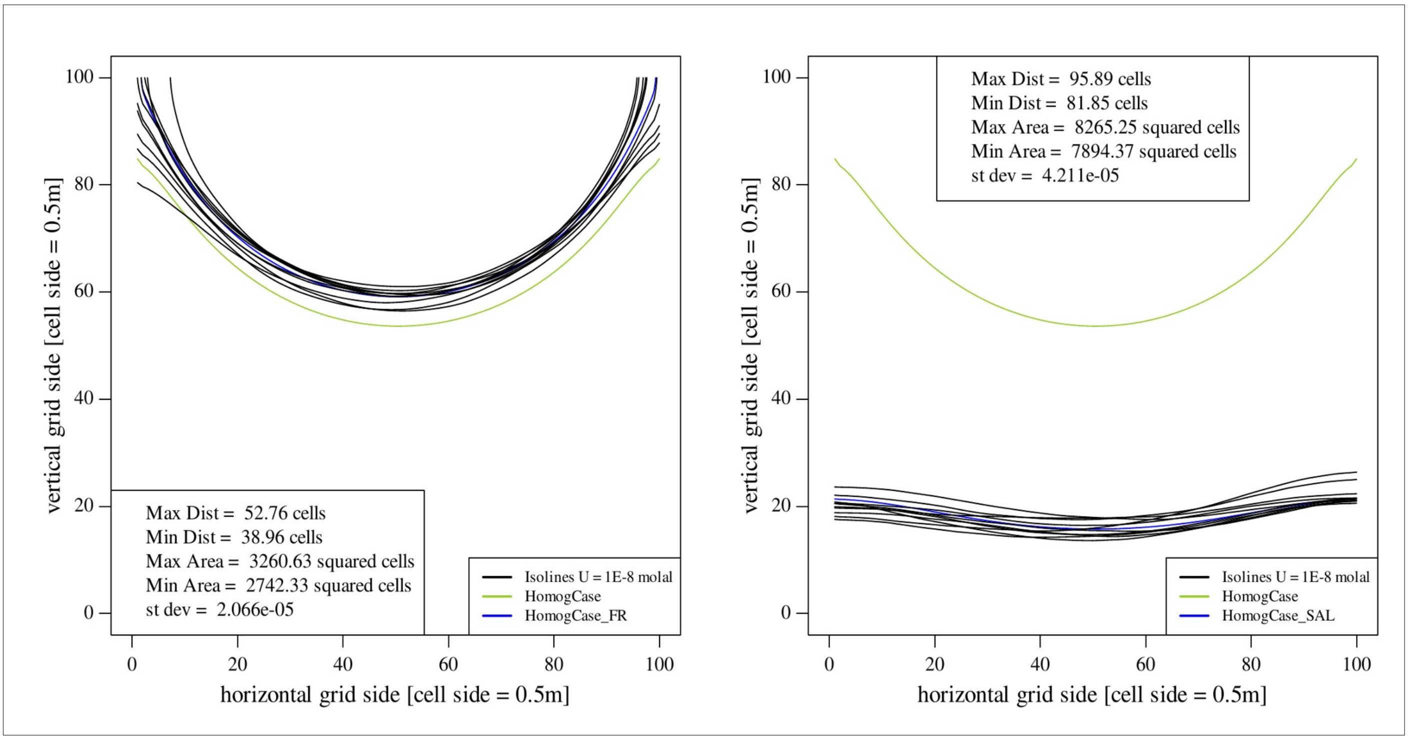

Figure9/8. Visual representation of the distance covered by the uranium concentration profiles after the implementation of the gradient for the carbonate-rich facies in SCENARIO2. The green line represents the distance covered by the uranium concentration profile for the homogeneous diffusion coefficient, without accounting for the geochemical gradient. The profile accounting for a homogeneous diffusion coefficient after the implementation of the gradient (blues) is plotted too. The plot on the right side refers to the "FRESH" condition, while the other one reports the results for the "SALINE" condition.

The trends related to the covered area and the in-flowed uranium present similar results as for the case of the sandy facies. Clear discrepancies are visible in the "saline" condition. Moreover, even for the "fresh" condition the two plots are not perfectly comparable. Looking in details, the first simulations do not present similar results in terms of concentration of the in-flowed uranium and covered area. Accordingly to what is mentioned in the previous paragraph, the implementation of the gradient seems to affect the compatibility of the two measures.

8.3.3 Shaly Facies

The last investigated case is the uranium migration inside the shaly facies. The results under “fresh” condition, the only one taken into consideration for the current facies, drift away from what is expected looking at the previous facies. The uranium migration is enhanced under “fresh” condition, without showing the concentration profiles strongly distancing themselves from the standard homogeneous scenario (green line) *[Figure10/8]*. Since the uranium migration does not involve the vertical borders of the grid, the trend related to the in-flowed uranium and the covered area are comparable *[Figure11/8]*. The differences with the scenario where the gradient is not accounted, in terms of maximum area, maximum distance, and standard deviation related to the in-flowed uranium, is herein reported *[Table8/8]*.

Condition inside the shaly facies (range = 20 meters)	Max Distance		Max Area		Standard Deviation (in-flowed uranium)
	Cells	m (rounded)	Sq. Cells	m^2 (rounded)	
No Gradient	26,16	13,1	874,92	218,7	$6.26\cdot10^{-6}$
Fresh	28,08	14	951,6	237,9	$8.38\cdot10^{-6}$

Table8/8. Resulting values for the investigated parameters as a consequence of simulating with “FRESH” boundary condition for a variogram range of 20 meters. The values related to the maximum distance and the maximum area are transformed into meters and squared meters. The results represents the uranium migration inside the shaly facies for SCENARIO2.

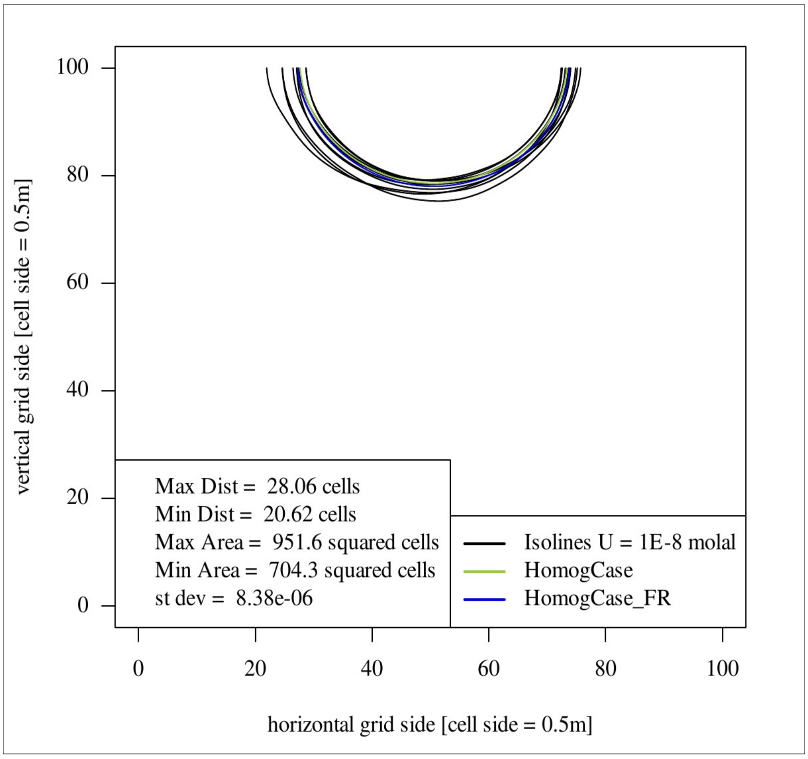

Figure10/8. Visual representation of the distance covered by the uranium concentration profiles after the implementation of the gradient for the shaly facies in SCENARIO2. The green line represents the distance covered by the uranium concentration profile for the homogeneous diffusion coefficient, without accounting for the geochemical gradient. The profile accounting for a homogeneous diffusion coefficient after the implementation of the gradient (blues) is plotted too. The plot reports the results under “FRESH” condition.

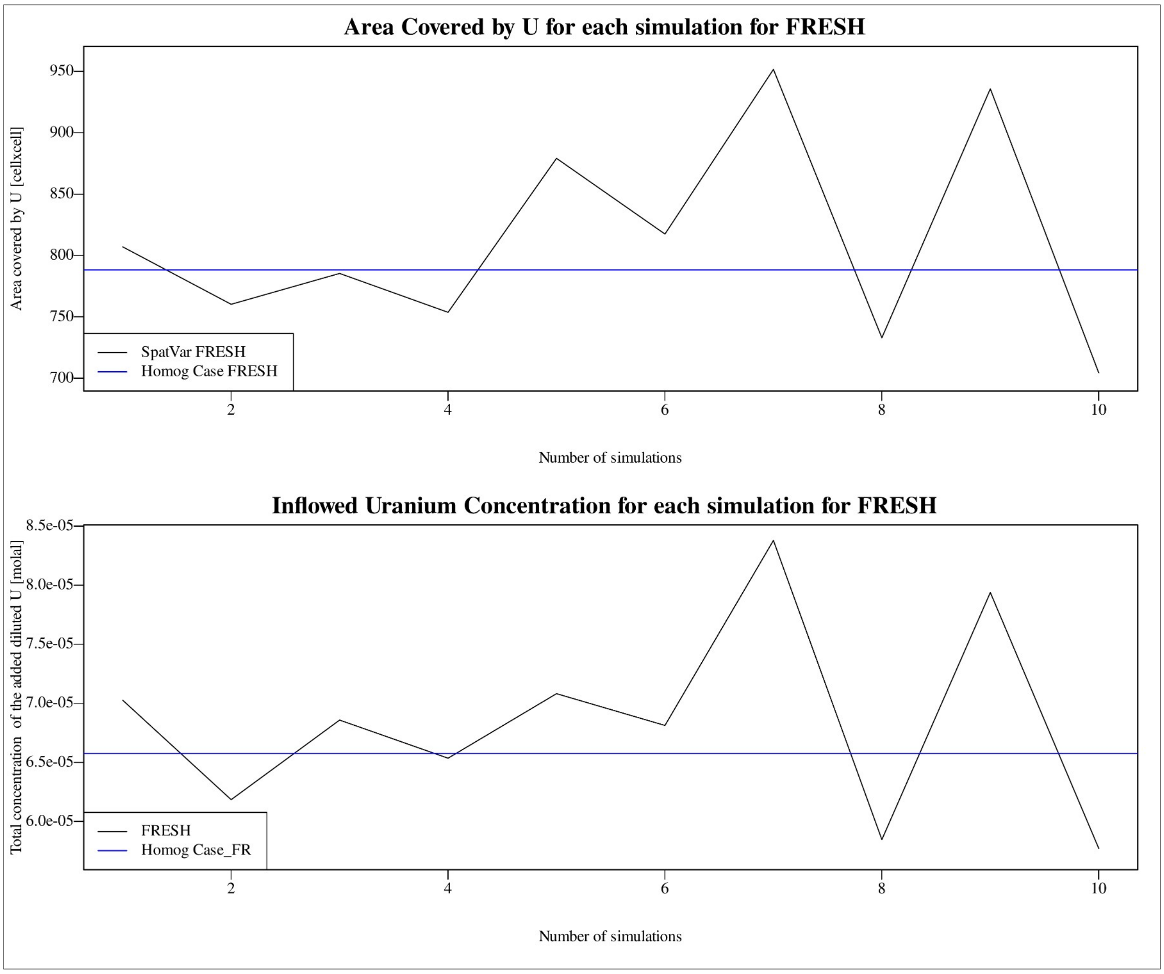

Figure11/8. Regarding the sandy facies, the trends of the total in-flowed uranium and the covered area are plotted for "FRESH" condition. The values related to each simulation are shown in black, while the constant value related to a homogeneous diffusion coefficient is reported in blue.

9 Simulating on a Representative-Geometry Model

The representation of cross-section of the Opalinus Clay reported in Chapter 1.2 shows a formation characterized by a thickness of 160 meter. The last step for the current analysis is to simulate the uranium diffusion in a model representing the whole formation with the three different facies. Herein, *Table1/9* presents the 5 horizontal layers of the Opalinus Clay.

Facies	Thickness [m]	Porosity Range [%]	Description
Sandy	40	6-14	Marly shales with lenses of gray sandy limestones
Silty-shaly	20	10-25	Argillaceous and marly shales
Sandy marly	10-15	6-14	Shales with layers of sandstones
Carbonate-rich sandy	5-15	6-14	Calcareous sandstones
Silty-shaly	80	10-25	Argillaceous and marly shales

Table1/9. Schematic description of the vertical cross-section of Opalinus Clay. In particular the thickness (mters), the porosity (%), and a brief mineralogical description are presented for each of the 5 layers.

In order to simulate the uranium migration for one million years inside the whole formation, a new grid is implemented. Not modifying the discretization approach, which is used for the totality of the previous results, the length of the side of a cell is 0.5 meters. The missing value is the length along the x-axis of the grid. A hypothetical horizontal length of 250 meters is selected. The new model is based on a 500x320 cells grid, which represents a 250x160 meters formation *[Figure1/9]*.

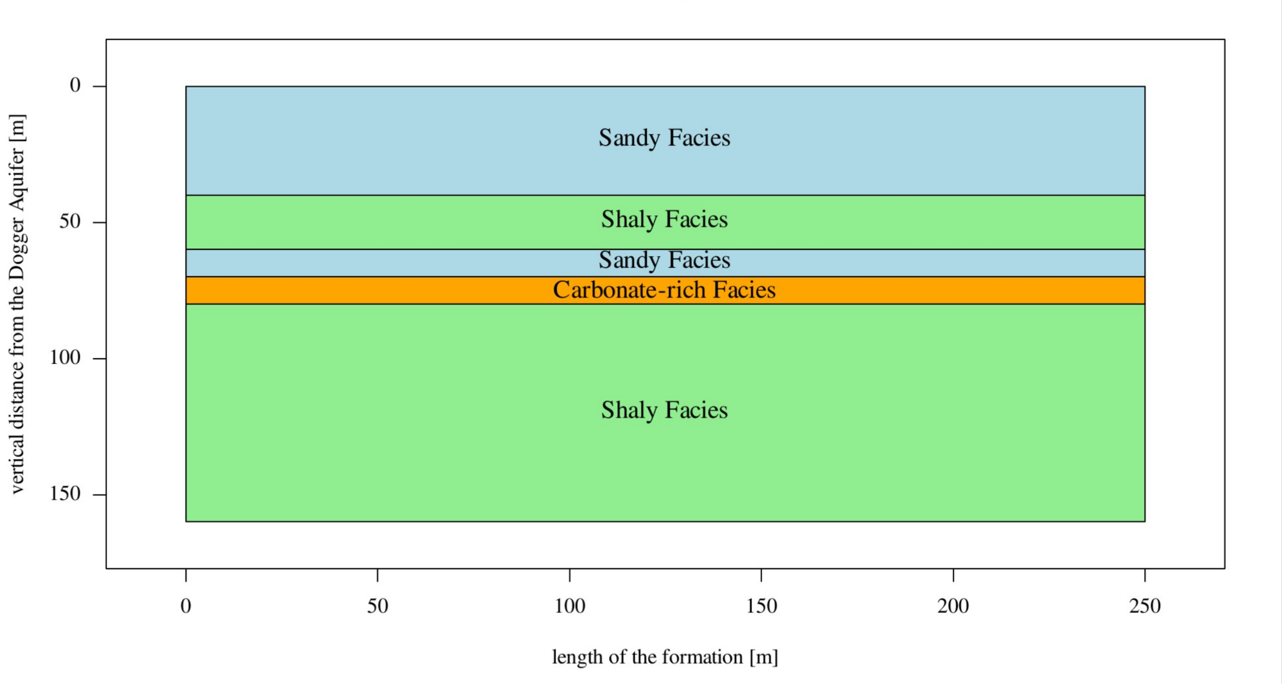

Figure1/9. Visual representation of the representative-geometry model.

Once the new grid is created, the entire gradient profile is implemented by equilibrating the whole model for 6 million years having set the lower boundary to the representative peak concentration of the shaly facies and the upper boundary to the representative concentration of the fresh water of the Dogger aquifer. The model simulated by Perason et al. [2] and Hennig et al. [6] differs from the one described. Their model does not only take into consideration the Oplainus Clay, but even a layer of Liassic shales. The consequence is that the lower boundary for their model does not correspond to the one fixed for the purpose of the current paper. *Figure1/8* shows a steep decrease in the Cl concentration passing the contact area between the Opalinus Clay and the Liassic shales.

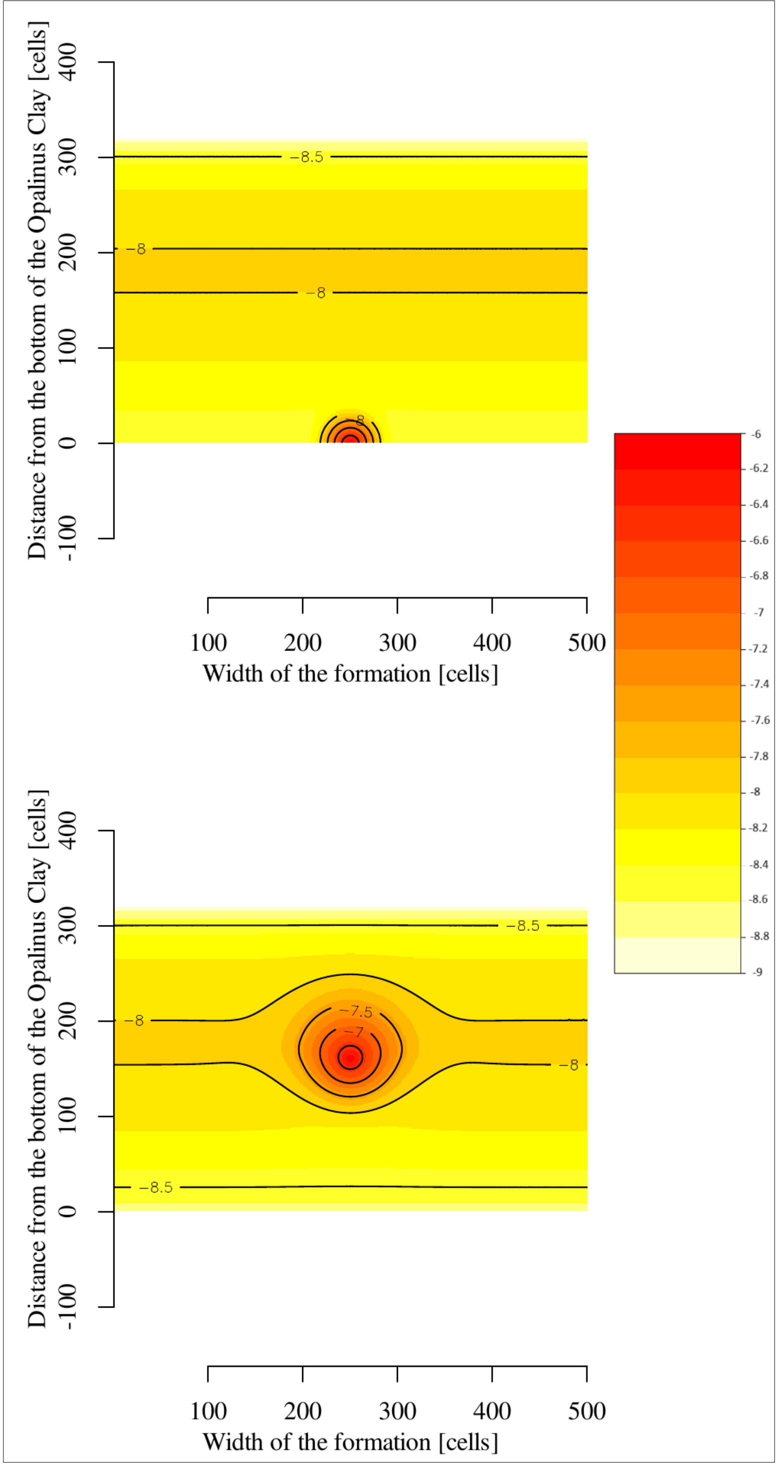

Figure2/9. Visual representation of the two simulated boundary conditions for the uranium diffusion inside a model with a more representative geometry. The plot at the top of the image shows the results once the shelter is located at the bottom of the Opalinus Clay (160 meters from the contact area with the Dogger aquifer). In the second scenario (plot at the bottom of the image) the uranium gets into the formation at a depth of 100 meters from the contact area with the Dogger aquifer. The measurement unit for the uranium concentration is the molality.

Two different locations for the injection are selected. Both cases are characterized by the second boundary condition (SCENARIO2), since, as it is already mentioned in Chapter 7, it is a more representative once the failing of the repository system takes place. The choice for the two involved cells follows the approach used by Hennig et al. [6] for the related studies. Inside her 1D simulations accounting the geochemical gradient, two different depths are selected. The values in meters represent the vertical distances form the contact area between the Opalinus Clay and the Dogger aquifer. The first location is at a depth of 100 m, and the second at 150 m. Regarding the current study, the first injection location does not vary, while the second one is shifted to a depth of 160 meters, which corresponds to the deepest point of the considered formation *[Figure2/9]*. For both the selected depths, the uranium source is located at the center of the grid in the horizontal axis. In other words, involving four cells for the injection, the selected cells are between (*ncol*/2)-2 and (*ncol*/2)+2 of the 200th and 320th row, with *ncol* equal to 500.

10 Approximated evaluation of the total CPU run time

A useful information for new coming studies is a coarse quantification of the total CPU run time for simulating all the presented scenarios and sub-cases. Regardless the investigation of a scenario with a representative-geometry, all the simulations ran on 16 CPUs. The averaged run time to simulate the diffusion of uranium inside the 50x50 meters model is estimated around 30 minutes. Looking at different scenarios, or at different sub-cases, the averaged value does not vary. The total number of simulations, that were launched for the purpose of the current study, is not precisely known. In particular, it was not kept track of the exact number of performed simulations in the context of the scoping analysis. The following list presents a hypothetical guess.
Regarding SCENARIO1, the simulations related to one facies are:

- 1 simulation accounting for a homogeneous diffusion coefficient,
- 30 simulations accounting for heterogeneous diffusion coefficients for 3 different ranges (isotropic variogram),
- 40 simulations accounting for heterogeneous diffusion coefficients for 2 different angles with 2 ratios (anisotropic variogram).

Concerning one facies, the total number of simulations is 71. The same approach must be applied to the other two facies. Accounting for both SCENARIO1 and SCENARIO2, the performed simulations are 426.
Regarding the investigation of the effects of the implementation of the geochemical gradient, the reactive-transport simulations of 6 Ma for equilibrating the new models have to be taken into account. Since the "SALINE" condition is not investigated for the shaly facies, 5 simulations in total were necessary. The CPU run time is 10 minutes for each one. Taking into consideration one facies, between the sandy and the carbonate-rich one, for SCENARIO1, the 1 million years simulations are:

- 2 simulation accounting for a homogeneous diffusion coefficient (there are two hydro-geochemical conditions),
- 20 simulations accounting for heterogeneous diffusion coefficients.

The total number is 22 simulations. While, concerning the shaly facies, the simulations are 11. Once both the scenarios are accounted for, the number turns into 110 simulations (1 Ma), plus the 5 simulations for the equilibrating phase.
Both the scoping analysis and the representative-geometry model have to be considered yet. Only three simulations are performed for the investigation of a more realistic model. However, its complexity required to simulate on a cluster which enabled the use of a large number of cores. For the 6 Ma equilibration, the simulation ran for 12 hours on 96 CPUs. Differently, the two sub-cases took 2 hours each on 128 CPUs. The number of simulations, and the related CPU run time, for the scoping analysis can not be clearly evaluated as for the previous scenarios. A hypothetical number is 40, with an assumed averaged run time of 20 minutes.
The results coming from this run-time analysis lead to a total number of iterations equal to 584 simulations, which are divided into:

- 536 simulations of 30 minutes (16 CPUs),
- 5 simulations of 10 minutes (16 CPUs),
- 40 simulations of 20 minutes (16 CPUs),
- 1 simulation of 12 hours (96 CPUs),
- 2 simulations of 2 hours (128 CPUs).

As a results, the total CPU run time is 17,890 minutes, which are around 298 hours, which means simulating for almost 12.5 days. In terms of hours/core the total CPU time is around 6179 h/core. The presented values aim to coarsely quantify the CPU time used to obtain the results shown herein. Moreover, it is a useful information for future studies.

11 Discussion and outlook

The Opalinus Clay is the formation chosen by the Swiss authority to build a repository and therefore the underground laboratory at Mont Terri. The consequent research projects have led to a detailed characterization of the formation aiming at investigating its suitability and in-depth characteristics as a host rock. The Opalinus Clay is furthermore still considered in Germany as as a possible solution for the storage of radioactive waste.
There are three main reasons behind this choice. The first one is related to the very low values of permeability which typically characterize clay formations. The consequence is the presence of the only diffusion as transport mechanism. The second reason focuses on the geochemistry potentially involved if uranium is released into the formation. Despite quite different mineralogical characteristics among the three facies, the whole formation shows a relevant content of argillaceous minerals which cause a retardation effect on the migration of radionuclides. Cation exchange phenomena and sorption mechanisms are believed to substantially reduce the length covered by uranium migration. The third reason is the intrinsic stability of the Opalinus Clay, but it is less relevant in the context of the current thesis. Previous studies [4] demonstrate that the major role in the uranium migration is played by the geochemistry of the pore water, in particular the partial pressure of the CO_2, which turns out to be even more relevant than the mineralogy. However, until now no predictive model assessing the uranium diffusion into the formation has taken into account the heterogeneity and spatial variability of the petrophysical properties of the host rock yet. Despite a clear complexity of the processes involved in retrieving data related to spatial variability of the properties of the host rock, using spatially homogeneous models results in a huge simplification of the real case scenario.

The current thesis aims at providing the first quantitative insights on the effects of the spatial variability of the host rock on the uranium migration. The presented results should be interpreted as starting point for further studies based on an innovative point of view. Moreover, the simulation of 2D models, and the consequent representation of 2D results, represent another massive step for the full characterization of the radionuclides migration inside the Opalinus Clay.

Herein, the four different study objectives are summarized:

- Optimization of the coupled simulations using POET
- Implementation of the spatial variability in terms of diffusion coefficients/tortuosity in the reactive transport simulations
- Investigation of the facies dependence for the uranium migration
- Simulation of a representative model accounting both for spatial variability and the realistic geochemical conditions.

Performing 2D coupled reactive transport simulations is a time consuming and complex task which has to be done with care. For this reasons, an in-depth scoping analysis related to the model of interest has been carried out. This led to the choice of a model of 50x50 meters, discretized into a 100x100 cells grid with a fixed time stepping of 2000 y to reach 1 million years. This choice ensured to have a low enough systematic error due to few coupling iterations but with a massive reduction in CPU time *[Figure7/3]*. This highlights the importance of a numerical scheme for the solution of diffusion allowing to relax the Courant-Friedrichs-Lewi stability condition (described in Chapter 3.1), as it is implemented in POET. The scoping analysis results in the choice of time step of 2000 years, and the consequent bearing of a systematic error of around 0.35 meters. In terms of number of iterations, the CPU time is reduced by 8 times, namely moving from 8000 iterations (accordingly to the stability condition) to 500 iterations.

The presence of heterogeneity inside the host rock, regarding reactive-transport simulations, and, even more in general, underground fluid modeling, is very difficult, and expensive, to be experimentally quantified. The consequence is the lack of extensive data for the characterization of the heterogeneity in the underground. Accordingly, the approach followed for accounting for spatial variability in the model is rather coarse and simplified, and it is based on the facies dependence of the porosity. As it is already mentioned, two main different ranges of porosity are identified:

- 6-14 % for the carbonate-rich and the sandy facies
- 10-25% for the shaly facies.

Due to a deficient characterization of the spatial variability of the Opalinus Clay, and similar formations, a general, but comprehensive, choice of the geostatistical parameter was taken in this work. Two main cases are investigated. The fist one considers anisotropic variogram for porosity. Two different main axes of anisotropy (parallel and perpendicular to the bedding) are investigated, with two different ratios of anisotropy: 4 and 10, and with a fixed range of 20 meters. The second case considers isotropic variogram and focuses on the effects of the range itself (5, 10, and 20 meters). The values of the range do not perfectly match with the few information retrieved from the literature, in particular considering the range of20 meters. Huysmans et al. [24] fits the sampled porosity of Bloom Clay (Belgium) with a spherical variogram of range 5.8 meters. The 2D seismic velocity distribution inside the sandy facies of the Opalinus Clay, which is simulated by Lüth et al. [25], presents a correlation distance that is assumed around 10 meters.

The anisotropic cases show a limited impact on uranium migration in the investigated models, both concerning the orientation of the anisotropy and the ratio between the ranges along the main and minimal anisotropy directions. In the isotropic case, however, the uranium migration show clear dependence on the range of the variogram, and in particular increased spread with larger ranges. The 10 uranium concentration profiles differ more from the one related to the homogeneous case once a range of 20 meters is taken into account. Moreover, in the facies where the chemistry as more limited sorption capacity and hence the uranium migration covers a longer distance, the effect of the spatial variability is enhanced. Accordingly, for the SCENARIO1, the highest value related to the maximum covered length corresponds to 33.133 meters, and it is observed for the carbonate-rich facies with a range of 20 meters. Looking at the relative increase between the maximum length covered for a range of 20 meters and the one related to range of 5 meters, the shaly facies shows the highest value *[Table1/10]*.

In order to replicate a more realistic scenario, a real quantification of the spread between the uranium concentration profiles is presented in *Table2/10*. It reports the mean value of the 100 standard deviations, obtained from the differences between the covered distance by each heterogeneous simulation (10 in total) and the one covered by the homogeneous simulation for every column of the grid. The quantitative results correspond to the qualitative evaluation given by the presented plot *[Chapter 6]* the spread increases as the correlation distance increases, and as the uranium migration is more enhanced by the chemistry.

Facies	**Maximum length [m] for range = 5 m**	**Maximum length [m] for range = 10 m**	**Maximum length [m] for range = 20 m**	**Relative increase** $\frac{l(20m)-l(5m)}{l(5m)}$
Sandy	22.961	23.283	23.659	3%
Carbonate-rich	31.76	32.275	33.017	4%
Shaly	14.703	14.972	15.322	4.2%

Table1/10. The maximum lengths covered by uranium migration inside the three facies are reported for all the investigated variogram ranges in SCENARIO1. The last column shows the relative increase in terms of maximum distances accounting for the values related to the a variogram range of 5 meters and 20 meters.

Facies	Range = 5 meters	Range = 10 meters	Range = 20 meters
	Mean of the st. dev.s of the relative distances for each column	**Mean of the st. dev.s of the relative distances for each column**	**Mean of the st. dev.s of the relative distances for each column**
Sandy	0.222	0.377	0.582
Carbonate-rich	0.239	0.416	0.657
Shaly	0.218	0.343	0.474

Table2/10. The mean of the standard deviations, related to each column of the grid (100), and obtained from the differences between the covered distance by each heterogeneous simulation and the one covered by the homogeneous simulation. Quantification of the spread between the uranium profiles for the three variogram ranges in SCENARIO1.

The trend in the results coming from SCENARIO2 is the same. Regarding each facies, both values related to length *[Table4/10]* and area*[Table5/10]*, together with the standard deviation related to the differences from the value of the homogeneous case for the in-flowed uranium quantities, simultaneously show the highest maximums and the lowest minimums for a range of 20 meters. In order to accurately investigate the effects of the spatial variability, since the evaluation of the distances for the SCENARIO2 is rather coarse, the same approach to estimate the relative increase is applied to the maximum covered areas. Looking at the values related to the standard deviation, the spread due to the variation in the range of the variogram is quantified. Accordingly to the table of SCENARIO1 *[Table2/10]*, the carbonate-rich facies shows the biggest spread *[Table3/10]*.

Facies	Range = 5 meters	Range = 10 meters	Range = 20 meters
	St. Dev. of the relative in-flowed U	**St. Dev. of the relative in-flowed U**	**St. Dev. of the relative in-flowed U**
Sandy	$8.17 \cdot 10^{-6}$	$1.107 \cdot 10^{-5}$	$1.304 \cdot 10^{-5}$
Carbonate-rich	$1.354 \cdot 10^{-5}$	$1.885 \cdot 10^{-5}$	$2.247 \cdot 10^{-5}$
Shaly	$4.16 \cdot 10^{-6}$	$5.37 \cdot 10^{-6}$	$6.26 \cdot 10^{-6}$

Table3/10. Standard deviation of the total in-flowed uranium, related to each facies, obtained for the three investigated ranges of the variogram in SCENARIO2.

Facies	Range = 5 meters		Range = 10 meters		Range = 20 meters	
	Distance [m]		**Distance [m]**		**Distance [m]**	
	Max	Min	Max	Min	Max	Min
Sandy	18.58	16.11	19.24	15.96	19.96	15.94
Carbonate-rich	26.66	22.23	27.12	22.00	27.94	21.96
Shaly	12.19	10.21	12.46	10.16	13.08	10.16

Table4/10. Maximum and minimum distances covered by uranium diffusion in each facies, which is obtained for the three investigated ranges of the variogram in SCENARIO2.

Facies	**Range of 5 meters**		**Range of 10 meters**		**Range of 20 meters**	
	Area [m^2]		**Area [m^2]**		**Area [m^2]**	
	Max	Min	Max	Min	Max	Min
Sandy	485.77	437.10	498.55	434.58	508.97	431.50
Carbonate-rich	941.24	867.54	960.38	866.51	974.88	861.5
Shaly	206.27	180.00	214.49	177.32	218.73	171.55

Table5/10. Maximum and minimum areas covered by uranium diffusion in each facies, which is obtained for the three investigated ranges of the variogram in SCENARIO2.

Facies	**Relative increase in terms of maximum areas** $\frac{A(20m)-A(5m)}{A(5m)}$
Sandy	4.8%
Carbonate-rich	3.6%
Shaly	6%

Table6/10. Difference between the maximum covered area for a variogram range of 20 meters and for a range of 5 meters. The resulting value is divided by the maximum covered area for a range of 5 meters. The relative increase, obtained in the SCENARIO2, is calculated for each facies.

Concerning the percentages related to the relative increase for SCENARIO2, it is important to underline that the uranium concentration profiles reach the vertical borders in the case of carbonate-rich facies. As a consequence, the reported value may be affected by this condition, resulting in a different trend with respect of the relative increase for SCENARIO1, which anyway is referred to the maximum length.

All the presented results bear the hypothesis of homogeneous initial background solution, which differs between the shaly and the sandy and carbonate rich facies. In other words, the diffusion of uranium is significantly affected by the differences in composition and concentrations of the initial pore water, assumed constant in both SCENARIO1 and SCENARIO2 boundary settings. This conceptualization differs from the actual formation from a hydro-geochemical perspective. It is experimentally demonstrated that the two embedding aquifers have established a geochemical gradient inside the Opalinus Clay throughout the last 6 million years. Since the chloride is a non-reactive component, its concentration profile clearly shows the presence of the gradient, and it is assumed as profile of reference for all the other pore water chemicals. The area of the Opalinus Clay closer to the Dogger aquifer presents lower values in terms of chloride concentration, while inside the shaly layer, at the bottom of the formation, the peak of the chloride concentration is observed.

The implementation of the gradient is performed in a simplified way, and it results in the assessment of two different models for each facies. The new models are equilibrated with different boundary conditions at the top and bottom boundaries intending to reproduce either the trend of the hydro-geochemical gradient towards the Dogger aquifer, which was labeled “FRESH” condition, or towards the increased concentration, labeled “SALINE” condition. Since the most relevant layer for the shaly facies is located at the same depth of the peak of the chloride concentration, the only simulated condition for this facies is the “FRESH”. The objective focuses on the coarse quantification of the combined effects of the implementation of the spatial variability and the geochemical gradient. As a consequence, only a variogram range equal to 20 meters is used. For both SCENARIO1 and SCENARIO2, the results coming from the simulations accounting the two different hydro-geochemical conditions emphasize the relevant role of the pore water chemistry. Regarding SCENARIO1 *[Table7/10]*, the uranium migration is buffered by the "FRESH" condition, with every uranium concentration profile which covers a shorter length than the distance related to the homogeneous case of the same scenario before the implementation of the gradient. Instead, the "SALINE" condition enhances the uranium diffusion, with all the profiles overcoming the one related to the homogeneous simulation not accounting for the gradient. The described results characterize the sandy and the carbonate-rich facies, while for the shaly facies the trend of the covered lengths does not correspond. In particular, the profiles are very close to the homogeneous of the previous case, and they overcome it, resulting in a longer mean and maximum distance covered.

Performing all the simulations with the same range does not technically allow to quantify the effects of the spatial variability. However, similar trend for different ranges are expected. Moreover, the effects of the combination of the use of a more representative model, from a hydro-geochemical point of view, and the implementation of the spatial variability can be quantified. Once the hydro-geochemical condition enhances the uranium migration, namely a longer length is covered, the uranium profiles distinctly drift away from the one related to the initially homogeneous simulation. In *Figure5/8* a different result is observed because the uranium diffusion reaches the bottom of the grid.

Facies	**Difference in terms of maximum length covered accounting and not accounting the gradient [m] (SCENARIO1)**	
	"SALINE" condition	**"FRESH" condition**
Sandy	15.08	- 2.26
Carbonate-rich	15.23	- 4.99
Shaly	/	0.851

Table7/10. The difference between the maximum covered length for the simulation accounting for the geochemical gradient and for the one not accounting for it is reported for the two new boundary conditions, and for each facies (SCENARIO1).

Concerning SCENARIO2 *[Table8/10; Table9/10]*, the trend in the results corresponds to the one just explained. Nevertheless, for the "FRESH" case, due to the different initial conditions, there is a smaller separation between the new profiles and the one related to the homogeneous simulation not accounting the gradient. On the other hand, the "SALINE" condition leads to a massive separation. The standard deviation of the relative in-flowed uranium follows the same trend of the covered length and area.

Facies	**Difference in terms of maximum length covered accounting and not accounting the gradient [m] (SCENARIO2)**	
	"SALINE" condition	**"FRESH" condition**
Sandy	15.08	- 0.6
Carbonate-rich	20.00	- 1.56
Shaly	/	0.96

Table8/10. The difference between the maximum covered length for the simulation accounting for the geochemical gradient and for the one not accounting for it is reported for the two new boundary conditions, and for each facies (SCENARIO2).

Facies	Difference in terms of maximum area covered accounting and not accounting the gradient [m^2] (SCENARIO2)	
	“SALINE” condition	**“FRESH” condition**
Sandy	931.62	- 54.62
Carbonate-rich	1091.43	- 159.72
Shaly	/	19.17

Table9/10. The difference between the maximum covered area for the simulation accounting for the geochemical gradient and for the one not accounting for it is reported for the two new boundary conditions, and for each facies (SCENARIO3).

After a comprehensive analysis of the results, the most important takeaway is the proportional relationship between the total length covered and the variance of the profiles accounting the spatial variability. Accordingly, the variance related to the all evaluating parameter show their peak, as expected, for the less sorbing carbonate-rich facies. Nevertheless, the uranium migration is largely facies-dependent due to the different chemistry involved in each facies, pore water chemistry and mineralogical composition of the host rock. To sum up, a list of the most relevant take-home messages is given. Regarding both SCENARIO1 and SCENARIO2, the highest values for the relative increases, at first in terms of covered length *[Table1/10]*, and then in terms of covered area *[Table6/10]*, are shown looking at the shaly facies. Namely, an increase of 4.2% and 6% are simulated. Accordingly, the most relevant effect of varying the correlation length is spectated for the sandy facies. Nevertheless, the largest spread between the concentration profiles of U, which is proportional to the variogram range, is simulated in the carbonate-rich facies. The enhancing chemical conditions leads to:

- for SCENARIO1, a maximum mean of the standard deviations for the relative distances equal to 0.657 *[Table2/10]*,
- for SCENARIO2, a maximum standard deviation of the in-flowed uranium of $2.247 \cdot 10^{-5}$ *[Table3/10]*.

Concerning the simulations after the implementation of the hydrogeochemical gradient, the carbonate-rich facies shows the biggest discrepancies from the previous results. Regarding the “SALINE” condition, an increase of 15.23 meters (SCENARIO1) and of 1091 m^2 (SCENARIO2) are simulated. While accounting for the “FRESH” condition, a reduction of 1.56 meters and 159.72 m^2 are observed. The results related to the sandy facies are affected by the implementation of the gradient in the opposite way.

Concerning all the chemical reactions that occur during the simulations, a more in-depth analysis is required to deeply quantify the influence of the variation of the chemical parameters (content of minerals, pH, content of the main pore water chemicals, etc.) on the model. The analysis should be carried out before accounting the spatial variability, in order to individually recognize the two influences. A detailed study of the involved chemistry would allow a more precise dimensioning of simulation grid and time stepping.

As it is observed in the results, the simulated model is rather simplified, and for the carbonate-rich facies, in SCENARIO2, its dimension may affect a comprehensive quantification of the total covered area.

New studies are required to efficiently implement the hydro-geochemical gradient inside the model. The influence of the gradient on the uranium migration in the Opalinus Clay is matter of different interesting ongoing studies, even at the GFZ. Regarding the current thesis, the results on the effects of the geochemical gradient on the uranium migration are insights for future studies. Since Hennig et al. [6] presents a series of simulations that show an enhanced migration towards the Dogger aquifer, the importance of the scoping analysis for the geochemical processes and the geochemical gradient is emphasized. Nevertheless, the thesis focuses on the effects related to the spatial variability of the petrophysical properties of the host rock. The quantity and the quality of the data related to the horizontal spatial correlation of the porosity (and, in perspective, of the relevant mineral fractions and sorption capacities) in the Opalinus Clay does not allow a detailed investigation yet. The availability of new data could be exploited for future simulations since POET allows to implement a variable porosity, despite it is considered constant for the purpose of the study. Moreover, it is possible to set an anisotropic diffusion coefficient. Regardless the availability of new data, a deeper investigation for the choice of the variogram parameters is necessary. The assumption of a spherical model, without any nugget effect, clearly affects the obtained results. New models should be tested, and the availability of a larger amount of data would enhance the process.

As an innovative study, the methods applied here may present some intrinsic assumptions which lead to a qualitative evaluation of the problem. However, the interesting results achieved in the context of the current thesis should provide relevant takeaways for future researches. For instance, the use of 3D models would allow a better understanding of the diffusive mechanisms of U. In particular, 3D models would result in a very useful tool for a comprehensive evaluation of the uranium diffusion for SCENARIO2. However, the implementation of 3D models will require the availability of a large quantity of data related to the petrophysical properties, and the mineralogy, of the host rock.

Webography

[S1] "Nuclear Power in the World Today - World Nuclear Association." Accessed: Nov., 2024. Available: https://world-nuclear.org/information-library/current-and-future-generation/nuclear-power-in-the-world-today

[S2] "IEA – International Energy Agency," IEA. Accessed: Nov., 2024. Available: https://www.iea.org/data-and-statistics

[S3] "Bentonite," *Wikipedia*. Jul. 25, 2024. Accessed: Nov., 2024. Available: https://en.wikipedia.org/w/index.php?title=Bentonite&oldid=1236599078

[S4] "Geochemistry of nuclear waste disposal." Accessed: Oct., 2024. Available: https://www.gfz.de/en/section/fluid-systems-modelling/topics/geochemistry-of-nuclear-waste-disposal

[S5] "Le Chatelier's Principle," Chemistry LibreTexts. Accessed: Dec., 2024. Available: https://chem.libretexts.org/Bookshelves/Physical_and_Theoretical_Chemistry_Textbook_Maps/Supplemental_Modules_(Physical_and_Theoretical_Chemistry)/Equilibria/Le_Chateliers_Principle

[S6] "Answer to 'How to transform/shift the mean and standard deviation of a normal distribution?", Mathematics Stack Exchange. Accessed: Dec., 2024. Available: https://math.stackexchange.com/a/2908415

Bibliography

[1] IAEA, 2021: *Spent Fuel Performance Assessment and Research*, 1st ed. Vienna: International Atomic Energy Agency, 2021.

[2] F. Pearson *et al., 2003: Mont Terri Project - Geochemistry of Water in the Opalinus Clay Formation at the Mont Terri Rock Laboratory.*

[3] S. Norris, 2017: "Radioactive waste confinement: clays in natural and engineered barriers – introduction", *Geol. Soc. Lond. Spec. Publ.*, vol. 443, Jan. 2017, doi: 10.1144/SP443.26.

[4] T. Hennig, 2022: "Uranium migration in the Opalinus Clay quantified on the host rock scale with reactive transport simulations", Universität Potsdam, 2022. doi: 10.25932/publishup-55270.

[5] T. Kneuker, R. Dohrmann, K. Ufer, and D. Jaeggi, 2023: "Compositional-structural characterization of the Opalinus Clay and Passwang Formation: New insights from Rietveld refinement (Mont Terri URL, Switzerland)," *Appl. Clay Sci.*, vol. 242, Sep. 2023. doi: 10.1016/j.clay.2023.107017.

[6] T. Hennig, 2021: "Potential Uranium Migration within the Geochemical Gradient of the Opalinus Clay System at the Mont Terri", *Minerals 2021, 11, 1087.* doi: 10.3390/min11101087.

[7] B. Hostettler, 2018: "Litho- and biostratigraphy of the Opalinus Clay and bounding formations in the Mont Terri rock laboratory (Switzerland)", in book: Mont Terri Rock Laboratory, 20 Years (pp.23-39). doi: 10.1007/978-3-319-70458-6_2.

[8] T. Kneuker and M. Furche, 2021: "Capturing the structural and compositional variability of Opalinus Clay: constraints from multidisciplinary investigations of Mont Terri drill cores (Switzerland)," *Environ. Earth Sci.*, vol. 80, Jun. 2021. doi: 10.1007/s12665-021-09708-1.

[9] M. Balhoff, 2022: "Chapter 7 - Component transport in porous media," in *Developments in Petroleum Science*, vol. 75, pp. 175–200. doi: 10.1016/B978-0-323-99235-0.00001-4.

[10] M. De Lucia, 2008: "Influence of spatial variability on reactive transport". Mathematics [math]. École Nationale Supérieure des Mines de Paris, 2008. Italian. NNT : 2008ENMP1552. pastel-00004649.

[11] C. A. J. Appelo and D. Postma, 2004: *Geochemistry, Groundwater and Pollution*, 0 ed. CRC Press, 2004. doi: 10.1201/9781439833544.

[12] J. Barthel, W. Kunz, and R. Neueder, 2003: "Electrolyte Solutions, Thermodynamics," in *Encyclopedia of Physical Science and Technology (Third Edition)*, R. A. Meyers, Ed., New York: Academic Press, 2003, pp. 219–241. doi: 10.1016/B0-12-227410-5/00208-8.

[13] M. De Lucia, M. Kühn, A. Lindemann, M. Lübke, and B. Schnor, 2021: "POET (v0.1): speedup of many-core parallel reactive transport simulations with fast DHT lookups," *Geosci. Model Dev.*, vol. 14, no. 12, pp. 7391–7409, Dec. 2021. doi: 10.5194/gmd-14-7391-2021.

[14] S. R. Charlton and D. L. Parkhurst, 2011: "Modules based on the geochemical model PHREEQC for use in scripting and programming languages," *Comput. Geosci.*, vol. 37, no. 10, pp. 1653–1663, Oct. 2011. doi: 10.1016/j.cageo.2011.02.005.

[15] T. Hennig, M. Stockmann, and M. Kühn, 2020: "Simulation of diffusive uranium transport and sorption processes in the Opalinus Clay," *Appl. Geochem.*, vol. 123, Dec. 2020. doi: 10.1016/j.apgeochem.2020.104777.

[16] T. Hennig and M. Kühn, 2021: “Surrogate Model for Multi-Component Diffusion of Uranium through Opalinus Clay on the Host Rock Scale,” *Appl. Sci.*, vol. 11, no. 2, Art. no. 2, Jan. 2021. doi: 10.3390/app11020786.

[17] T. Hennig and M. Kühn, 2021: “Uranium migration through the Swiss Opalinus Clay varies on the metre scale in response to differences of the stability constant of the aqueous, ternary uranyl complex $Ca_2UO_2(CO_3)_3$,” in *Advances in Geosciences*, Copernicus GmbH, Nov. 2021, pp. 97–105. doi: 10.5194/adgeo-56-97-2021.

[18] M. Mazurek *et al.*, 2023: “Swiss deep drilling campaign 2019–2022: Geological overview and rock properties with focus on porosity and pore-space architecture,” *Appl. Geochem.*, vol. 159, p. 105839, Dec. 2023. doi: 10.1016/j.apgeochem.2023.105839.

[19] M. E. Houben, G. Desbois, and J. L. Urai, 2014: “A comparative study of representative 2D microstructures in Shaly and Sandy facies of Opalinus Clay (Mont Terri, Switzerland) inferred form BIB-SEM and MIP methods,” *Mar. Pet. Geol.*, vol. 49, pp. 143–161, Jan. 2014. doi: 10.1016/j.marpetgeo.2013.10.009.

[20] H. Cai, N. S. N. Lam, and L. Zou, 2022: “Incorporating neighborhood scale effects into land loss modeling using semivariograms,” *J. Geogr. Syst.*, vol. 24, no. 3, pp. 419–439, Jul. 2022. doi: 10.1007/s10109-021-00372-4.

[21] S. S. Rocha, C. S. Pitombo, L. H. M. Costa, and S. de F. Marques, 2021: “Applying optimization algorithms for spatial estimation of travel demand variables,” *Transp. Res. Interdiscip. Perspect.*, vol. 10, p. 100369, Jun. 2021. doi: 10.1016/j.trip.2021.100369.

[22] D. J. Mulla, 2012: “Chapter 20 - Modeling and Mapping Soil Spatial and Temporal Variability,” in *Hydropedology*, H. Lin, Ed., Boston: Academic Press, 2012, pp. 637–664. doi: 10.1016/B978-0-12-386941-8.00020-4.

[23] B. Yven, S. Sammartino, Y. Géraud, F. HOMAND, and F. Villiéras, 2007: “Mineralogy, texture and porosity of Callovo-Oxfordian argillites of the Meuse/Haute-Marne region (eastern Paris Basin),” *Bull. Soc. Geol. Fr.*, vol. Mém. Soc. géol. France, pp. 73–90, Jan. 2007. hal-03698812.

[24] M. Huysmans and A. Dassargues, 2006: “Stochastic analysis of the effect of spatial variability of diffusion parameters on radionuclide transport in a low permeability clay layer,” *Hydrogeol. J.*, vol. 14, no. 7, Art. no. 7, Nov. 2006. doi: 10.1007/s10040-006-0035-2.

[25] S. Lüth *et al.*, 2024: “Characterization of heterogeneities in the sandy facies of the Opalinus Clay (Mont Terri underground rock laboratory, Switzerland),” *Geophys. J. Int.*, vol. 236, no. 3, pp. 1342–1359, Mar. 2024. doi: 10.1093/gji/ggad494.